Dissertation
zum Erwerb des Doctor of Philosophy (Ph.D.)
an der Medizinischen Fakultät der
Ludwig-Maximilians-Universität zu München

Effector functions and dependencies of myeloid cell subsets in colitis, colitis associated cancer and sporadic intestinal cancer

vorgelegt von:
(*First name, last name*)

Rebecca Metzger
.....

aus:
(*Place of birth*)

Landsberg a. Lech
.....

am:

13.02.2020

Supervisor(s): Prof. Dr. med. Anne Krug
Prof. Dr. rer. nat. Thomas Brocker
PD. Dr. rer. nat. Hubertus Hochrein

Dean: Prof. Dr. med. dent. Reinhard Hickel

Date of oral defense: 9.10.2020

LMU LUDWIG-MAXIMILIANS-UNIVERSITÄT MÜNCHEN

Dean's Office
Medical Faculty

MMRS

Affidavit

Metzger, Rebecca

Surname, first name

Street

Zip code, town

Country

I hereby declare, that the submitted thesis entitled

Effector functions and dependencies of myeloid cell subsets in colitis, colitis associated cancer and sporadic intestinal cancer

is my own work. I have only used the sources indicated and have not made unauthorised use of services of a third party. Where the work of others has been quoted or reproduced, the source is always given.

I further declare that the submitted thesis or parts thereof have not been presented as part of an examination degree to any other university.

München, 28.11.2020

Place, date

Rebecca Metzger

Signature doctoral candidate

Table of contents

1. List of abbreviations

cDC	conventional dendritic cell
CRC	colorectal cancer
DC	dendritic cell
NK cells	natural killer cells
PMN-MDSC	polymorphonuclear myeloid derived suppressor cell
TAM	tumor associated macrophage
TAN	tumor associated neutrophil

2. List of Publications

1 Markota A, Metzger R, Heiseke AF, Jandl L, Dursun E, Eisenächer K, Reindl W, Haller D, Krug AB. Comparison of iron-reduced and iron-supplemented semisynthetic diets in T cell transfer colitis. PloS one 2019; 14: e0218332.

2 Metzger R, Maruskova M, Krebs S, Janssen K-P, Krug AB. Increased Incidence of Colon Tumors in AOM-Treated Apc1638N/+ Mice Reveals Higher Frequency of Tumor Associated Neutrophils in Colon Than Small Intestine. *Frontiers in Oncology* (Methods) 2019; 9.

3. Introductory summary

3.1 Introduction

This work focuses on the intestinal myeloid compartment in colitis and colon cancer. Intestinal myeloid cells are shaped by their environment and in turn have decisive roles in intestinal homeostasis and disease. To gain further insights into the intertwined dependencies in the intestinal ecosystem the influence of dietary iron on intestinal myeloid cells and colitis, as well as the role of the myeloid effector molecule CCL17 in colitis associated cancer and the impact of tumor localization on myeloid cell infiltrates in sporadic intestinal tumors were analyzed.

The intestinal myeloid cell compartment is comprised of granulocytic cells and mononuclear phagocytes. The group of granulocytic cells contains neutrophils, eosinophils, basophils and mast cells with neutrophils being the most abundant leukocytes and playing crucial roles in infection and inflammation. Neutrophils are able to kill intracellular or nearby pathogens with their intracellular or secreted granules containing antimicrobial proteins which can also modulate other immune cells [1]. Murine neutrophils are characterized by the expression of Ly6G and CD11b.

Neutrophils are crucial for maintaining intestinal homeostasis by their antimicrobial activity and have a dual role during intestinal inflammation [2]. While their abundance correlates with disease severity and they are responsible for detrimental tissue damage they also produce mediators to resolve inflammation and to support epithelial integrity [3, 4]. In the tumor, the $Ly6G^+$ $CD11b^+$ population contains classical neutrophils (tumor associated neutrophils, TANs) with proinflammatory functions and an immunosuppressive subset (polymorphonuclear myeloid derived suppressor cells, PMN-MDSC). For TANs anti- and pro-tumoral functions have been described and their role in colorectal cancer (CRC) is controversial [5, 6]. The PMN-MDSC subset was shown to promote tumor initiation, progression and metastasis [6]. Intestinal mononuclear phagocytes can be subdivided into in dendritic cells (DCs) and cells of the monocyte macrophage lineage. Intestinal DCs

mainly consist of conventional DCs (cDC), whereas plasmacytoid DCs are rare in the intestine. Markers for murine intestinal cDC subpopulations are CD11b, Sirpα, CD103 and XCR1. The cDC1 subset expresses CD103 and XCR1 and is low for CD11b, while cDC2 express $CD11b^+$ and $Sirp\alpha^+$. Within this population and second subset can identified in the intestine by co-expression of CD11b and CD103. In colitis cDC1 have a rather anti-inflammatory role by e.g. their production of retinoic acid and subsequent regulatory T cell induction, whereas cDC2 are potent producers of pro-inflammatory cytokines and inducers Th17 responses [7, 8]. In the tumor microenvironment both cDC subsets have been shown to play crucial roles. As cDC1 are especially capable of antigen uptake and cross-presentation they are vital for mounting an anti-tumor immune response of cytotoxic $CD8^+$ T cells [9]. The cDC2 subset is able to activate $CD4^+$ T cells to elicit Th1 driven antitumor responses, which can be enhanced by depletion of regulatory T cells [10]. Intestinal cDC2 are closely related to intestinal macrophages, which belong to the monocyte-macrophage lineage and are derived from circulating monocytes [7]. Expression of CD64 and F4/80 allows the distinction of monocyte/macrophages from cDC2 in the intestine. In the steady state the macrophage pool in the gut is constantly replenished by infiltrating classical monocytes in a CCR2-dependent manner [11] unlike in other tissues, where the tissue resident macrophages are replenished by yolk-sac derived tissue resident stem cells [12]. These monocytes differentiate via an intermediary state into mature, anti-inflammatory macrophages [11]. This differentiation process can be followed by monitoring Ly6C and MHCII expression. Newly infiltrating $Ly6C^{hi}$ $MHCII^{lo}$ monocytes develop into inflammatory $Ly6C^{hi}$ $MHCII^{hi}$ monocytes before differentiating into $Ly6C^{lo}$ $MHCII^{hi}$ macrophages. Colitis is marked by a massive increase of infiltrating monocytes, which do not undergo the complete differentiation process but maintain high levels of pro-inflammatory activity and responsiveness to toll-like receptor ligands [13]. In intestinal tumors an additional $MHCII^{lo}$ macrophage population is found, which has been shown to possess an immunosuppressive signature, which is also observed in tumor-associated macrophages (TAMs) in other tumor entities [14, 15]. Tumor infiltrating monocytes can secrete tumoricidal mediators, but on the

other hand differentiate into immunosuppressive TAMs, which promote tumor growth [16]. Tumor associated macrophages have been shown to secrete CCL17, a chemokine of the C-C family, which is known to bind to the chemokine receptor CCR4, which is expressed on T-, natural killer cells (NK-cells), DCs and macrophages [17-21], CCR4. CCL17 has been shown to play a role in several inflammatory diseases, such as dermatitis, atherosclerosis, as well as in colitis [22-24].

3.2 Summary of publication 1 - Comparison of iron-reduced and iron-supplemented semisynthetic diets in T cell transfer colitis

Maintenance of intestinal homeostasis is a fine balancing act which can be disturbed by multiple internal but also external factors. As intestinal cells are in close contact with the environment via the gut lumen, dietary components can act on the cells in the gut directly and or via influencing the intestinal microbiota, which colonizes the luminal space. Not only macronutrients such as indigestible saccharides, which lead to anti-inflammatory effects via short chain fatty acid production by bacteria [25], but also micronutrients like selenium at sub-toxic levels have been shown to influence colitis severity [26]. The micronutrient iron was shown to induce a pro-inflammatory response in macrophages [27] and luminal iron depletion led to disease amelioration in an ileitis model [28]. However, the effect of dietary iron reduction in colitis was not investigated so far. In our study, we therefore compared the disease severity and the immune cell compartment in the T cell transfer colitis model conducted with Rag-deficient recipient mice on iron-depleted, normal, or iron-enriched diets [29]. As the transferred T cells were obtained from mice receiving normal chow, we mainly studied the effects of dietary iron modulation on the innate immune system and its effects on the transferred T cells. While we could observe massive monocyte infiltration and increase of the inflammatory monocyte proportion during the course of colitis we did not detect differences in immune cell frequencies or effector functions including T- helper cell responses with respect to the diets corresponding to the course and severity of colitis which was not affected by the iron content of the diets. Thus, we concluded that the frequencies

and effector functions of the analyzed intestinal myeloid cells during colitis were independent of the luminal iron availability, which is in contrast to the results obtained in the ileitis model and illustrates that inflammatory processes in the intestine are highly dependent on the location within the gastrointestinal tract.

3.3 Summary of the unpublished manuscript – CCL17 promotes colitis associated tumorigenesis dependent on the microbiota

Colitis is a strong risk-factor for the development of colorectal cancer [30] and chemokines are important immune regulators in inflammation and cancer with functions beyond cell recruitment [31, 32]. We show in this study that chemokine CCL17 is mainly expressed by myeloid cells (cDC2 and macrophages) in the colon and that it is strongly upregulated upon inflammation and tumorigenesis. Further we firstly describe a pro-tumorigenic role for this chemokine in the development of colitis associated cancer. We found that CCL17-deficiency influenced the microbiota directly or indirectly and reduced tumor incidence without altering the infiltrating immune cell frequencies, highlighting its importance beyond its role in immune cell recruitment. Instead, we found effects on tumor infiltrating myeloid cell function and on apoptosis in the mucosa of the colon at an early stage of the disease. Moreover, our study provides new insights about the gene expression profile of the myeloid subpopulations, which infiltrate colitis induced tumors with implications for their functionalities in colitis associated cancer development.

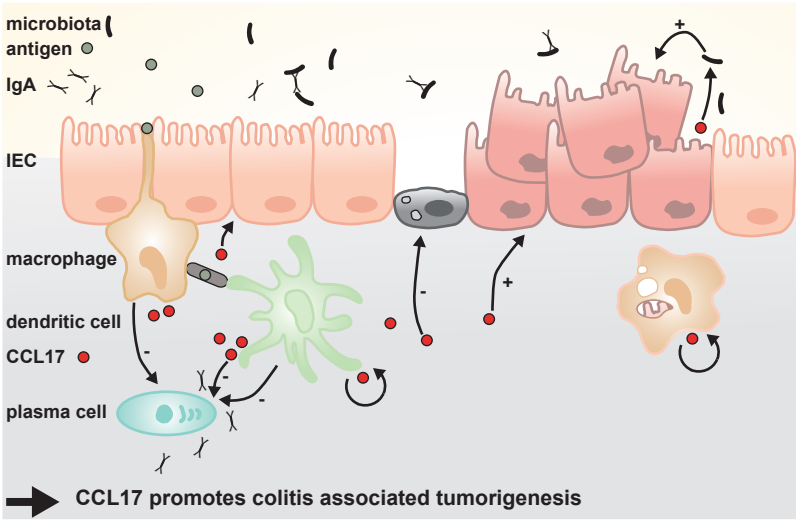

Figure 1 Graphical abstract of the unpublished manuscript - CCL17 promotes colitis associated tumorigenesis dependent on the microbiota. CCL17 is expressed by intestinal macrophages and DCs, altering their phenotype. Moreover, CCL17 decreases luminal IgA levels and bacterial IgA coating and leads to lowered apoptosis, thereby promoting outgrowth of transformed intestinal epithelial cells. (-) inhibits, (+) promotes

3.4 Summary of publication 2 – Increased Incidence of Colon Tumors in AOM-Treated Apc1638$^{N/+}$ Mice Reveals Higher Frequency of Tumor Associated Neutrophils in Colon Than Small Intestine

As illustrated with the above described study, myeloid cells play vital roles for inflammation-related colon tumor development. However, they also shape the tumor microenvironment of sporadic colon tumors and influence their incidence and progression [33]. Unfortunately, to date mouse models for sporadic intestinal tumorigenesis show lesions predominantly in the small intestine while human intestinal tumors are mostly found in the colon. In this study we present a model with 90 % incidence of colon tumors which allows the analysis of small intestinal as well as colonic sporadic tumors in parallel and illustrate the marked differences regarding the tumor immune cell infiltrate when comparing tumors from small intestinal versus colonic locations [34]. We found a 6-fold higher percentage of infiltrating granulocytes in colonic versus small intestinal tumors, highlighting the dependency of the myeloid immune cell infiltrate on the tumor location. Given the functional relevance of both TANs and PMN-MDSC, it is of great importance to model the human situation as close as possible to investigate the influence of these cell types on colon tumor development and

use this information to design novel treatment strategies for human patients with colorectal cancer. The model presented in this study not only provides a closer resemblance to the human disease but also allows direct comparisons between the different tumor locations, which enables to estimate whether promising findings from the small intestinal tumor models might be valid also for sporadic colonic tumors. Furthermore, we found an accumulation of CCL17-expressing macrophages and DCs in the colon tumors in this model which is in line with our findings in the colitis-associated cancer model and shows that CCL17 could be a relevant modulator of the tumor microenvironment also in sporadic colon tumors.

3.5 Conclusion

Taken together, this work highlights the complexity of the intestinal myeloid cell compartment and the multiple dependencies for cell frequencies and functions. It illustrates the limitations of dietary interventions in the treatment of colitis, but on the other hand shows that CCL17 could be an interesting target for treating colitis associated cancer and points to the microbiota as an important player in colitis associated colon tumorigenesis. Further, it provides a detailed analysis of the gene expression profiles of myeloid populations in colitis induced tumors. This resource can be used to study the contribution of each of these populations to the initiation and progression of colon tumors in a well-established mouse model which may lead to novel approaches for targeting pro-tumorigenic mechanisms or for enhancing myeloid cell mediated anti-tumor responses. My study using the sporadic intestinal tumor model shows that small intestinal tumors markedly differ from colonic lesions with regard to the infiltration of myeloid cells. These findings have implications for developing strategies to prevent the influx or change the functionality of tumor infiltrating myeloid cells in intestinal cancers and demonstrate the importance of the location of the lesion within the gastrointestinal tract.

3.6 Contributions to publication 1 - Comparison of iron-reduced and iron-supplemented semisynthetic diets in T cell transfer colitis

The study was conceptualized by A. Krug, D. Haller and W. Reindl. A. Krug acquired funding.

Data interpretation and conceptualization of the manuscript were performed by all co-authors.

Figure 1: A. Markota conducted the experiments with my support in scoring and tissue sampling together with L. Jandl and A. Heiseke. E. Dursun provided help with histology. Histoscoring was supported by A. Krug.

Figures 2-5: Flow cytometric analyses were performed by A. Markota with my support in tissue sampling and data analysis.

Supplementary Figure A: I established, performed, analyzed and interpreted the histological assessment of the intestinal iron, which showed a reduction of the intestinal iron in the dietary iron depleted group and laid the ground for the interpretation of the obtained results in the colitis model.

Supplementary Figure B: Flow cytometric analyses were performed by A. Markota with my support in tissue sampling and data analysis.

Supplementary Table A: K. Eisenächer obtained sample material for hematological analysis.

Supplementary Table B: Flow cytometric analyses were performed by A. Markota with my support in tissue sampling, data analysis and - interpretation.

3.7 Contributions to the unpublished manuscript – CCL17 promotes colitis associated tumorigenesis dependent on the microbiota

The study was conceptualized and funding was acquired by A. Krug

Figure 1: I performed the tissue preparation and the flow cytometric analysis/ immuno-fluorescent staining/gene expression analysis shown in Figure 1 A-D

Figure 2: I conducted the experiments and performed the tissue preparation with support of S. Krebs. I performed flow cytometric analysis and cell sorting prior to global gene expression analysis, as well as the flow cytometric validation of the sequencing results (Figure 2 D). Library preparation was performed by R. Öllinger. Data analysis and heatmap generation (Figure 2 C, E) was performed with T. Engleitner and K. Lutz, I performed GO term analyses shown in Figure 2F.

Figure 3: The experiments shown in figure 3 were performed with support of S. Krebs, who also helped in tissue preparation. I performed immunohistochemical and immunofluorescence stainings and analyses as well as the size measurements.

Figure 4: I performed the fecal sample preparation for the microbiome analysis, library preparation and bioinformatical analyses were done by D. Garzetti. I performed fecal IgA staining and flow cytometric analyses with the advice and reagents from V. Friedrich and T. Brocker.

Figure 5: I performed the experiment and flow cytometric as well as gene expression analyses. K. Lutz and E. Winheim were participating in tissue preparation.

Figure 6: I performed the analyses shown in Figure 6A-D.

Supplementary Figure 1: I performed the flow cytometric analyses shown in supplementary Figure 1.

Supplementary Figure 2: I analyzed the depicted comparisons of surface protein/gene expression based on the gene expression data obtained and analyzed with the support of R. Öllinger, T. Engleitner and K. Lutz.

Supplementary Figure 3: I performed the flow cytometric and gene expression analyses shown in supplementary Figure 3.

3.8 Contributions to publication 2 – Increased Incidence of Colon Tumors in AOM-Treated Apc$^{1638N/+}$ Mice Reveals Higher Frequency of Tumor Associated Neutrophils in Colon Than Small Intestine

The study was conceptualized and funding was acquired by A. Krug. K.P. Janssen provided Apc1638$^{N/+}$ mice and participated in conceptualization of the manuscript.

Figure 1: I conducted the experiment and the analyses shown in Figure 1 with the support of M. Maruskova in mouse scoring and colony management.

Figure 2: I conducted the histology shown in Figure 2A. Scoring was done by myself, A. Krug and K.P. Janssen. I conducted the gene expression analysis with reagents from K.P. Janssen. I established the immunofluorescence staining and analysis. Stainings were conducted with the support of S. Krebs.

Figure 3: I performed the flow cytometric analyses shown in Figure 3A-D with support of M. Maruskova in tissue sampling. I performed the gene expression analysis shown in Figure 3E with the help of S. Krebs in RNA isolation and cDNA preparation.

Figure 4: I performed the flow cytometric analyses shown in Figure 4A-C with support of M. Maruskova in tissue sampling. I established and performed the immunofluorescence staining shown in Figure 4D.

Supplementary Figures 1 and 2: I performed the flow cytometric analyses shown in the supplementary figures with support of M. Maruskova in tissue sampling. I established and performed the immunofluorescence staining.

PLOS ONE

RESEARCH ARTICLE

Comparison of iron-reduced and iron-supplemented semisynthetic diets in T cell transfer colitis

Anamarija Markota[1], Rebecca Metzger[1], Alexander F. Heiseke[1], Lisa Jandl[1], Ezgi Dursun[1], Katharina Eisena¨cher[1], Wolfgang Reindl[3], Dirk Haller[2], Anne B. Krug[1]*

1 Institute for Immunology, Biomedical Center, Ludwig-Maximilians-University Munich, Martinsried, Germany, **2** Chair for Nutrition and Immunology, Technical University Munich, Freising, Germany, **3** Klinikum Mannheim, II. Medizinische Klinik, Mannheim, Germany

* anne.krug@med.lmu.de

Citation: Markota A, Metzger R, Heiseke AF, Jandl L, Dursun E, Eisena¨cher K, et al. (2019) Comparison of iron-reduced and iron-supplemented semisynthetic diets in T cell transfer colitis. PLoS ONE 14(7): e0218332. https://doi.org/10.1371/journal.pone.0218332

Editor: Jo¨rn Karhausen, Duke University, UNITED STATES

Received: February 6, 2019

Accepted: May 30, 2019

Published: July 5, 2019

Data Availability Statement: All relevant data are within the manuscript and its Supporting Information files.

Funding: A.M. A.H., A.K. W.R. and D.H. were supported by the GRK 1482 of the German Research Foundation. A.K., A.H. E.D, R.M., L.J. and K.E. received funding from German Research Foundation grants SFB1054/TPA06, KR2199/3-2, KR2199/6-1, KR2199/9-1. The funders had no role in study design, data collection and analysis,

Abstract

Clinical observations in inflammatory bowel disease patients and experimental studies in rodents suggest that iron in the intestinal lumen derived from iron-rich food or oral iron supplementation could exacerbate inflammation and that iron depletion from the diet could be protective. To test the hypothesis that dietary iron reduction is protective against colitis development, the impact of iron reduction in the diet below 10 mg/kg on the course of CD4+ CD62L+ T cell transfer colitis was investigated in adult C57BL/6 mice. Weight loss as well as clinical and histological signs of inflammation were comparable between mice pretreated with semisynthetic diets with either < 10mg/kg iron content or supplemented with 180 mg/kg iron in the form of ferrous sulfate or hemin. Accumulation and activation of Ly6C^{high} monocytes, changes in dendritic cell subset composition and induction of proinflammatory Th1/Th17 cells in the inflamed colon were not affected by the iron content of the diets. Thus, dietary iron reduction did not protect adult mice against severe intestinal inflammation in T cell transfer induced colitis.

Introduction

Inflammatory bowel diseases (IBD)—ulcerative colitis and Crohn's disease—are chronic inflammatory disorders of the gastrointestinal tract resulting from a dysregulated immune response to the intestinal microbiota which is influenced by the genetic susceptibility of the host and environmental factors [1]. In addition to dietary intake of macronutrients (fat, carbohydrates and proteins), micronutrients including iron influence the epithelial barrier function, the mucosal immune response and directly or indirectly the microbiota [2]. The consumption of red meat containing heme iron has been associated with a higher risk for IBD and colorectal cancer [3, 4]. Oral iron supplementation is often avoided during phases of active IBD, because it is poorly tolerated by some IBD patients and may promote IBD symptoms [5]. Results of recent clinical studies however do not provide clear evidence for exacerbation of IBD as a consequence of oral iron supplementation [6]. Animal studies performed in rodents using

decision to publish, or preparation of the manuscript.

Competing interests: The authors have declared that no competing interests exist.

chemically induced erosive colitis models demonstrated a proinflammatory effect of iron in the intestinal lumen by showing that high dose oral iron supplementation causes an increase in disease activity, inflammatory score and oxidative stress [7–12]. Luminal iron, especially in the form of heme iron was shown to induce oxidative stress and cytotoxicity in the intestinal epithelium [13]. However, it was shown recently that exposure of intestinal macrophages to hemin inhibited their expression of LPS-induced proinflammatory cytokines and this effect was reversed by dietary iron reduction [14]. The effect of dietary iron reduction for the development of intestinal inflammation has been explored in the spontaneous Crohn's disease-like ileitis model in tumor necrosis factor $(TNF)^{\Delta ARE}$ mice, which developed less severe intestinal inflammation when treated with an iron-reduced diet [15]. In this study, mice fed with an iron-free (< 10 mg/kg) semisynthetic diet for 11 weeks depleted hepatic iron stores without developing anemia and the protective effect of the iron-reduced diet was still observed when systemic iron stores were repleted by parenteral iron administration demonstrating that luminal iron depletion was responsible for the observed effect [15]. However, iron reduction has not been tested as dietary intervention in the T cell transfer induced colitis model, which causes T cell driven microbiota-dependent colonic inflammation resembling human IBD.

How luminal iron could promote intestinal inflammation is not fully understood. Excess luminal iron induces reactive oxygen species (ROS) and nitric oxide (NO) production which activate the nuclear factor (NF)-κB signalling pathway and induce inflammatory cytokine production [8, 9, 13, 16]. Luminal iron was also shown to trigger endoplasmic reticulum (ER)-stress leading to apoptosis of intestinal epithelial cells and alterations in the composition of the intestinal microbiota [15], but little is known about how changes in the concentration of luminal iron affect intestinal immune responses. Especially the impact of dietary iron on the mononuclear phagocyte (MNP) system and potential subsequent effects on T cell responses during colitis has not been investigated.

The MNP system in the intestine is composed of macrophages and dendritic cells (DCs) that have complementary yet distinct functions [17]. Intestinal $CX3CR1^{high}$ macrophages are equipped with transepithelial dendrite extensions that enable them to sense and internalize microbial antigens and micronutrients (including iron) in the gut lumen [18, 19]. Macrophages are equipped to take up, store and export iron, but may accumulate iron under inflammatory conditions [20]. Iron overload triggers an unrestrained M1 type proinflammatory program in macrophages as observed for example in chronic venous leg ulcers and atherosclerosis [21, 22]. Resident anti-inflammatory $Ly6C^{low}$ intestinal macrophages [23, 24] are continuously replenished by $Ly6C^{high}$ blood-derived monocytes [25] that then downregulate Ly6C and upregulate MHCII, CD64 and F4/80 [26]. During inflammation, $Ly6C^{high}$ monocytes are massively recruited to the colon and differentiate into proinflammatory cytokine producing macrophages which promote and maintain pathogenic T helper (Th) cells producing IL-17 (Th17) and Interferon (IFN)-xγ (Th1) in the inflamed colon [27]. Luminal antigens taken up by non-migratory macrophages can be transferred to intestinal DCs which migrate to the draining lymph nodes (LN) where they present antigens and induce T helper (Th) cell polarization into regulatory (Treg) and effector Th cells [17, 28]. The CD103+ CD11b- intestinal DCs which preferentially induce gut-homing Tregs were found to be decreased in the lamina propria of the colon during colitis in mice and humans concomitant with an increase in the percentage of CD11b+ DCs, which promote differentiation of proinflammatory effector Th cells [29, 30, 31, 32].

Here we investigated the impact of dietary iron reduction in T cell transfer induced murine colitis as a model of human IBD focusing on the effect of luminal iron on intestinal macrophages and DCs as well as Th cell differentiation. Colitis activity was comparable in mice pretreated with iron-reduced and iron-supplemented semisynthetic diets in T cell transfer colitis

and no significant differences in the macrophage and DC compartment or in the proinflammatory Th1/Th17 cell frequency in the inflamed colon were observed. Thus, our results show that dietary iron reduction neither changed the intestinal inflammatory immune response nor altered the clinical course of murine experimental colitis induced by T cell transfer.

Methods

Mice

Wild type and *Rag1*$^{-/-}$ mice (C57BL/6) were bred and held in the mouse facility of the Institute of Medical Microbiology, Immunology and Hygiene at the Technical University Munich. Health monitoring was performed according to the recommendations of the Federation of European Laboratory Animal Science Association (FELASA). Sentinels occasionally tested positive for *Helicobacter* spp. Mice entered experiments at 10–12 weeks of age. Mice were sacrificed by cervical dislocation. All experimental procedures involving mice were performed in accordance with the regulations of and were approved by the local government (Regierung von Oberbayern, Az 205–2012).

Dietary treatment

The following diets were used: iron-deficient experimental diet (Altromin C1038, < 10 mg Fe/kg, Altromin, Lage, Germany), iron sulphate containing experimental diet ($FeSO_4$, Altromin C1000, 180 mg Fe/kg) or iron-deficient experimental diet (Altromin C1038) supplemented with hemin (Sigma Aldrich, Seelze, Germany), which was incorporated into the diet (equalling 180 mg Fe/kg). Mice were held on standard chow (Harlan Global rodent diet 2018, Harlan, Germany) until the age of 10–12 weeks, which was then gradually replaced by the experimental diets over a period of 2 weeks. Mice were fed experimental diets for 9 weeks and were then sacrificed for analysis or subjected to T cell transfer colitis and continued on the experimental diets until the end of the experiments. Mice were held in small groups of 3–4 mice per cage throughout the entire experimental time.

Colitis model

For T cell transfer colitis, 3 x 10^5 $CD4^+CD62L^+$ splenic T cells were injected intraperitoneally into *Rag1*$^{-/-}$ mice. Colitis activity was evaluated by bodyweight measurements and cumulative clinical score (0: absent symptoms, 1: mild symptoms, 2: moderate, 3: severe for inactivity, hunched posture, ruffled fur, diarrhea, rectal prolapse and rectal bleeding). Mice were sacrificed when they had lost up to 20% bodyweight compared to the starting weight or when clinical criteria for euthanasia were reached.

T cell isolation

For T cell transfer, T cells were isolated from splenocytes of C57BL/6 WT mice (fed normal chow) using $CD4^+$ $CD62L^+$ Isolation Kit II (Miltenyi Biotech, Bergisch-Gladbach, Germany). The purity of $CD4^+$ $CD62L^+$ T cells as well as the percentage of $Foxp3^+$ Tregs within the isolated T cell population was evaluated by FACS analysis before each transfer experiment (purity: > 90% $CD4^+$ $CD62L^+$ containing 7–10% $Foxp3^+$ as shown previously[33]).

Isolation of cells from mLNs and colon

Mesenteric lymph nodes (mLNs) were minced and digested with collagenase D (500 μg/mL) and DNase I (100 μg/mL) (Roche, Mannheim, Germany) at 37˚C for 30 min. The digested tissue fragments were passed through a 100 μm cell strainer.

Colons were excised and attached mesenteric fat was carefully removed. The whole colons were cut longitudinally and flushed 3 times with ice cold Ca^{2+}/Mg^{2+} free HBSS (Invitrogen, Thermo Fisher Scientific, Waltham, MA, USA) and then cut in 3 mm long pieces and incubated in Ca^{2+}/Mg^{2+}-free HBSS with 2 mM DTT (Roth, Karlsruhe, Germany) and 5 mM EDTA (Invitrogen, Thermo Fisher Scientific) for 30 min at 37˚C stirring in the incubator (5% CO_2). The treated colon pieces were collected using a 100 μm filter. The filtrate was further passed through glass wool (Roth) to remove epithelial cells and isolate the IELs. For isolation of LPLs, the remaining colon pieces were digested in RPMI 1640 medium (Thermo Fisher Scientific) containing DNase I (100 μg/mL), collagenase D (500 μg/mL) and collagenase V (850 μg/mL, Sigma Aldrich, St. Louis, MO, USA) for 30 min at 37˚C and passed through a 100 μm cell strainer.

Flow cytometry

Cells were stained with fluorescently labelled antibodies against the following surface markers: CD3ε CD4, CD11b, CD11c, CD45.2, I-A^b (all eBioscience, San Diego, CA, USA), CD64 (BioLegend, San Diego, CA, USA), CD62L, CD103, Ly6-C (BD Biosciences, Heidelberg, Germany) at 1:200 final dilution in FACS buffer (PBS, 2% FCS) with 50% HB197 hybridoma supernatant containing Fc blocking antibody 2.4G2 (ATCC, Manassas, VA, USA). Dead cells were excluded by propidium-iodide (PI) staining (Sigma Aldrich). For intracellular cytokine staining single cells from mLNs and colonic LPLs were resuspended in complete medium (RPMI 1640, 1% GlutaMAX-I, 1% non-essential amino acids, 1% Penicillin/Streptomycin, 1 nM Sodium Pyruvate Solution (all from Invitrogen) and β-mercaptoethanol (Sigma-Aldrich), Cell were stimulated at 10^6 cells/96-well with 20 ng/mL Phorbol 12-myristate 13-acetate (PMA) (Sigma-Aldrich), 1 μg/ml Ionomycin (Sigma-Aldrich), Golgi Plug (0.2% v/v) and Golgi Stop (0.14% v/v) (BD Biosciences) for 6h at 37˚C. Cells were stained for CD3ε and CD4 and then treated with IC fixation buffer and 1X Permeabilization Buffer (eBioscience). Intracellular staining was performed using anti IL-17A-APC and anti IFN-γ-PE antibodies (BD Bioscience). Intracellular Foxp3 staining was performed using the Intracellular Foxp3 staining kit (eBioscience). Flow cytometry analysis was performed using a Gallios Flow cytometer (Beckman Coulter, Brea, CA, USA) and data were analysed using FlowJo software (Tree Star, Stanford, USA).

Histology

Colons were cut longitudinally and "swiss rolls" were prepared and fixed in 4% formaldehyde (Roti-Histofix, Karl-Roth, Karlsruhe, Germany) over night and embedded in paraffin. Tissue blocks were cut in 4 μm sections and stained with hematoxylin and eosin (H&E). Histological scoring was performed observer-blinded by adding the scores (0–3) for leucocytes infiltration and epithelial damage as described (maximal score 6) [34].

Statistical analysis

Statistical analysis was performed using Graph Pad Prism software (Version 6.0, GraphPad Software San Diego, CA, USA). The results are presented as mean ± SD. One way ANOVA test followed by Tukey's post-hoc test was used for multiple comparisons and histology scores were compared using Kruskal-Wallis non-parametric test. p values < 0.05 were considered to indicate significant differences.

Results

Dietary iron reduction does not protect against colitis induced by CD4 + CD62L+ T cell transfer in Rag1-/-mice

It was shown previously that oral iron supplementation influences chemically-induced colitis activity in rodents and that dietary iron reduction below 10 mg/kg protects mice from spontaneous Crohn's disease-like ileitis in tumor necrosis factor (TNF)$^{\Delta ARE}$ mice when compared to normal dietary iron content. Therefore, our hypothesis was that dietary iron reduction below 10 mg/kg could protect mice from colitis and this was tested in C57BL/6/Rag1$^{-/-}$ mice using the CD4^{+} CD62L^{+} T cell transfer colitis model (see experiment outline in Fig 1A). Hemin was used to mimic heme iron contained in red meat or in hemoglobin from mucosal bleeding for example. Mice on iron-depleted diet did not develop anemia as determined by blood hemoglobin concentration 13.9 g/dl [35] (w/o Fe: 14.9 ± 3.9; $FeSO_4$: 16.4 ± 3.6; Hemin: 15.8 ± 3.4 g/dl; table A in S1 File). After T cell transfer mice lost weight progressively in all 3 groups and by day 17 more than 50% of the mice in each group had lost 15–20% of their starting bodyweight (w/o Fe: 85.3 ± 8.0, $FeSO_4$: 91.4 ± 9.9, Hemin; 91.2 ± 7.4, mean ± SD, Fig 1B). The bodyweight loss was accompanied by similarly increased clinical disease activity in all experimental groups (clinical score: w/o Fe: 2.1 ± 1.9, $FeSO_4$: 3.4 ± 1.1, Hemin: 2.5 ± 1.1, mean ± SD, Fig 1C). Leucocytosis and increased haematocrit (indicating fluid loss) were observed in all dietary groups during colitis (table A in S1 File). The histological colitis score was also comparable between the 3 groups (w/o Fe: 4.7 ± 0.8, $FeSO_4$: 4.2 ± 0.4, Hemin: 4.3 ± 0.5, Fig 1D). Similar degrees of epithelial damage with presence of transmural ulcerations and extensive immune cell infiltration were observed in the colon sections (Fig 1E). Ferric iron was detected by histochemical staining in the lamina propria of the inflamed colon at a higher level in mice which had received iron-supplemented diets than in mice which were iron-depleted diet (Fig A in S1 File). These results show that the induction and development of T cell transfer colitis was not affected by reduction of the iron concentration in the diet or by the form of iron (ferrous iron sulphate or hemin), which was added to the experimental diet.

Recruitment of Ly6C^{high} monocytes to the colon is not impaired by dietary iron reduction during T cell transfer colitis

The composition of colonic MNPs changes dramatically during colitis and the increased influx of blood-derived monocytes into the colon is a sensitive parameter of inflammation. To investigate whether the luminal iron content has an impact on monocyte recruitment and maturation, the monocyte/macrophage compartment in the colon was analysed by flow cytometry after exposure to the experimental diets during T cell transfer colitis (Fig 2A). The frequencies of CD11b^{+}CD64^{+} macrophages in colon lamina propria leucocyte (LPL) and intraepithelial leucocyte (IEL) fractions were comparable between the groups (Fig 2B and 2C). Analysis of Ly6C and MHCII expression in this population distinguished three distinct subsets: Ly6C^{high}MHCII^{-} (P1) and Ly6C^{high}MHCII^{+} (P2) cells are derived from circulating Ly6C^{high} monocytes and give rise to Ly6C^{low}MHCII^{+} macrophages (P3) [25, 26]. The composition of the monocyte/macrophage compartment in the colon was not affected by changes in dietary iron content as reflected in similar frequencies of P1, P2 and P3 subsets in the 3 experimental groups during colitis (Fig 2D and 2E).

The development of colitis after T cell transfer resulted in a marked shift of the Ly6C^{low} P3 population to the Ly6C^{high} MHCII$^{+/-}$ population (P1/P2) in colon LPL compared to *Rag1*$^{-/-}$ mice treated with the same type of the diet without T cell transfer in all conditions. The ratio of Ly6C^{high} (P1/P2) to Ly6C^{low} (P3) populations increased during colitis to a similar extent in

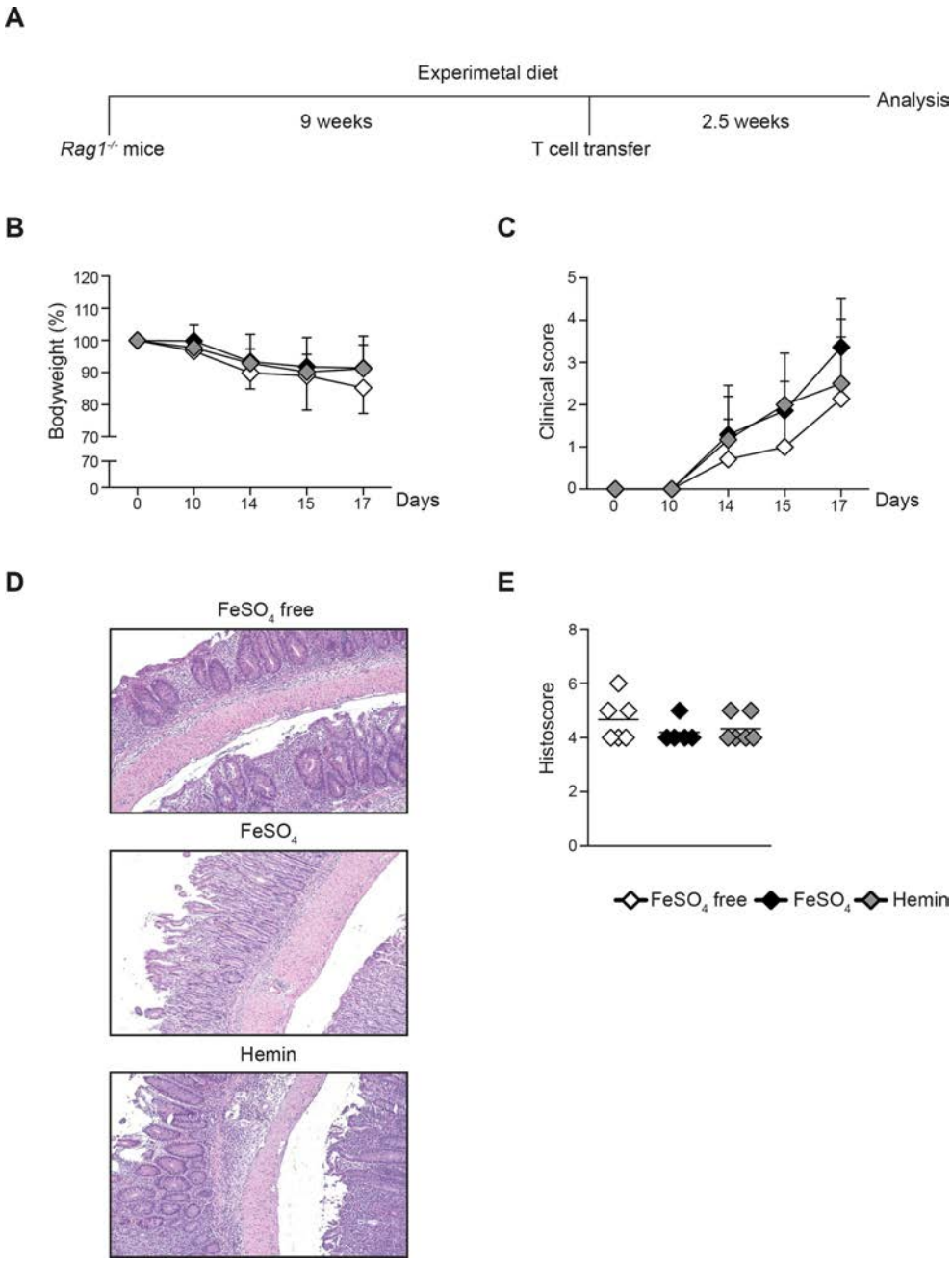
A
Experimetal diet
Analysis
9 weeks
2.5 weeks
Rag1-/- mice
T cell transfer
B
Bodyweight (%)
120
110
100
90
80
70
70
0
0
10
14
15
17
Days
C
Clinical score
5
4
3
2
1
0
0
10
14
15
17
Days
D
FeSO4 free
FeSO4
Hemin
E
Histoscore
8
6
4
2
0
FeSO4 free
FeSO4
Hemin

Fig 1. Dietary iron reduction does not protect against T cell transfer colitis. (A) Experimental design for T cell transfer colitis in *Rag1*$^{-/-}$ recipient mice fed with iron depleted (w/o Fe) or iron supplemented experimental diets ($FeSO_4$ or Hemin). **(B)** Bodyweight development at indicated time points after transfer of $CD4^+$ $CD62L^+$ T cells to *Rag1*$^{-/-}$ mice fed with experimental diets (one of 3 independent experiments with 4–6 animals in each group is displayed; mean ± SD; one way ANOVA, not significant). **(C)** Clinical colitis scores at indicated time points of mice from (A) (one of 3 independent experiments with 4–6 animals in each group is displayed; mean ± SD; one way ANOVA, n.s.). **(D)** Representative H&E staining of colon tissues sections of mice from (A) at day 17 after T cell transfer. **(E)** Histological colitis scores of mice from (A) (each symbol represents one animal and horizontal lines indicate mean values for each dietary group; Kruskall-Wallis test, n.s.).

https://doi.org/10.1371/journal.pone.0218332.g001

all 3 experimental groups and was not affected by the dietary treatment itself (Fig 3A and 3B). These results indicate that neither the constant migration of monocytes into the colon and their maturation into $Ly6C^{low}MHCII^+$ macrophages in the steady state nor the increased influx of blood-derived monocytes into the colon during colitis were affected by modulation of dietary iron in the T cell transfer colitis model.

Intestinal DC subset composition is not affected by dietary iron reduction during T cell transfer colitis

Besides the macrophages, DCs play an important role in colitis development as inducers of proinflammatory T cell responses [31]. To address if dietary iron content can influence their frequency and phenotype in the colon and their shift from the $CD103^+$ to the $CD11b^+$ subpopulations during colitis, DC subpopulations in colon LPL and IEL fractions were analyzed by flow cytometry in *Rag1*$^{-/-}$ mice in the steady state and during T cell transfer colitis after exposure to different diets. Three distinct DC subsets were distinguished based on CD103 and CD11b expression (Fig 4A). We observed a decrease in the percentage of $CD103^+$ $CD11b^-$ DCs and an increase in the percentage of $CD103^+$ $CD11b^+$ DCs after colitis induction (table B in S1 File). However, modulation of dietary iron content had no major effects on the total frequency of DCs or the DC subset composition in the colon during T cell transfer colitis (Fig 4B–4E). Thus, the dietary iron content did not influence DC recruitment to the inflamed colon or DC subset composition during colitis.

Dietary iron reduction does not influence in vivo T cell differentiation and activation during T cell induced colitis

T cell transfer colitis in lymphopenic mice is driven by CD4+ T cells which get activated, expand and differentiate in response to commensal bacterial antigens and innate immune signals delivered by DCs. Therefore, we explored the effect of luminal iron on $CD4^+$ T cell numbers and differentiation in this model. The frequencies of $CD4^+$ T cells found in the spleens, mLNs and colon LPL and IEL fractions on day 17 after T cell transfer were comparable between the different dietary treatments (Fig B in S1 File). A small population of $Foxp3^+$ Tregs was detected in mLNs and colon LPL as well as spleen and colon IELs with similar frequencies in the 3 dietary groups (Fig 5A and 5C, Fig B in S1 File). The frequencies of $CD4^+$ T cells producing IFN-γ^+, IL-$17A^+$ or both cytokines after restimulation in mLNs and colon LPL were also comparable between the groups (Fig 5B and 5C). Thus, in the T cell transfer colitis model dietary iron reduction had no influence on the accumulation of CD4+ T cells in the colon, mLN and spleen and their capacity to produce IFN-γ and IL-17 was not affected. We conclude that iron deprivation in the diet does not protect adult C57BL/6 mice against severe intestinal inflammation in the T cell transfer colitis model and does not change the frequency of relevant immune cell populations in the colon and mLNs.

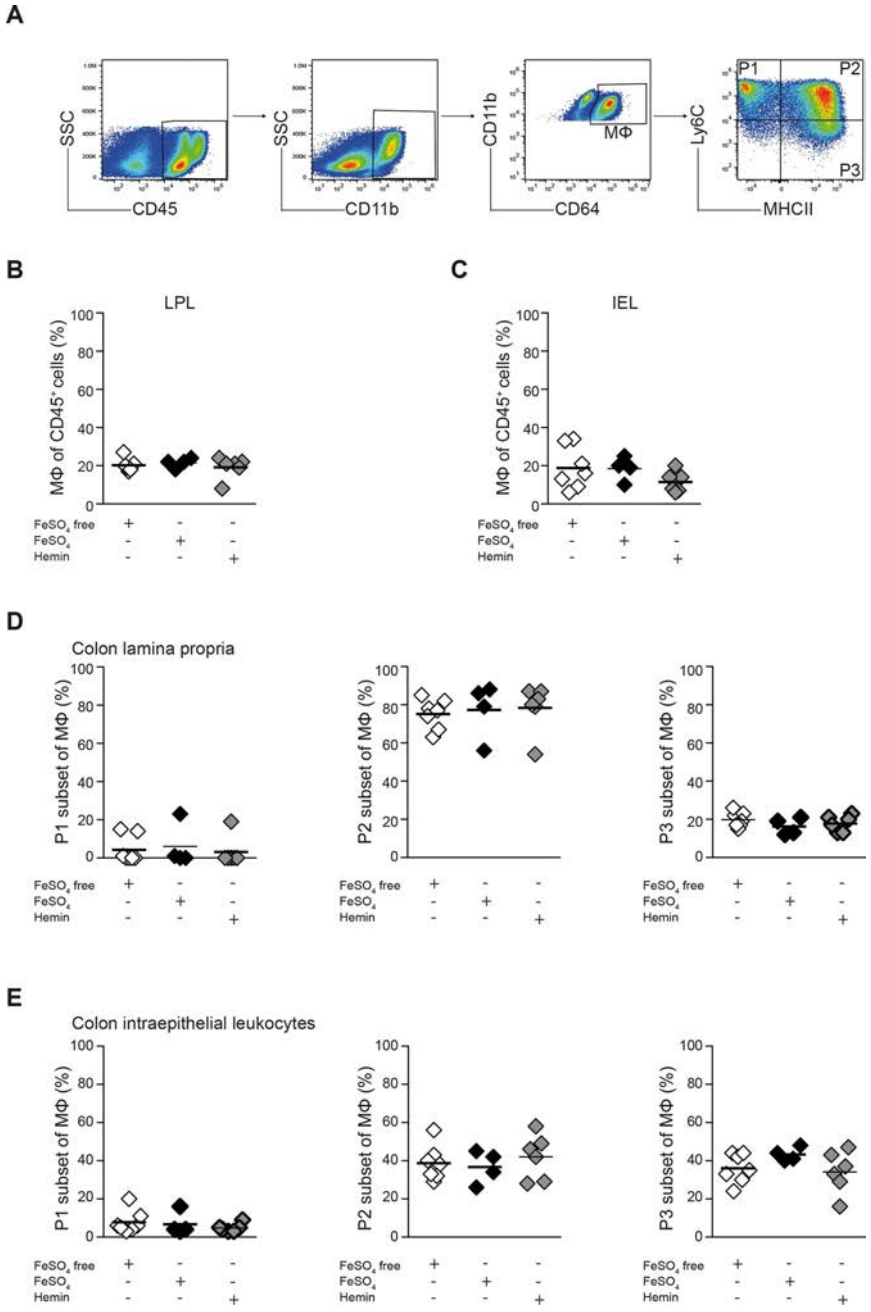
A
SSC
CD45
SSC
CD11b
CD11b
CD64
MΦ
Ly6C
MHCII
P1
P2
P3
B
LPL
MΦ of CD45+ cells (%)
C
IEL
MΦ of CD45+ cells (%)
FeSO4 free
FeSO4
Hemin
D
Colon lamina propria
P1 subset of MΦ (%)
P2 subset of MΦ (%)
P3 subset of MΦ (%)
E
Colon intraepithelial leukocytes
P1 subset of MΦ (%)
P2 subset of MΦ (%)
P3 subset of MΦ (%)

Fig 2. No effect of luminal iron depletion on monocyte/macrophage composition in the inflamed colon. *Rag1*$^{-/-}$ mice were treated with iron depleted (w/o Fe) or iron supplemented experimental diets ($FeSO_4$ or Hemin) and colitis was induced by T cell transfer. Colon LPLs and IELs were prepared on day 17 after T cell transfer and analyzed by flow cytometry. **(A)** Gating strategy used for characterization of the monocyte/macrophage compartment in LPL and IEL colon fraction. **(B, C)** The percentages of $CD11b^+$ $CD64^+$ monocytes/macrophages within viable $CD45^+$ leucocytes in LPL (B) and IEL (C) colon fractions are shown. **(D, E)** The percentages of P1, P2 and P3 subsets in LPL (D) and IEL (E) colon fractions are shown. (B-E) Results of one representative of 2 independent experiments with 4–6 animals in each dietary group are shown. Crossbars indicate mean values; one way ANOVA, n. s.).

https://doi.org/10.1371/journal.pone.0218332.g002

Discussion

Clinical observations in IBD patients and experimental studies suggested that iron in the intestinal lumen derived from iron-rich food or iron supplementation exacerbates inflammation in IBD patients [4, 5, 7–12]. This led to the assumption that oral iron replacement therapy for iron-deficiency anemia should be avoided during active IBD and that iron reduction in the diet may be protective. Indeed, evidence for a protective effect of luminal iron depletion was found in a murine model of ileitis [15]. In this model the beneficial effect of luminal iron depletion correlated with reduced ER-stress in the epithelium and changes in the microbiota composition. In contrast, we found that colitis activity in the T cell transfer induced mouse model of colitis was not affected by alterations in the iron content of the experimental diet in recipient mice. Examination of the frequency and activation of relevant innate and adaptive immune cell populations in the colon during colitis revealed that the iron-reduced diet had no significant effect on these parameters of intestinal inflammation.

To investigate the influence of the iron depleted diet on colitis development, we chose to study the $CD4^+$ $CD62L^+$ T cell transfer induced colitis model. In contrast to chemically induced colitis models in which epithelial disruption is the primary event, T cell transfer colitis is driven by microbiota-dependent proinflammatory Th1/17 cell responses. This is a valid preclinical model, that has been widely used for the development of approved drugs, which are effective in the therapy of Crohn's disease and ulcerative colitis, such as anti-TNF-α and anti-α4β7-integrin antibodies and probiotics [36, 37, 38] for example. The advantage of this model is that epithelial disruption is not the primary event as in chemically induced colitis models.

As iron cannot be removed from normal chow, the animals were adapted to an experimental semisynthetic diet, which was either iron-free (< 10 mg/kg) or contained 180 mg/kg iron in the form of FeSo4 or hemin–a concentration of iron corresponding to that contained in normal chow [15]. The same semisynthetic diets (with or without FeSo4) have been used in the $TNF^{\Delta ARE/WT}$ ileitis model where the iron-reduced diet changed the microbiota composition and prevented development of inflammation [15]. In that study it was also shown that the iron-free diet led to depletion of hepatic iron stores but did not cause anemia. This is in line with our results where mice treated with the iron-free diet did not develop overt anemia but showed reduced iron staining in colon tissue sections [15].

Purified diets with different iron concentrations have been tested in chemically induced colitis models in mice and rats where inflammation is initiated by epithelial disruption and massive entry of luminal bacteria into the mucosa of the colon. Seril et al. showed using the DSS colitis model in 8 weeks old mice, that colitis activity and tumor incidence increased with increasing doses of iron (49–490 mg/kg) in the purified diet [12, 39]. Barollo et al. reported increased inflammation and tissue damage in the dinitrobenzene sulfonic acid (DNBS)-induced colitis model in rats fed with a high iron diet (200 mg/kg and 1.7 g/kg) [7]. Furthermore, in several publications, normal chow was supplemented with high doses of iron in different formulations. Carrier et al. observed exacerbation of DSS-induced colitis in rats by addition of 3 and 30 g/kg iron pentacarbonyl iron to the chow correlating with oxidative stress,

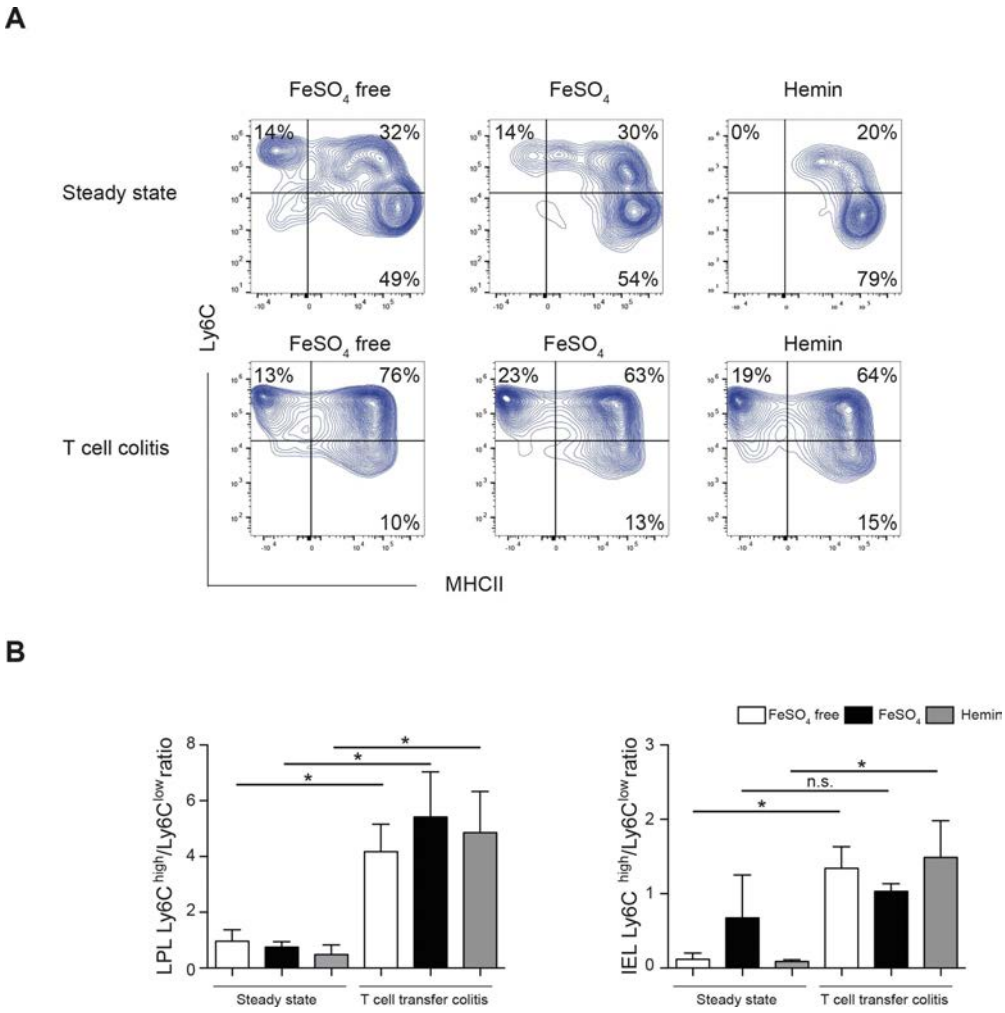

Fig 3. Recruitment of monocytes to the colon during colitis is not influenced by dietary iron reduction. (A) The expression of Ly6C and MHCII by $CD11b^+CD64^+$ colonic monocyte/macrophages in the steady state and on day 17 of T cell transfer colitis in *Rag1*$^{-/-}$ mice fed with experimental diets is shown in the dot plots. Numbers in the quadrants indicate percentages. Representative results of one of 2 independent experiments are shown. **(B)** Ratios of $Ly6C^{high}$(P1/P2): $Ly6C^{low}$(P3) $CD11b^+CD64^+$ cells in colon LPL and IEL isolated from *Rag1*$^{-/-}$ mice fed with experimental diets without colitis induction and on day 17 after colitis induction by T cell transfer. An increase in the $Ly6C^{high}$ to $Ly6C^{low}$ ratio indicates recruitment of monocytes to the inflamed colon. Representative results of one of 2 independent experiments with 4–6 animals per each dietary group are shown (mean ± SD; one-way ANOVA with Tukey's multiple comparison test, n.s.).

https://doi.org/10.1371/journal.pone.0218332.g003

neutrophil infiltration, NFκB activation and inflammatory cytokine production [8, 16]. Similarly, supplementation with 1% (10 g/kg) carbonyl iron in the chow for 6 weeks started at 4 weeks of age exacerbated colitis and promoted tumor development in the Azoxymethan/DSS mouse model of colitis-associated colon cancer [9]. On the other hand, a recent study using a

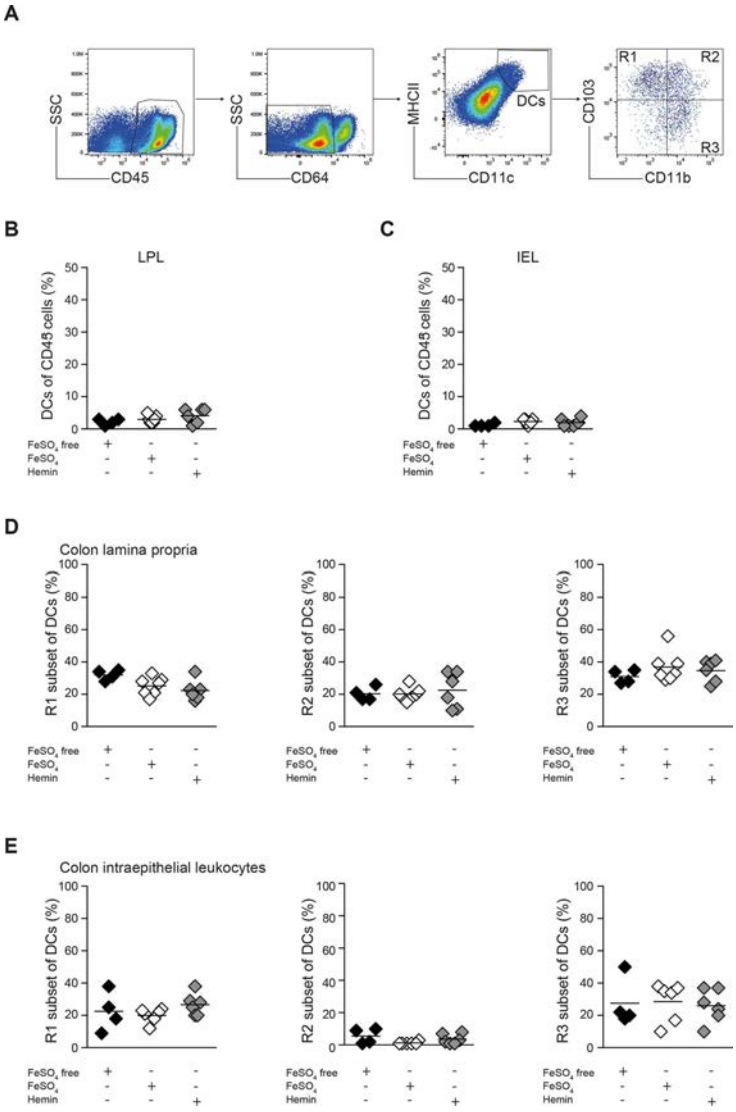

Fig 4. DC subset composition in the colon is not influenced by dietary iron reduction during T cell transfer colitis. *Rag1*$^{-/-}$ mice were treated with iron depleted (w/o Fe) or iron supplemented experimental diets ($FeSO_4$ or Hemin) and colitis was induced by T cell transfer. Colon LPLs and IELs were prepared on day 17 after T cell transfer and analyzed by flow cytometry. **(A)** Gating strategy for DC subpopulations in colon LPL and IEL fractions. **(B, C)** The frequencies of DCs within viable $CD45^+$ leucocytes in colon LPL (b) and IEL (C) are shown. **(D, E)** The frequencies of R1, R2 and R3 subsets within $CD64^+CD11c^+MHCII^{high}$ DCs within colon LPL (D) and IEL (E) are shown (one of 2 independent experiments with 4–6 animals in one of each dietary group; each dot represents one animal and horizontal lines indicate mean values; one way ANOVA, n.s.).

https://doi.org/10.1371/journal.pone.0218332.g004

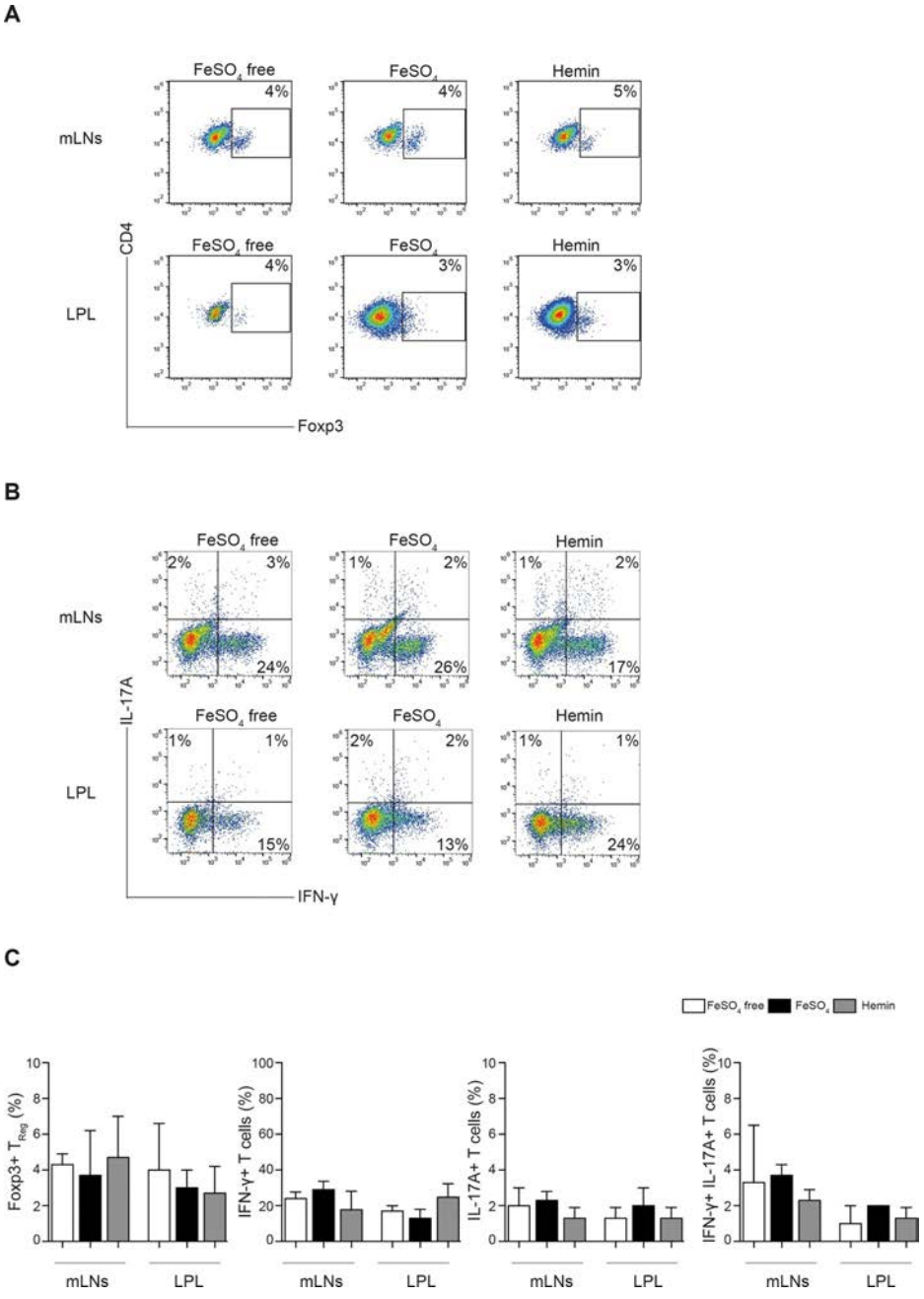
A
FeSO4 free
FeSO4
Hemin
mLNs
LPL
4%
4%
5%
4%
3%
3%
CD4
Foxp3
B
FeSO4 free
FeSO4
Hemin
mLNs
LPL
2%
3%
24%
1%
2%
26%
1%
2%
17%
1%
1%
15%
2%
2%
13%
1%
1%
24%
IL-17A
IFN-γ
C
FeSO4 free
FeSO4
Hemin
Foxp3+ TReg (%)
IFN-γ+ T cells (%)
IL-17A+ T cells (%)
IFN-γ+ IL-17A+ T cells (%)
mLNs
LPL

Fig 5. Frequency of Tregs and proinflammatory Th1/Th17 effector cells is not affected by dietary iron content during T cell mediated colitis. *Rag1*$^{-/-}$ mice were treated with iron depleted (w/o Fe) or iron supplemented experimental diets ($FeSO_4$ or Hemin) and colitis was induced by T cell transfer. MLN cells and colon LPLs were prepared on day 17 after T cell transfer and analyzed by flow cytometry. **(A)** Representative dot plots show Foxp3 expression in $CD3^+CD4^+$ T cells isolated from mLNs and colon LPL fraction for the 3 experimental groups. Numbers indicate percentages of $Foxp3^+$ cells. **(B)** MLN cells and colon LPLs were stimulated with PMA/Ionomycin in the presence of secretion blockers for 6 hours. Representative dot plots show the intracellular IFN-γ and IL-17A content in $CD3^+CD4^+$ T cells for the respective dietary groups. **(C)** The percentages of $Foxp3^+$ Tregs, IFN-γ single positive, IL-17A single positive and IFN-γ/IL-17A double positive Th cells isolated from the indicated organs are shown as mean values ± SD (n = 3 mice per group, one way ANOVA, n.s.).

https://doi.org/10.1371/journal.pone.0218332.g005

chronic low dose DSS colitis model in mice demonstrated that a diet with 500 mg/kg ferrous sulfate reduced colitis susceptibility compared to a diet with 50 mg/kg ferrous sulfate [10]. Taken together, most studies that described increased disease severity and tissue damage in chemically induced colitis models supplemented oral iron using much higher doses than those recommended for oral iron replacement therapy in human patients and much higher than the concentrations found in iron-rich foods (e.g. pork liver 180 mg/kg, Canadian Nutrient File, Health Canada, 2015). Our study is the first to investigate the impact of iron reduction in the diet below 10 mg/kg compared to an iron-rich diet with 180 mg/kg ferrous sulfate or hemin in the T cell transfer colitis model and we could not observe a beneficial effect of this intervention. These results contrast with previous observations in the ileitis model in $TNF^{\Delta ARE}$ mice, where the same semisynthetic iron-depleted diet reduced inflammation compared to the 180mg/kg ferrous sulfate supplemented diet [15].

How can we explain the different results of these two studies? One important aspect is the different pathophysiology of the models which were used. In $TNF^{\Delta ARE}$ mice intestinal pathology is restricted to the terminal ileum and proximal colon like in human Crohn's disease. Ileal epithelial cells have a higher basal level of ER-stress and are more responsive to induction of ER-stress *ex vivo* than colon epithelial cells [40]. Therefore the observed effects of dietary iron reduction on ER-stress and intestinal epithelial cell apoptosis may be more pronounced in the ileitis model [15] than in the colitis models.

In $TNF^{\Delta ARE}$ mice inflammation is driven by dysregulated TNF-α production in response to the microbiota [41, 42] and critically depends on $CD8^+$ T cell responses [43]. In contrast, unrestrained microbiota-triggered $CD4^+$ Th1/Th17 cells cause inflammation in the T cell transfer colitis model. It cannot be excluded that in the T cell transfer colitis model T cells isolated from mice fed with iron-free diet would have behaved differently after transfer than T cells isolated from mice fed with iron-supplemented diet. Indeed, it was reported that iron can promote expression of GM-CSF and IL-2 in T cells by stabilizing RNA binding protein PCBP1, which promotes stability of Csf2 and Il2 mRNA [44]. However, CD4+ T cells isolated from spleen of $TNF^{\Delta ARE/WT}$ mice fed with iron-free or iron sulfate supplemented diets did not differ in their ability to produce TNF-α and IFN-γ after TCR stimulation [15].

Another major difference is the kinetic of the inflammatory response. Ileitis develops spontaneously over a period of 8–16 weeks in the heterozygous $TNF^{\Delta ARE}$ mice, whereas severe colitis develops within 2–3 weeks in the $CD4^+CD62L^+$ T cell transfer colitis under our experimental conditions. The duration of dietary treatment was comparable between the two studies (8–11 weeks) and allows for full adaptation to the diet as shown previously [15]. Constante et al. reported that even 4 weeks of experimental diet with different concentrations of iron were sufficient to induce changes in the intestinal microbiota composition in adult mic [10]. In that study however microbiota changes did not translate into different susceptibility to colitis induced by low dose DSS. This is in line with the results of a recent clinical trial, which showed that oral iron replacement therapy induces major changes in intestinal bacterial diversity and composition in IBD patients without affecting clinical disease activity [6]. Similarly, an epidemiological study published recently found no significant associations of dietary total

iron and heme iron intake with risk of IBD in two large prospective cohorts (from the Nurses Health Study). Only in a subgroup of patients with a specific ulcerative colitis susceptibility locus (a functional coding variant of *FcγRIIA*) heme iron consumption was significantly associated with risk of ulcerative colitis suggesting that dietary heme iron may promote the development of ulcerative colitis in genetically predisposed individuals but does not have a major effect in the general population [45].

It has been reported that calcium phosphate in the diet can counteract cytotoxic and hyperproliferative effects of luminal hemin [46] and a hemin-supplemented low calcium diet was shown to aggravate chemically induced colitis in rats and mice [47, 48]. However, another study investigated the effect of hemin-supplemented diet with normal calcium content on microbiota and DSS-induced colitis and showed an aggravation of acute DSS colitis by hemin in the diet although the diet was not calcium-depleted [49], which may be due to direct effects of luminal heme iron on the microbiota. In our study dietary iron reduction led to reduced accumulation of iron in the colonic lamina propria and this was prevented by iron supplementation in the form of iron sulfate or hemin. We observed a similar extent of iron staining in colonic lamina propria of mice fed with a hemin-supplemented *vs*. iron-sulfate-supplemented diet with normal calcium content. It is therefore unlikely, but cannot be excluded, that hemin-supplementation did not affect colitis activity in our study is due to the presence of calcium (9450 mg/kg) in the diet.

In our study, we investigated sensitive immunological parameters of inflammation, such as recruitment of monocytes into the colon, changes in DC subset distribution, and activation of Th cells in the colon. Although monocytes/macrophages are equipped to sense luminal iron directly, their response during colitis was not different between mice exposed to iron -reduced diet or diet supplemented with ferrous sulfate or hemin at moderate concentrations corresponding to those found in iron-rich food. Furthermore, accumulation of transferred $CD4^+$ T cells in the colon of *Rag1*$^{-/-}$ mice and the production of IFN-γ and IL-17 by these cells as well as the frequency of $Foxp3^+$ Tregs were unaltered by the iron content of the diet given to recipient mice. These results indicate that in this model which is driven by a microbiota-dependent proinflammatory $CD4^+$ T cell response the reduction of dietary iron in the recipient mice did not affect the proinflammatory responses of the transferred T cells. Thus, our results do not provide evidence for a protective effect of dietary iron reduction in this standard mouse model of colitis. It remains to be investigated if such an intervention could be beneficial in a subgroup of ulcerative colitis patients which may be particularly sensitive to luminal iron [45].

Supporting information

S1 File.
(PDF)

Acknowledgments

This work is part of the thesis of Anamarija Markota. We would like to thank Andrea Musumeci for assistance with experiments.

Author Contributions

Conceptualization: Wolfgang Reindl, Dirk Haller, Anne B. Krug.

Funding acquisition: Anne B. Krug.

Investigation: Anamarija Markota, Rebecca Metzger, Alexander F. Heiseke, Lisa Jandl, Ezgi Dursun, Katharina Eisena¨cher.

Project administration: Anne B. Krug.

Supervision: Katharina Eisena¨cher, Wolfgang Reindl, Dirk Haller, Anne B. Krug.

Writing – original draft: Anamarija Markota, Anne B. Krug.

Writing – review &editing: Anne B. Krug.

References

1. Garrett WS, Gordon JI, Glimcher LH. Homeostasis and inflammation in the intestine. Cell. 2010; 140 (6):859–70. Epub 2010/03/23. S0092-8674(10)00024-3 [pii] https://doi.org/10.1016/j.cell.2010.01.023 PMID: 20303876,
2. Rapozo DC, Bernardazzi C, de Souza HS. Diet and microbiota in inflammatory bowel disease: The gut in disharmony. World J Gastroenterol. 2017; 23(12):2124–40. https://doi.org/10.3748/wjg.v23.i12.2124 PMID: 28405140; PubMed Central PMCID: PMC5374124.
3. Fonseca-Nunes A, Jakszyn P, Agudo A. Iron and cancer risk—a systematic review and meta-analysis of the epidemiological evidence. Cancer Epidemiol Biomarkers Prev. 2014; 23(1):12–31. https://doi.org/10.1158/1055-9965.EPI-13-0733 PMID: 24243555,
4. Hou JK, Abraham B, El-Serag H. Dietary intake and risk of developing inflammatory bowel disease: a systematic review of the literature. Am J Gastroenterol. 2011; 106(4):563–73. https://doi.org/10.1038/ajg.2011.44 PMID: 21468064,
5. Erichsen K, Hausken T, Ulvik RJ, Svardal A, Berstad A, Berge RK. Ferrous fumarate deteriorated plasma antioxidant status in patients with Crohn disease. Scand J Gastroenterol. 2003; 38(5):543–8. PMID: 12795468,
6. Lee T, Clavel T, Smirnov K, Schmidt A, Lagkouvardos I, Walker A, et al. Oral versus intravenous iron replacement therapy distinctly alters the gut microbiota and metabolome in patients with IBD. Gut. 2017; 66(5):863–71. https://doi.org/10.1136/gutjnl-2015-309940 PMID: 26848182; PubMed Central PMCID: PMC5531225.
7. Barollo M, D'Inca R, Scarpa M, Medici V, Cardin R, Bortolami M, et al. Effects of iron manipulation on trace elements level in a model of colitis in rats. World J Gastroenterol. 2005; 11(28):4396–9. https://doi.org/10.3748/wjg.v11.i28.4396 PMID: 16038040; PubMed Central PMCID: PMC4434668.
8. Carrier JC, Aghdassi E, Jeejeebhoy K, Allard JP. Exacerbation of dextran sulfate sodium-induced colitis by dietary iron supplementation: role of NF-kappaB. Int J Colorectal Dis. 2006; 21(4):381–7. https://doi.org/10.1007/s00384-005-0011-7 PMID: 16133010,
9. Chua AC, Klopcic BR, Ho DS, Fu SK, Forrest CH, Croft KD, et al. Dietary iron enhances colonic inflam- mation and IL-6/IL-11-Stat3 signaling promoting colonic tumor development in mice. PLoS One. 2013; 8(11):e78850. https://doi.org/10.1371/journal.pone.0078850 PMID: 24223168; PubMed Central PMCID: PMC3819375.
10. Constante M, Fragoso G, Lupien-Meilleur J, Calve A, Santos MM. Iron Supplements Modulate Colon Microbiota Composition and Potentiate the Protective Effects of Probiotics in Dextran Sodium Sulfate-induced Colitis. Inflamm Bowel Dis. 2017; 23(5):753–66. https://doi.org/10.1097/MIB.0000000000001089 PMID: 28368910,
11. Oldenburg B, van Berge Henegouwen GP, Rennick D, Van Asbeck BS, Koningsberger JC. Iron supplementation affects the production of pro-inflammatory cytokines in IL-10 deficient mice. Eur J Clin Invest. 2000; 30(6):505–10. PMID: 10849019,
12. Seril DN, Liao J, Ho KL, Warsi A, Yang CS, Yang GY. Dietary iron supplementation enhances DSS-induced colitis and associated colorectal carcinoma development in mice. Dig Dis Sci. 2002; 47 (6):1266–78. PMID: 12064801,
13. Ijssennagger N, Rijnierse A, de Wit NJ, Boekschoten MV, Dekker J, Schonewille A, et al. Dietary heme induces acute oxidative stress, but delayed cytotoxicity and compensatory hyperproliferation in mouse colon. Carcinogenesis. 2013; 34(7):1628–35. https://doi.org/10.1093/carcin/bgt084 PMID: 23455377,
14. Kayama H, Kohyama M, Okuzaki D, Motooka D, Barman S, Okumura R, et al. Heme ameliorates dextran sodium sulfate-induced colitis through providing intestinal macrophages with noninflammatory profiles. Proc Natl Acad Sci U S A. 2018; 115(33):8418–23. Epub 2018/08/01. https://doi.org/10.1073/pnas.1808426115 PMID: 30061415; PubMed Central PMCID: PMC6099887.

15. Werner T, Wagner SJ, Martinez I, Walter J, Chang JS, Clavel T, et al. Depletion of luminal iron alters the gut microbiota and prevents Crohn's disease-like ileitis. Gut. 2011; 60(3):325–33. https://doi.org/10.1136/gut.2010.216929 PMID: 21076126.
16. Carrier J, Aghdassi E, Platt I, Cullen J, Allard JP. Effect of oral iron supplementation on oxidative stress and colonic inflammation in rats with induced colitis. Aliment Pharmacol Ther. 2001; 15(12):1989–99. PMID: 11736731.
17. Joeris T, Muller-Luda K, Agace WW, Mowat AM. Diversity and functions of intestinal mononuclear phagocytes. Mucosal Immunol. 2017; 10(4):845–64. https://doi.org/10.1038/mi.2017.22 PMID: 28378807.
18. Niess JH, Brand S, Gu X, Landsman L, Jung S, McCormick BA, et al. CX3CR1-mediated dendritic cell access to the intestinal lumen and bacterial clearance. Science. 2005; 307(5707):254–8. https://doi.org/10.1126/science.1102901 PMID: 15653504.
19. Rescigno M, Urbano M, Valzasina B, Francolini M, Rotta G, Bonasio R, et al. Dendritic cells express tight junction proteins and penetrate gut epithelial monolayers to sample bacteria. Nat Immunol. 2001; 2(4):361–7. https://doi.org/10.1038/86373 PMID: 11276208.
20. Cairo G, Recalcati S, Mantovani A, Locati M. Iron trafficking and metabolism in macrophages: contribution to the polarized phenotype. Trends Immunol. 2011; 32(6):241–7. https://doi.org/10.1016/j.it.2011.03.007 PMID: 21514223.
21. Sindrilaru A, Peters T, Wieschalka S, Baican C, Baican A, Peter H, et al. An unrestrained proinflammatory M1 macrophage population induced by iron impairs wound healing in humans and mice. J Clin Invest. 2011; 121(3):985–97. https://doi.org/10.1172/JCI44490 PMID: 21317534; PubMed Central PMCID: PMC3049372.
22. Nairz M, Schroll A, Demetz E, Tancevski I, Theurl I, Weiss G. 'Ride on the ferrous wheel'—the cycle of iron in macrophages in health and disease. Immunobiology. 2015; 220(2):280–94. https://doi.org/10.1016/j.imbio.2014.09.010 PMID: 25240631.
23. Shouval DS, Biswas A, Goettel JA, McCann K, Conaway E, Redhu NS, et al. Interleukin-10 receptor signaling in innate immune cells regulates mucosal immune tolerance and anti-inflammatory macrophage function. Immunity. 2014; 40(5):706–19. https://doi.org/10.1016/j.immuni.2014.03.011 PMID: 24792912; PubMed Central PMCID: PMC4513358.
24. Zigmond E, Bernshtein B, Friedlander G, Walker CR, Yona S, Kim KW, et al. Macrophage-restricted interleukin-10 receptor deficiency, but not IL-10 deficiency, causes severe spontaneous colitis. Immunity. 2014; 40(5):720–33. https://doi.org/10.1016/j.immuni.2014.03.012 PMID: 24792913.
25. Bain CC, Bravo-Blas A, Scott CL, Perdiguero EG, Geissmann F, Henri S, et al. Constant replenishment from circulating monocytes maintains the macrophage pool in the intestine of adult mice. Nat Immunol. 2014; 15(10):929–37. https://doi.org/10.1038/ni.2967 PMID: 25151491; PubMed Central PMCID: PMC4169290.
26. Tamoutounour S, Henri S, Lelouard H, de Bovis B, de Haar C, van der Woude CJ, et al. CD64 distinguishes macrophages from dendritic cells in the gut and reveals the Th1-inducing role of mesenteric lymph node macrophages during colitis. Eur J Immunol. 2012; 42(12):3150–66. https://doi.org/10.1002/eji.201242847 PMID: 22936024.
27. Zigmond E, Varol C, Farache J, Elmaliah E, Satpathy AT, Friedlander G, et al. Ly6C hi monocytes in the inflamed colon give rise to proinflammatory effector cells and migratory antigen-presenting cells. Immunity. 2012; 37(6):1076–90. https://doi.org/10.1016/j.immuni.2012.08.026 PMID: 23219392.
28. Mazzini E, Massimiliano L, Penna G, Rescigno M. Oral tolerance can be established via gap junction transfer of fed antigens from CX3CR1(+) macrophages to CD103(+) dendritic cells. Immunity. 2014; 40(2):248–61. Epub 2014/01/28. https://doi.org/10.1016/j.immuni.2013.12.012 PMID: 24462723.
29. Annacker O, Coombes JL, Malmstrom V, Uhlig HH, Bourne T, Johansson-Lindbom B, et al. Essential role for CD103 in the T cell-mediated regulation of experimental colitis. J Exp Med. 2005; 202(8):1051–61. https://doi.org/10.1084/jem.20040662 PMID: 16216886; PubMed Central PMCID: PMC2213206.
30. Wenzel UA, Jonstrand C, Hansson GC, Wick MJ. CD103+ CD11b+ Dendritic Cells Induce Th17 T Cells in Muc2-Deficient Mice with Extensively Spread Colitis. PLoS One. 2015; 10(6):e0130750. https://doi.org/10.1371/journal.pone.0130750 PMID: 26121642; PubMed Central PMCID: PMC4487685.
31. Laffont S, Siddiqui KR, Powrie F. Intestinal inflammation abrogates the tolerogenic properties of MLN CD103+ dendritic cells. Eur J Immunol. 2010; 40(7):1877–83. https://doi.org/10.1002/eji.200939957 PMID: 20432234.
32. Magnusson MK, Brynjolfsson SF, Dige A, Uronen-Hansson H, Borjesson LG, Bengtsson JL, et al. Macrophage and dendritic cell subsets in IBD: ALDH+ cells are reduced in colon tissue of patients with ulcerative colitis regardless of inflammation. Mucosal Immunol. 2016; 9(1):171–82. https://doi.org/10.1038/mi.2015.48 PMID: 26080709; PubMed Central PMCID: PMC4683124.
33. Heiseke AF, Faul AC, Lehr HA, Forster I, Schmid RM, Krug AB, et al. CCL17 promotes intestinal inflammation in mice and counteracts regulatory T cell-mediated protection from colitis. Gastroenterology.

2012; 142(2):335–45. Epub 2011/11/08. S0016-5085(11)01501-0 [pii] https://doi.org/10.1053/j.gastro.2011.10.027 PMID: 22057112.

34. Siegmund B, Rieder F, Albrich S, Wolf K, Bidlingmaier C, Firestein GS, et al. Adenosine kinase inhibitor GP515 improves experimental colitis in mice. J Pharmacol Exp Ther. 2001; 296(1):99–105. PMID: 11123368.

35. Raabe BM, Artwohl JE, Purcell JE, Lovaglio J, Fortman JD. Effects of weekly blood collection in C57BL/6 mice. J Am Assoc Lab Anim Sci. 2011; 50(5):680–5. PMID: 22330715; PubMed Central PMCID: PMC3189672.

36. Kurmaeva E, Lord JD, Zhang S, Bao JR, Kevil CG, Grisham MB, et al. T cell-associated alpha4beta7 but not alpha4beta1 integrin is required for the induction and perpetuation of chronic colitis. Mucosal Immunol. 2014; 7(6):1354–65. https://doi.org/10.1038/mi.2014.22 PMID: 24717354; PubMed Central PMCID: PMC4417258.

37. McRae BL, Levin AD, Wildenberg ME, Koelink PJ, Bousquet P, Mikaelian I, et al. Fc Receptor-mediated Effector Function Contributes to the Therapeutic Response of Anti-TNF Monoclonal Antibodies in a Mouse Model of Inflammatory Bowel Disease. J Crohns Colitis. 2016; 10(1):69–76. https://doi.org/10.1093/ecco-jcc/jjv179 PMID: 26429698.

38. Schultz M, Strauch UG, Linde HJ, Watzl S, Obermeier F, Gottl C, et al. Preventive effects of Escherichia coli strain Nissle 1917 on acute and chronic intestinal inflammation in two different murine models of colitis. Clin Diagn Lab Immunol. 2004; 11(2):372–8. Epub 2004/03/12. https://doi.org/10.1128/CDLI.11.2.372-378.2004 PMID: 15013990; PubMed Central PMCID: PMC371200.

39. Seril DN, Liao J, Yang CS, Yang GY. Systemic iron supplementation replenishes iron stores without enhancing colon carcinogenesis in murine models of ulcerative colitis: comparison with iron-enriched diet. Dig Dis Sci. 2005; 50(4):696–707. PMID: 15844705.

40. Bogaert S, De Vos M, Olievier K, Peeters H, Elewaut D, Lambrecht B, et al. Involvement of endoplasmic reticulum stress in inflammatory bowel disease: a different implication for colonic and ileal disease? PLoS One. 2011; 6(10):e25589. https://doi.org/10.1371/journal.pone.0025589 PMID: 22028783; PubMed Central PMCID: PMC3196494.

41. Kontoyiannis D, Pasparakis M, Pizarro TT, Cominelli F, Kollias G. Impaired on/off regulation of TNF biosynthesis in mice lacking TNF AU-rich elements: implications for joint and gut-associated immunopathologies. Immunity. 1999; 10(3):387–98. PMID: 10204494.

42. Roulis M, Bongers G, Armaka M, Salviano T, He Z, Singh A, et al. Host and microbiota interactions are critical for development of murine Crohn's-like ileitis. Mucosal Immunol. 2016; 9(3):787–97. https://doi.org/10.1038/mi.2015.102 PMID: 26487367; PubMed Central PMCID: PMC5027991.

43. Kontoyiannis D, Boulougouris G, Manoloukos M, Armaka M, Apostolaki M, Pizarro T, et al. Genetic dissection of the cellular pathways and signaling mechanisms in modeled tumor necrosis factor-induced Crohn's-like inflammatory bowel disease. J Exp Med. 2002; 196(12):1563–74. https://doi.org/10.1084/jem.20020281 PMID: 12486099; PubMed Central PMCID: PMC2196068.

44. Wang Z, Yin W, Zhu L, Li J, Yao Y, Chen F, et al. Iron Drives T Helper Cell Pathogenicity by Promoting RNA-Binding Protein PCBP1-Mediated Proinflammatory Cytokine Production. Immunity. 2018; 49 (1):80–92.e7. Epub 2018/07/01. https://doi.org/10.1016/j.immuni.2018.05.008 PMID: 29958803.

45. Khalili H, de Silva PS, Ananthakrishnan AN, Lochhead P, Joshi A, Garber JJ, et al. Dietary Iron and Heme Iron Consumption, Genetic Susceptibility, and Risk of Crohn's Disease and Ulcerative Colitis. Inflamm Bowel Dis. 2017; 23(7):1088–95. https://doi.org/10.1097/MIB.0000000000001161 PMID: 28604414; PubMed Central PMCID: PMC5549140.

46. Sesink AL, Termont DS, Kleibeuker JH, Van der Meer R. Red meat and colon cancer: dietary haem-induced colonic cytotoxicity and epithelial hyperproliferation are inhibited by calcium. Carcinogenesis. 2001; 22(10):1653–9. Epub 2001/09/29. https://doi.org/10.1093/carcin/22.10.1653 PMID: 11577005.

47. Schepens MA, Vink C, Schonewille AJ, Dijkstra G, van der Meer R, Bovee-Oudenhoven IM. Dietary heme adversely affects experimental colitis in rats, despite heat-shock protein induction. Nutrition (Burbank, Los Angeles County, Calif). 2011; 27(5):590–7. Epub 2010/08/14. https://doi.org/10.1016/j.nut.2010.05.002 PMID: 20705428.

48. van der Logt EM, Blokzijl T, van der Meer R, Faber KN, Dijkstra G. Westernized high-fat diet accelerates weight loss in dextran sulfate sodium-induced colitis in mice, which is further aggravated by supplementation of heme. The Journal of nutritional biochemistry. 2013; 24(6):1159–65. Epub 2012/12/19. https://doi.org/10.1016/j.jnutbio.2012.09.001 PMID: 23246033.

49. Constante M, Fragoso G, Calve A, Samba-Mondonga M, Santos MM. Dietary Heme Induces Gut Dysbiosis, Aggravates Colitis, and Potentiates the Development of Adenomas in Mice. Frontiers in microbiology. 2017; 8:1809. Epub 2017/10/07. https://doi.org/10.3389/fmicb.2017.01809 PMID: 28983289; PubMed Central PMCID: PMC5613120.

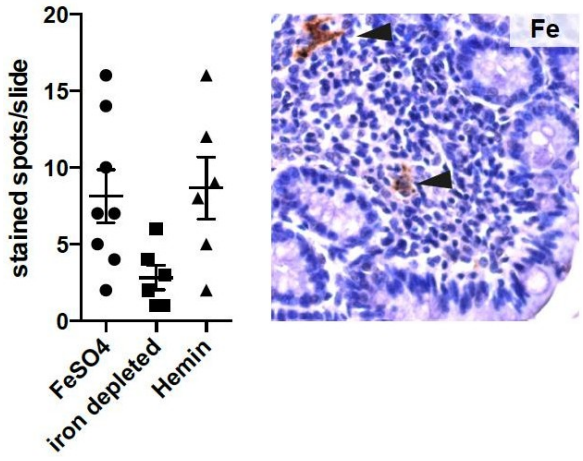

Figure A Detection of iron in colon tissue sections
Left panel: Iron was detected in colon tissue FFPE sections obtained from mice after T cell transfer colitis by DAB-enhanced Prussian blue staining. The number of stained spots per slide was counted. Mean values and SD are shown (pooled results of 2 experiments, n = 8 for FeSo4, n=6 for iron-free and hemin). * p< 0.025 (unpaired t-test for FeSO4 vs iron-free and hemin vs iron-free with Bonferroni adjusted significance level). Right panel: Exemplary result of iron staining in colon tissue section, counterstained with hematoxylin. Scale bar: 50 µm.

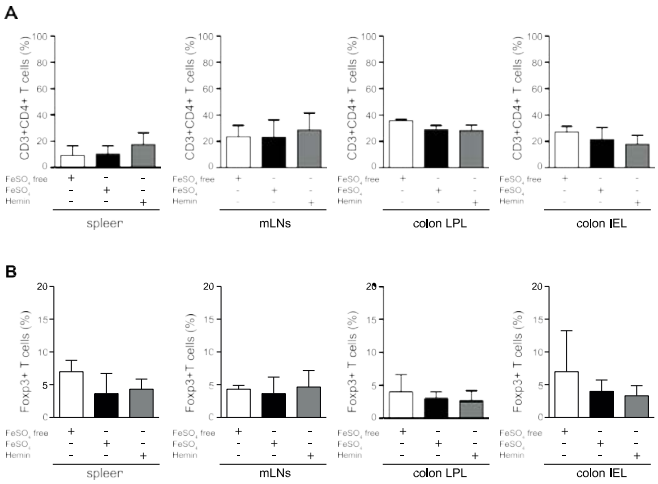

Figure B Frequency of Tregs and proinflammatory Th1/Th17 effector cells during T cell mediated colitis

Rag1$^{-/-}$ mice were treated with iron depleted (w/o Fe) or iron supplemented experimental diets ($FeSO_4$ or Hemin) for 9 weeks and colitis was induced by T cell transfer. Cells were isolated from spleen, MLNs, colon LPLs and colon IELs on day 17 after T cell transfer and analyzed by flow cytometry. The percentages of CD4+ T cells (A) and the percentages of Foxp3$^+$ Tregs within CD4+ T cells (B) were determined (mean values ± SD, n= 3 mice per group, one way ANOVA, n.s.).

Table A*

Diet		WBC (10^9/l)	RBC (10^{12}/l)	Hb (g/l)	HCT (%)	MCV (fl)*	MCH (pg)
$FeSO_4$ -free	Before colitis	2.6 ± 1.4	7.6 ± 3.0	14.9 ± 3.9	43.6 ± 9.1	53.3 ± 1.1	14.4 ± 2.5
	During colitis	11.7 ± 3.0	10.9 ± 1.3	19.4 ± 2.6	64.7 ± 11.1	43.87 ± 2.1	14.3 ± 1.7
$FeSO_4$	Before colitis	2.3 ± 1.8	7.2 ± 4.1	16.4 ± 3.6	40.9 ± 7.6	50.7 ± 2.0	14.8 ± 1.3
	During colitis	10.1 ± 2.9	12.8 ± 2.9	22.2 ± 2.5	69.5 ± 10.6	47.9 ± 1.6	14.8 ± 0.9
Hemin	Before colitis	4.3 ± 3.2	6.7 ± 2.9	15.8 ± 3.4	44.6 ± 8.1	52.5 ± 1.6	13.9 ± 2.2
	During colitis	9.6 ± 3.8	9.9 ± 1.1	21.5 ± 2.9	61.1 ± 6.3	44.6 ± 2.4	15.4 ± 1.2

***Hematological parameters before and after colitis induction**

Rag1$^{-/-}$ mice were treated with three different experimental diets (iron depleted (w/o Fe) or iron supplemented ($FeSO_4$ or Hemin) diet) for 9 weeks, colitis was induced by T cell transfer. Blood samples were analysed after 9 weeks of diet before T cell transfer and on day 17 after T cell transfer. White blood cell count (WBC); red blood cell count (RBC), hemoglobin (Hb), hematocrit (HCT), mean corpuscular volume (MCV) and mean corpuscular hemoglobin (MCH) were analysed. Mean and SD are shown (n=7 for $FeSO_4$; n=6 for w/o Fe; n=6 for Hemin). One-way analysis of variance (ANOVA) was performed to compare differences between dietary groups. * indicates $p < 0.05$. Only MCV was significantly different between the dietary groups both before and during colitis.

Table B*

Diet		$CD103^+CD11b^-$ of DCs (%)	$CD103^+CD11b^+$ of DCs (%)	$CD103^-CD11b^+$ of DCs (%)
$FeSO_4$-free	Steady state	38.8 ± 5.1	11.2 ± 3.8	16.6 ± 5.0
	Colitis	32.0 ± 3.2	20.3 ± 4.3*	31.0 ± 4.1*
$FeSO_4$	Steady state	42.2 ± 9.0	4.8 ± 3.1	19.2 ± 7.8
	Colitis	25.1 ± 5.6*	20.1 ± 4.1*	36.9 ± 9.3*
Hemin	Steady state	33.3 ± 9.0	8.5 ± 2.4	33.3 ± 6.2#
	Colitis	22.3 ± 6.3	22.5 ± 11.0*	34.6 ± 6.6

***Frequency of DC subpopulations in colon LPL in steady state vs. colitis**
Cells were isolated from colon LPL and DC subpopulation frequency analyzed by flow cytometry after dietary treatment (steady state) or on day 17 after T cell transfer into Rag1-/- mice treated with the indicated diets (colitis). The percentages of indicated DC subpopulation within the DC gate are shown (mean ± SD). * indicate significant differences between colitis and steady state (unpaired t test, $p < 0.05$, n = 4-6 mice per group). # indicates that mice receiving hemin-supplemented diet had a significantly higher percentage of CD103- CD11b+ cDCs in the steady state compared to the two other diet groups (2-way ANOVA, Tukey's multiple comparison test, $p < 0.05$).

Supplementary Materials and Methods

Hematological analysis

Blood samples were collected from either facial vein or postmortem by cardiac puncture, depending on the time point of the sampling in the feeding experiments. For facial blood collection, mice were pinched behind the jawbone using a 5 mm lancet and blood was collected into EDTA containing collection tubes. Cardiac puncture was performed for terminal blood collection. Mice were sacrificed by CO_2 asphyxia. The blood was drawn from the heart using a 0.5 ml insulin syringe and transferred into EDTA containing collecting tubes. Blood samples were diluted in phosphate-buffered saline (1:3). White blood cell count (WBC), haemoglobin (Hb), haematocrit (HCT), mean corpuscular volume (MCV) and mean corpuscular haemoglobin (MCH) were measured by the Clinical Chemistry department using Sysmex XT- 2000i-1 Hematology Analyzer (Sysmex Europe GmbH, Norderstadt, Germany).

Iron staining in tissue sections

Ferric iron staining in colon tissue FFPE sections was performed according to Meguro et al. (1) using the Iron Stain Kit (Sigma Aldrich) for Prussian Blue staining and the DAB-Substrate Kit (Vector Laboratories, Burlingame, CA, USA) for enhancement. Counterstaining was performed with Hematoxylin (Merck Millipore, Burlington, MA, USA).

Reference

1. Meguro R, Asano Y, Odagiri S, Li C, Iwatsuki H, Shoumura K. Nonheme-iron histochemistry for light and electron microscopy: a historical, theoretical and technical review. Archives of histology and cytology. 2007;70(1):1-19.

Unpublished manuscript – CCL17 promotes colitis associated tumorigenesis dependent on the microbiota

Abstract

Colorectal cancer is one of the most common cancers and a major cause of mortality. Pro-inflammatory and anti-tumor immune responses play a critical role in colitis associated colon cancer. CCL17, a chemokine of the C-C family which is a ligand for CCR4, is expressed by intestinal dendritic cells in the steady state and is upregulated during colitis in mouse models and in inflammatory bowel disease patients. Using CCL17eGFP-knock in mice we could show that during colitis CCL17 was also expressed by macrophages and intermediary monocytes in addition to dendritic cells. We characterized the tumor infiltrating monocyte and macrophage populations of colitis induced tumors by global gene expression analysis revealing that the Ly6C^{lo} MHCII^{hi} myeloid cells which showed the highest level of CCL17 expression also showed a higher expression of genes enriched in cytokine activity, endocytosis and positive regulation of the inflammatory response compared to the Ly6C^{hi} monocytes subset and the Ly6C^{lo} MHCII^{lo} macrophages. We found indeed a significantly lower tumor number in CCL17-deficient mice compared to control mice after AOM DSS treatment, indicating a functional relevance of CCL17 in colitis-associated tumorigenesis. As this effect was microbiota-dependent we analyzed the microbiota of CCL17-deficient mice housed separately or together with CCL17-competent mice and found marked changes in microbiota diversity and composition. Elevated cecal IgA concentration and a higher portion of IgA-coated fecal bacteria in CCL17-deficient mice were observed together with the observed microbiota changes. While we did not find significantly reduced inflammation we observed an increased ratio of pro- vs anti-apoptotic gene expression in the colon of separately housed CCL17-deficient compared CCL17-competent control mice during the early phase of tumor initiation. In addition, alterations in the gene expression signatures of the tumor infiltrating myeloid cells were observed in CCL17-deficient mice. Taken together our results indicate a role of CCL17 in colitis associated

tumorigenesis by influencing the composition of the intestinal microbiome, the apoptosis levels in the early tumor development and myeloid cell functionality.

Introduction

Colorectal cancer (CRC) is the third most frequent malignancy worldwide with increasing incidence and has led to almost 860.000 deaths in 2018 [1]. The pathophysiology of CRC is multifactorial with genetic, environmental and life style factors playing major roles [2]. There is clear evidence that inflammation is closely linked to colorectal tumorigenesis [3]. Inflammatory bowel disease (IBD) patients have a 5-to 8-fold increased risk to develop CRC [4]. Inflammatory mechanisms play a pro-tumorigenic role also for sporadic CRC which develops in the absence of intestinal inflammatory disease [5, 6]. An important driver for inflammation is the gut microbiome consisting of more than 100 trillion aerobic and anaerobic bacteria [7], of which several have been linked to increased tumorigenesis [8], while others have been shown to produce protective metabolites [9]. In the inflammatory tumor microenvironment immune cells can have both pro- and anti-tumoral effects [10]. Of the T helper cell subsets (Th1, Th2, Th17, Treg) Th1 cells are considered to be the main drivers of anti-tumor immunity [11]. But also tumor-infiltrating myeloid cells, such as macrophages and neutrophils, can be skewed towards a pro- or anti-tumor activity by the tumor microenvironment [12]. Therapy for unresectable CRC includes chemo- and radiotherapy, targeted therapy and immunotherapy with limited efficacy [13, 14]. Therefore, new therapeutic strategies which promote anti-tumor immunity without causing tumor-promoting inflammation are needed for the treatment of advanced CRC. Promising targets for therapeutic intervention are factors of the tumor microenvironment including cytokines, growth factors, hypoxia by angiogenesis-blockade [15], as well as chemokines. Besides their role for migration and homing of immune cells [16] chemokines can influence immune and cancer cell functionality. For example, it was shown that blocking CCR5 and CCL2 induced anti-tumor activity in macrophages [17, 18]. Non-chemotactic functions, which promoted tumor progression were also described for CCL5, which increased S100A4 dependent tumor cell dissemination and metastatic burden and for CXCL1, which promoted breast cancer metastasis by activating NFκB signaling [19, 20]. The

C-C chemokine CCL17 binds to CCR4 and induces chemotaxis of CCR4-expressing NK cells and $CD4^+$ T cells including regulatory T cells (Treg) and effector Th2 and Th17 cells [21-23]. The chemotactic activity of CCL17 is partially redundant with that of CCL22 which also binds to CCR4 [24, 25]. However, CCL17 specifically promotes migration and activation of murine DCs [26-28] and was found to play an important proinflammatory role in models of organ-specific inflammation, such as atopic dermatitis, neuroinflammation, atherosclerosis, arthritis and colitis [26-30]. Its role for tumorigenesis especially in the inflamed colon remained to be investigated. CCL17 was shown to be expressed by non-granulocytic $CD11b^+$ myeloid cells, such as $CD11b^+$ dendritic cells (DC) and macrophages [31-33], which make up a major proportion of the immune cells in the colonic tumor microenvironment [34].

The myeloid immune compartment in the colon consists of granulocytic cells and mononuclear phagocytes (MNPs). Besides sensing pathogens, MNPs interact with ILC and T- and B lymphocytes, while granulocytic cells, predominantly neutrophils, directly destroy pathogens by degranulation or uptake and subsequent degradation [35, 36]. DCs are subdivided in conventional and plasmacytoid DCs. Conventional DCs (cDCs) are far more abundant in the colon [37, 38] while pDCs which are rare in the intestine have a highly specialized role in the anti-viral defense [39]. The cDC population consists of two main subsets with functional specializations [37]. The cDC1 subset has been shown to possess superior cross-presentation capacities [40], while the cDC2 subset was found to be critical for the defense against bacterial and fungal infections [41]. The cDC2 subpopulation is characterized by CD11b and SIRPα expression, while cDC1 express CD103 and XCR1 [37]. Further, there is a cDC2 subset which is marked by co-expression of CD103 and CD11b and plays a critical role in the induction of Th17 and ILC3 responses [41, 42]. Besides DCs, MNPs of the monocyte-macrophage lineage are abundant in colonic mucosa. Unlike in other tissues, intestinal macrophages are derived from circulating monocytes, which constantly enter the lamina propria of the intestine and differentiate into macrophages [43]. Infiltrating monocytes lose their Ly6C expression and upregulate MHCII expression during the 5-7 day long differentiation process with $Ly6C^+$ $MHCII^+$ representing intermediary or intermediary monocytes with high cytokine production capacities

[44]. Intestinal macrophages are predominantly characterized by a high MHCII expression and need to be distinguished from cDC2 by CD64 or F4/80 expression. Besides exerting similar functions as cDC2 such as Th17 and ILC3 induction [45], intestinal macrophages can promote tissue repair and are able to sample luminal antigens, which they transfer to cDCs [45, 46].

Intestinal DCs and macrophages can influence tumor incidence and progression by several means: DCs take up and present tumor antigens to T cells to induce adaptive anti-tumor immunity; DCs and macrophages release cytokines and other factors with direct and indirect effects on tumor development and progression and intestinal DCs and macrophages influence the composition of the microbiota e.g. by regulating intestinal IgA production [47-49]. Thus, myeloid cell derived CCL17 appeared to be a promising molecule in potentially regulating the inflammatory tumor microenvironment of colitis associated colon tumors and we analyzed its role in AOM DSS induced tumorigenesis, which closely resembles CAC [50].

In the current study we have found a strong upregulation of CCL17 expression in AOM DSS induced colon tumor tissue and identified intratumoral DCs and macrophages as main CCL17 producing cell types. We provide evidence for a microbiota-dependent tumor-promoting role of CCL17 in this model.

Materials and methods

Animals and In Vivo Procedures

CCL17-eGFP mice on the C57BL/6J background (at east 10 generations backcrossed) were obtained from the laboratory of Irmgard Förster {Alferink , 2003 #245}, bred in-house and rederived into C57BL/JRccHsd mice, purchased from Envigo (Huntingdon, UK). All mice were housed under specific pathogen-free conditions. Health monitoring was performed according to the recommendations of the Federation of European Laboratory Animal Science Association (FELASA). All experimental procedures involving mice were performed in accordance with the regulations of and were approved by the local government (Regierung von Oberbayern, license numbers: ROB-55.2-2532.Vet_02-13-36 and ROB-55.2-2532.Vet_02-17-22).

For AOM DSS treatments, mice were injected with 10 mg/kg Azoxymethane (AOM, Sigma-Aldrich, St. Louis, USA, #A5486) i.p. and after five days were treated with three cycles of Dextran sodium sulphate (DSS, MP-Biomedical, Santa Ana, USA, #02 160110 80) (2.5 % w/w) for 5 days each with 2 weeks in between the cycles. The mice were sacrificed on day 85 of the experiment or at an earlier time point when they met the euthanization critera. On the day of the analysis the colon was cut longitudinally, washed with ice-cold PBS and the tumor numbers and sizes were recorded. Tumors of similar sizes were excised and used for flow cytometric analyses, histology and gene expression analysis respectively.

For short term AOM DSS experiments mice were injected 10 mg/kg AOM i.p. and after five days were treated with DSS (2.5 % w/w) for 5 days. Four days after completion of the DSS treatment the mice were sacrificed and analyzed as described.

Cell Preparation and Flow Cytometry

After excision of the tumors remaining normal intestinal tissue was cut into 5 mm long pieces and incubated with 2 mM DTT (Sigma-Aldrich, #D0632), 10 mM HEPES, 10 mM EDTA in HBSS (without Ca^{2+}/Mg^{2+}) for 10 minutes at 37 °C and 125 rpm. Subsequently, tumor and normal tissue was digested with DNAse (0.5 µg/ml, Sigma-Aldrich, #10104159001), Collagenase D (2.5 µg/ml, Sigma-Aldrich, #11088858001), Collagenase V (5 µg/ml, Sigma-Aldrich, #C9263) and Collagenase IV (157 Wuensch Units/ml, Worthington, Columbus, USA #LS004188) in RPMI-1640 for 30 minutes at 37°C with gentle shaking and pushed through a 100 µm and a 40 µm filter, which were washed with ice-cold HBSS containing Mg^{2+} and Ca^{2+} (HBSS+). The obtained single cell suspensions were incubated for 10 min on ice with anti-CD16/anti-CD32 containing cell culture supernatant and surface-stained with the respective antibodies [Supplementary Table 1] for 20 minutes on ice protected from light. For intracellular cytokine staining the cells were restimulated with 20 ng/ml PMA and 1 ug/ml ionomycin for 5 hours in the presence of Golgi Plug (0.2 % v/v) and Golgi Stop (0.14 % v/v) (BD Biosciences, Franklin Lakes, USA, #555029, #554724). For intracellular staining the cells were fixed and

permeabilized using the Foxp3 fixation/permeabilization kit (Thermo-Fischer, Waltham, USA, #00-5521-00) after surface antibody staining. Cells were analyzed on a Cytoflex (Beckman Coulter, Brea, USA) or Fortessa (Beckton Dickinson, Franklin Lakes) flow cytometer or sorted using an Aria Fusion (Beckton Dickinson). Data analysis was conducted with FlowJo v. 10 (Beckton Dickinson).

Histology, Immunohistochemistry, and Microscopy

Selected tumors of similar sizes were fixed in 4% PFA for 1 hour at 4°C and subsequently incubated in 20% sucrose o/n at 4°C. Tumors were then embedded in OCT (Leica, Wetzlar, Germany) and stored in -80°C. For H&E staining cryosections (5–8 µm) were incubated in Hematoxylin solution (Merck, Darmstadt, Germany), washed in H2O and subsequently stained in Eosin solution (J.T. Baker, Philipsburg, USA), washed in H2O, dehydrated and mounted with Roti® Histokitt (Carl Roth, Karlsruhe, Germany). For immunofluorescent staining cyrosections (5-8 µm) were blocked with phosphate buffered saline (PBS) containing 5% goat serum (Vector Labs, #S-1000) and 0.5% Triton-X-100 for 1h at RT and then stained with primary antibodies (anti-GFP, Abcam, Cambridge, UK, #6556; anti-Ki67, Cell Signaling Technologies, Danvers, USA, #12202; anti-mouse E-Cadherin BD Biosciences, #610181; anti-mouse CD3, Thermo-Fischer, #14-0031-82; anti-mouse CD11c, BD Biosciences, #550283) at 4°C o/n, protected from light. Secondary antibodies were used and incubated for 1h at RT (anti-mouse IgG-AF555, Thermo-Fischer, #A32727; anti-rabbit IgG AF488, Thermo-Fischer, #A11008; anti-hamster IgG DyeLight647, Biolegend, San Diego, USA #405505). For staining nuclei DAPI (Sigma-Aldrich, #D9542) was used. Imaging was conducted with a Leica SP8X WLL upright confocal microscope or a Olympus BX41 fluorescence microscope. Quantification of $Ki67^+$ cells was performed using ImageJ . The number of total cells ($DAPI^+$) and the number of $Ki67^+$ cells ($AF488^+$) were determined and the frequency of $Ki67^+$ cells was calculated.

Microbiota analysis

Microbiota analysis was performed as described in [51] with feces instead of rectal swabs as sample material.

Data analysis was conducted with QIIME v 1.9 [52]. Open-reference OTU clustering and taxonomy assignment of sequences were done with UCLUST [53] against the Silva database Release 119 [54] at the 97% similarity level. Alpha diversity and beta diversity metrics were finally calculated, after rarefying over 2,000 sequences per sample. Linear discriminant analysis (LDA) coupled with effect size measurement (Lefse analysis) was conducted (non-parametric Wilcoxon sum-rank test followed by LDA analysis) [55]. Bray Curtis distance matrices were calculated with QIMME for principal component analysis and statistical testing was done with Adonis (permutational multivariate analysis of variance using the Bray-Curtis distance matrices).

Gene expression analysis

qPCR

RNA was isolated from snap-frozen tissue using Trizol (Thermo-Fischer, #15596018) reagent and reverse transcribed using the SuperScript III (Thermo-Fischer, #18080-044) according to the manufacturer's instructions. The real-time PCR was performed on a Light Cycler 480 (Roche, Basel, Switzerland) using predeveloped primer-probe sets [Supplementary Table 2] and the data was analyzed with the 2^{ddct}-Method [56].

RNA-seq

Library preparation and sequencing was conducted as described earlier [57]. Downstream analysis was conducted with R v3.4.4 and DESeq2 v1.18.1, resulting in gene transcript count tables, which were subsequently used for gene set enrichment (using the GSEA v4.0.3 Mac App) and GO term analyses (using the online tools available on genemania.org, string-db.org, reactome.org and geneontology.org).

IgA quantification

Cecal contents were homogenized in 100 µl 0.5% Tween in PBS per 10 mg cecal content and centrifuged at 100 g for 15 min at 4 °C in order to pellet large particles. The supernatant was transferred into a new tube, protease inhibitor was added and it was centrifuged for 10 min at 10000 g at 4°C. The supernatant was transferred into clean tubes and used for quantification with an anti-mouse IgA ELISA kit (Thermo Fischer, #88-50450-22) according to the manufacturer's instructions. Serum was directly used for quantification of IgA with the same kit.

Feces were homogenized in 100 µl PBS per 10 mg, centrifuged at 50 g for 15 min at 4 °C and the pellet was discarded. After two washes in 1% BSA in PBS the fecal bacteria were stained with anti-IgA-PE antibody (Thermo, #12-4204-81) in PBS with 20% normal rat serum and 1% BSA and analyzed on a Canto II (Beckton Dickinson) flow cytometer.

Colon tumor explant culture

Colon tumors were excised, weighed and cultured in RPMI-1640, supplemented with 10% FCS, penicillin/streptomycin, glutamine, non-essential amino acids and 50 mM BME, o/n at 37 °C, 5% CO2.

Multiplex Cytokine analysis

Cytokine analysis from cell culture supernatants was performed using the Legendplex mouse inflammation panel (Biolegend, #740446) according to the manufacturer's introductions.

Statistical Analysis

For standard statistical analyses Prism v. 7 (Graphpad, San Diego, USA) was used. Unless specified otherwise, individual data points, mean and SEM are depicted. Depending on the data distribution unpaired, two-tailed Student's t-tests or Mann-Whitney tests were performed

for two-group comparisons. For three- or more group comparisons one-way-ANOVA with Holm Sidak's multiple comparison test or Kruskal-Wallis with Dunn's multiple comparison tests were used depending on the data distribution. P-values <0.05 and FDRs <0.25 were considered significant.

Results

CCL17 is expressed in cDC and macrophages in the inflamed mucosa of the colon and in colon tumors

In order to gain insights into the role of CCL17 in the formation and progression of colitis associated cancer we sought to identify the CCL17 expressing cells in the colon. CCL17 has been shown to be expressed in various lymphoid and non-lymphoid tissues predominantly by DCs. However, less is known about the contribution of the several DC subsets and the expression dynamics upon inflammation and tumorigenesis, especially in the colon. To answer the question whether a distinct DC subset expresses CCL17 in the colon and whether the expression pattern changes under different conditions we used the CCL17-eGFP knock-in mice [31] and detected CCL17-eGFP expressing cells by flow cytometry. Within the $CD45^+$ $CD11b^+$ $Ly6G^-$ lamina propria leucocyte (LPL) fraction of the colon 4 populations were distinguished by Ly6C and MHCII expression, $Ly6C^{hi}$ $MHCII^{lo}$ monocytes (p1), $Ly6C^{hi}$ $MHCII^{hi}$ intermediate monocytes (p2), $Ly6C^{lo}$ $MHCII^{hi}$ macrophages/DC (p3) and $Ly6C^{lo}$ $MHCII^{lo}$ cells (p4) [Figure 1A]. The $Ly6C^{lo}$ $MHCII^{hi}$ population was further separated by CD64 expression into $MHCII^{hi}$ macrophages (p5) and $CD11b^+$ cDCs (p6). DCs were separately gated as $CD45^+$ $CD64^-$ $MHCII^{hi}$ $CD11c^{hi}$ cells and contained $CD11b^-$ $CD103^+$ cDC1, $CD11b^+$ $CD103^-$ cDC2 and $CD11b^+$ $CD103^+$ (DP) cDCs [Figure 1A]. In the steady state 13.2±0.9% cDC2 and 16.4±1.0% $CD103^+$ $CD11b^+$ DC were positive for CCL17 expression, whereas the frequency of monocytes and macrophages expressing CCL17 was below 1.2 % [Figure 1B]. In the inflamed colon during acute colitis induced by dextran sodium sulfate (DSS) also intermediate monocytes (p2, 9.6±2.0%) and macrophages (p5, 23.1±3.8%) expressed the CCL17-eGFP reporter and the

expression in DCs was increased compared to the steady state with the highest expression in the $CD11b^+$ $CD103^+$ DC subset (38.2±7.5%) [Figure 1B]. In colon tumors induced by administration of Azoxymethan (AOM) and 3 cycles of DSS a significant increase of CCL17 expressing cells compared to the non-tumorous colon tissue was found within the intermediate monocytes, $CD11b^+$ DCs and $MHCII^{hi}$ macrophages. The expression pattern was similar to the inflamed colon with the exception of $Ly6C^{lo}$ $MHCII^{lo}$ cells, which were not expressing CCL17 in the inflamed colon (p4, 0.2±0.03%) but contained a small population of CCL17 expressing cells in the colon tumor tissue (p4, 2.1±0.5%) [Figure 1B]. CCL17-eGFP reporter expression was not detected in other colonic cells than DCs or macrophages in the tested conditions [suppl. Figure 1]. The enrichment of CCL17-positive cells in the tumor compared to adjacent tissue was also observed by immunofluorescence [Figure 1C]. As GM-CSF is a known inducer for CCL17 expression [33], we quantified *Csf2* and *Ccl17* mRNA expression in the tumor tissue. *Ccl17* transcripts were found to be 9.1-fold increased in tumor tissue compared to adjacent colon tissue in accordance with the higher frequency of CCL17 expressing cells in tumors compared to surrounding colon tissue [Figure 1D]. *Csf2* transcripts, encoding GM-CSF were concomitantly 9.7-fold increased suggesting that CCL17 is induced in the tumor microenvironment by locally produced factors including GM-CSF, a known inducer of CCL17 expression. Thus, our results show that CCL17 expression is increased in colitis-associated colon tumors especially in tumor-associated macrophages.

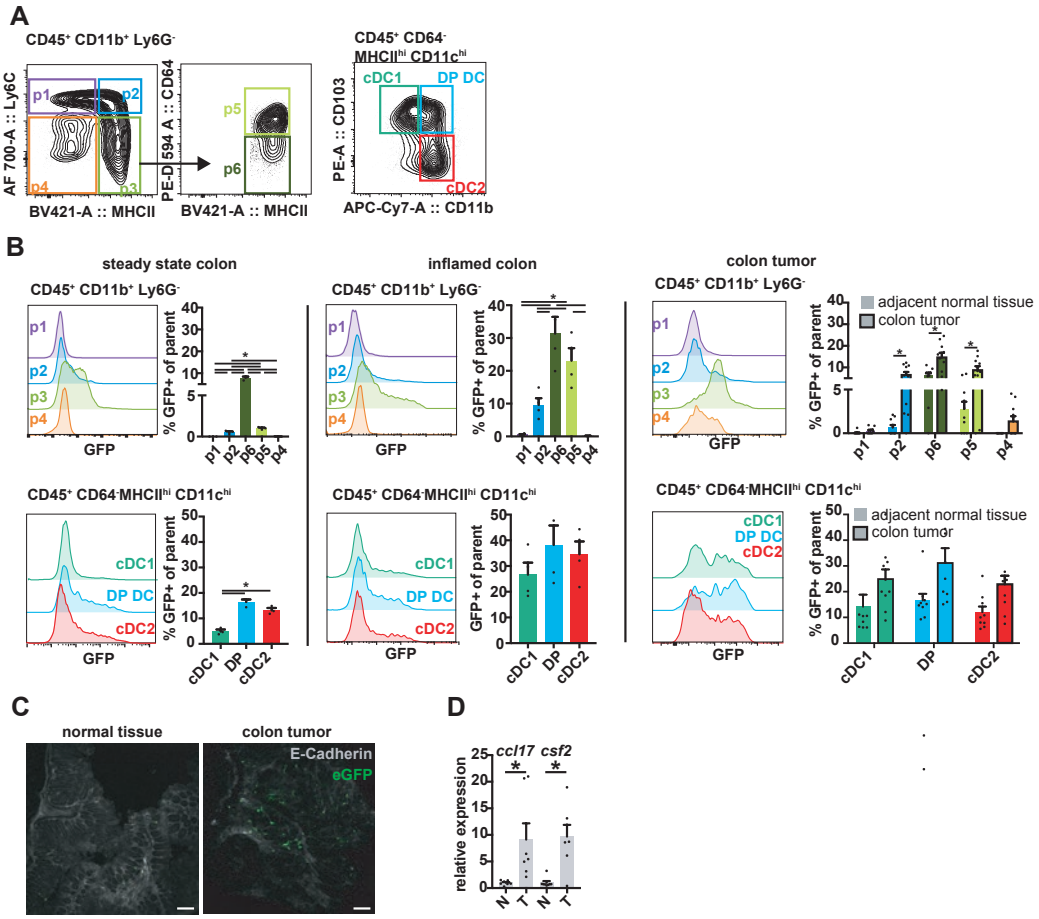

Figure 1 Colonic CCL17 expression. Using CCL17-reporter (eGFP) mice we detected CCL17-eGFP expressing cells by flow cytometry and determined the phenotype of CCL17 producing cells in the colon under different conditions. **A** Gating strategy for CD11b+ Ly6G- myeloid cells (left) and for dendritic cells (right). **B** CCL17-eGFP reporter expression in steady state (left), DSS-inflamed (mid) and colon tumor and adjacent normal tissue (right) in CD11b+ Ly6G- cells (upper row) and DCs (lower row). Mean ± SEM. Each data point represents one mouse (n ≥ 3). Histograms show one representative example. *p<0.05, unpaired, two-tailed Student's t-test. Data is representative for n ≥ 3 independent experiments. **C** Immunofluorescence staining of normal colonic (left) and colon tumor (right) tissue stained for GFP (green) and E-Cadherin (grey). Scale bar = 10 µm. Data is representative for n > 3 independent experiments. **D** Relative expression of Ccl17 and Csf2 transcripts in AOM DSS induced colon tumor tissue (T) and adjacent normal tissue (N). Mean ± SEM. Each data point represents one mouse (n ≥ 7). *p<0.05 unpaired, two-tailed Mann-Whitney test. Data is pooled from three independent experiments.

Differential CCL17- and surface marker expression in tumor infiltrating myeloid cell populations

It is known that the different tumor infiltrating myeloid subpopulations shape the tumor microenvironment promoting or inhibiting tumor growth. However, a detailed analysis of these cells in the colitis associated cancer mouse model is lacking to date. To further characterize these cells in AOM DSS induced tumors whole transcriptome analysis by RNA sequencing of Ly6C^{hi} monocytes, Ly6C^{hi} MHCII^{hi} intermediary monocytes, Ly6C^{lo} MHCII^{hi} and Ly6C^{lo} MHCII^{lo}

cells, gated as shown in [Figure 2A], was performed. CCL17 expression was mainly detected in Ly6C^{lo} MHCII^{hi} cells (p3), consistent with the mean fluorescence intensity (MFI) of the CCL17-eGFP signal detected by FACS [Figure 2B]. Of the top 200 highly variable genes [supplementary PDF] we validated the differential expression of CD209a (DC-SIGN), CD206 (mannose receptor) and CD24a (Small Cell Lung Carcinoma Cluster 4 Antigen) by flow cytometry [Figure 2E], identifying additional markers to distinguish these populations. For flow cytometric analyses cDC2 and MHCII^{hi} macrophages within the Ly6C^{lo} MHCII^{hi} cells were analyzed separately, gated as shown in [Fig 2E], whereas global gene expression analysis was performed on the entire Ly6C^{lo} MHCII^{hi} population due to limited numbers of DCs. The C-type lectin receptor CD209a (mouse DC-SIGN) was expressed at higher levels on cDC2, macrophages and Ly6C^{hi} MHCII^{hi} cells, than MHC^{lo} populations [58]. The CD209a MFI values were comparable in CCL17-eGFP^{+} cells, cDC2, total DCs and MHCII^{hi} macrophages [Figure S2A]. The endocytic mannose receptor CD206 which is known as a marker for immunosuppressive tumor-associated macrophages [59] was found to be expressed mainly by MHCII^{hi} macrophages and at low levels by cDC2 and intermediate monocytes. CCL17-eGFP^{+} cells showed similar CD206 levels as the cDC2 population [Figure S2A]. When comparing the gene expression levels of known markers for pro-inflammatory (M1) and suppressive (M2) macrophages [60], several M1 markers (*Il1b*, *Cxcl2*, *Il1a*, *Nfkbiz*, *Peli1*) were highest expressed in monocytes, followed by MHCII^{hi} macrophages, while their expression was low in intermediary monocytes and MHCII^{lo} macrophages [Figure S2B]. Regarding the analyzed M2 marker genes no such repetitive expression pattern could be found with highest expression of *Ccl8* in MHCII^{hi} macrophages, of *Chil3* in monocytes and of *Cd36* in MHCII^{lo} macrophages. CCL22, the other ligand for CCR4, showed a similar expression pattern as CCL17, indicating a coregulation of these chemokines. Taking into account the expression of the analyzed M1 and M2 marker genes besides *Mrc1* (encoding for CD206) MHCII^{hi} macrophages in AOM DSS induced colonic tumors did not show an overall increase of M2 marker genes, nor a decrease of M1 marker genes, suggesting that CD206 might not be a useful marker for immunosuppressive TAMs in the AOM DSS tumor model. Monocytes were

found to express CD24 at the highest levels [Figure 2C, 2D]. While the gene expression levels were lowest in Ly6C^{lo} MHCII^{hi} cells [Figure 2C] the surface protein levels were lowest in Ly6C^{lo} MHCII^{lo} cells [Figure 2D]. Total DCs showed increased CD24 levels compared to cDC2 and MHCII^{hi} macrophages, likely due to higher expression in cDC1 [Figure S2A]. Gene ontology (GO) term analysis of the gene clusters with increased expression by the respective populations revealed proteolytic activity of monocytes, expression of hemoglobin genes by intermediary monocytes, endocytic and proinflammatory activity in Ly6C^{lo} MHCII^{hi} cells and pattern recognition receptor (PRR) binding in MHCII^{lo} cells [Figure 2E]. These results provide insights into the functionality of tumor infiltrating myeloid populations in AOM DSS induced tumors. Further, they showed that CCL17 expression is highest in the Ly6C^{lo} MHCII^{hi} subset of tumor-associated myeloid cells, which is comprised by cDC2 and MHCII^{hi} macrophages and is marked by higher expression of CD206 and CD209a and a gene expression profile enriched for inflammatory cytokines and endocytosis.

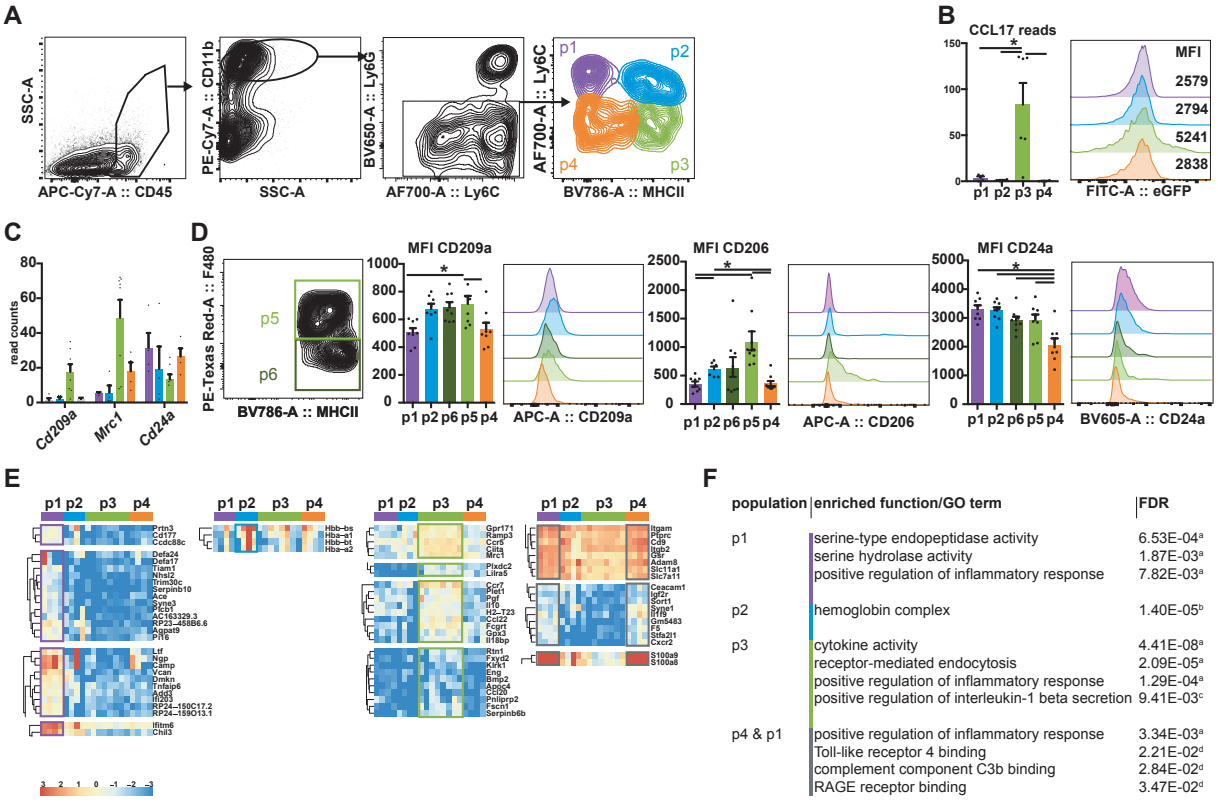

Figure 2 Differential CCL17 and surface marker expression in tumor infiltrating myeloid cell populations. Myeloid subsets of tumor infiltrating cells in AOM/DSS induced tumors were analyzed by RNA sequencing. **A** Gating strategy used for sorting of tumor infiltrating myeloid cell populations. **B** *Ccl17* transcript expression in the sorted myeloid cell populations (left: transcript read counts, right: eGFP-reporter expression). Mean ± SEM. Each data point represents pooled tumors (similar size) of one

mouse (n ≥ 4). **C** Transcript expression of *Cd209a*, *Mrc1* and *Cd24a* in AOM DSS induced tumors. Mean ± SEM. Each data point represents pooled tumors (similar size) of one mouse (n ≥ 4). **D** Gating strategy to separate cDC2 and MHCII^{hi} macrophages for flow cytometric analyses (left). Mean fluorescence intensities and representative histograms of validated surface proteins. Mean ± SEM. Each data point represents pooled tumors (similar size) of one mouse (n ≥ 8). **E** Gene expression of gene clusters used for GO term analysis. **F** Functional gene enrichment analysis for genes with elevated expression in the depicted populations. GO term: gene ontology term; FDR: false discovery rate; a-d: used database. a: GeneMANIA prediction server, b: STRING database, c: REACTOME pathway database, d: PANTHER Classification System

CCL17-deficient single-housed mice show decreased colon tumor formation in the AOM DSS model

Given the strong upregulation of CCL17 in the colon tumor tissue we investigated whether CCL17 plays a nonredundant role in the tumorigenesis of AOM DSS induced colon tumors. Therefore CCL17-deficient (homozygous CCL17-eGFP knock-in, ki/ki) and CCL17-competent (wt/ki and wt/wt) mice received one injection of AOM and were subjected to 3 cycles of low dose DSS as depicted in [Figure 3A]. To control for microbiota mediated effects we bred CCL17-deficient mice from a homozygous ki/ki breeding pair for one generation and compared the offspring (ki single housed, SiHo) with CCL17-deficient (ki cohoused, CoHo) and with CCL17-competent (ctrl) mice generated from a heterozygous breeding pair. Both breeding pairs were derived from the same heterozygous breeding pair to minimize genetic drift between the experimental groups. There was no difference in the relative bodyweight during AOM DSS treatment between the experimental groups. However, tumor formation was significantly decreased in single-housed CCL17-deficient mice (ki SiHo, 12.4±1.3 tumors) compared to CCL17-competent (ctrl, 16.1±1.1) and cohoused CCL17-deficient mice (ki CoHo, 19.9±2.0). The tumors did not show overt histological differences between the experimental groups [Figure 3E]. The average tumor area was slightly elevated in the single-housed CCL17-deficient group compared to the other groups (single-housed CCL17-deficient 6.5±0.5 mm^2, CCL17-competent 4.7±0.4 mm^2, cohoused CCL17-deficient 5.0±0.4 mm^2) and a trend towards a higher percentage of Ki67$^+$ tumor cells in this group was observed, indicating that tumor multiplicity but not tumor growth is reduced in single-housed CCL17-deficient mice [Figure 3F, 3G].

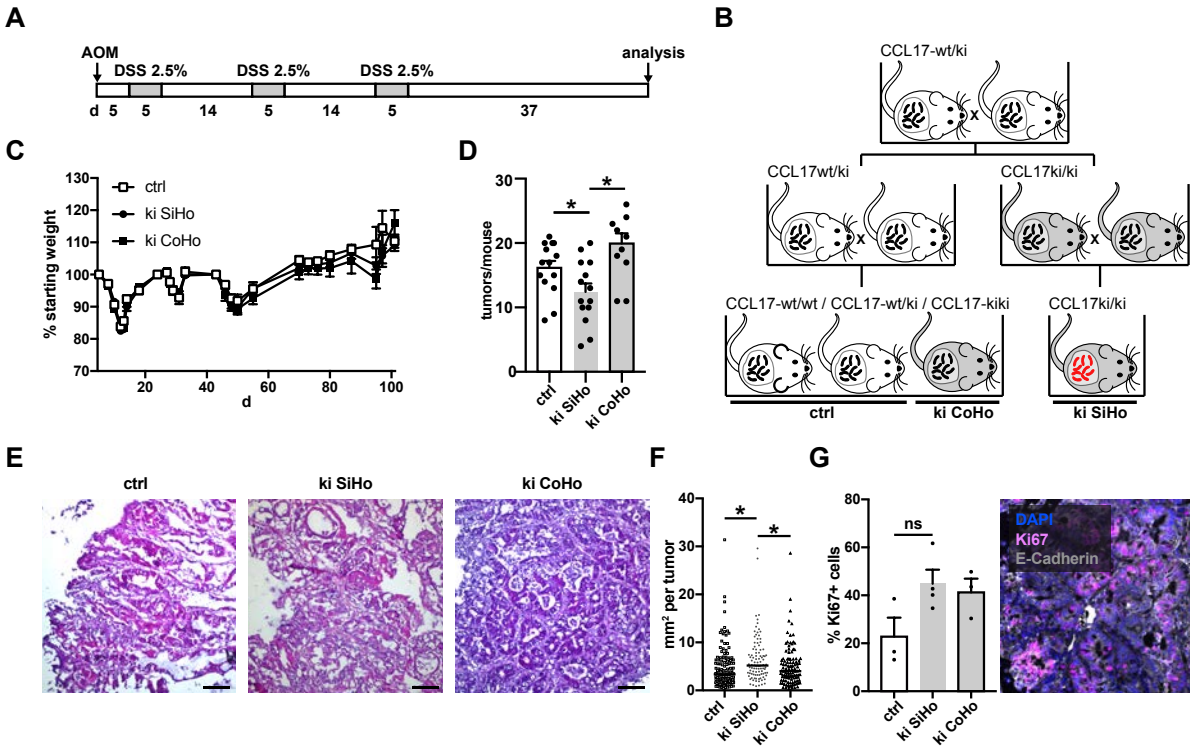

Figure 3 CCL17-deficient single housed mice show decreased tumor formation upon AOM DSS treatment. Single-bred/-housed CCL17-deficient (ki/ki) and cohoused CCL17-ki/ki and CCL17-competent (wt/ki and wt/wt) littermates were treated with AOM and three cycles of DSS. **A** Experimental scheme of the AOM DSS treatment. AOM: Azoxymethane, DSS: Dextran sulfate sodium, dissolved in drinking water (%wt/wt). **B** Breeding strategy for obtaining the experimental groups ctrl (CCL17-wt/wt and CCL17-wt/ki), ki CoHo (CCL17-ki/ki with CCL17-wt/wt and CCL17-wt/ki cohoused littermates) and ki SiHo (CCL17-ki/ki with CCL17-ki/ki littermates, separately housed from CCL17-wt/wt and CCL17-wt/ki mice). **C** Relative bodyweight during AOM DSS treatment. The bodyweight was normalized to the starting weight at the beginning of each DSS cycle. Open rectangles: ctrl, filled circles: kiSiHo, filled rectangles: kiCoHo. Mean ± SEM. Each data point represents one mouse (n ≥ 11, pooled from two experiments). **D** Number of tumors per mouse after AOM DSS treatment. Each data point represents one mouse (n ≥ 11, pooled from two experiments). Mean ± SEM. *p<0.05, two-tailed Mann-Whitney test. **E** Representative hematoxylin-eosin (H&E) stained cryosections from AOM DSS induced tumors. Scale bar: 10 µm. **F** Area per tumor. Each data point represents one tumor (n ≥ 98). Line: median, *p<0.05, unpaired, two-tailed Student's t-test. **G** Left: Percentage of Ki67+ cells, determined by immunofluorescence staining (Ki67+/DAPI+ cells). Each data point represents one mouse (n ≥ 3). Mean ± SEM. Right: Representative section stained for DAPI (blue), Ki67 (magenta) and E-Cadherin (grey). Scale bar: 10 µm.

CCL17 deficiency leads to an altered microbiota

The observed reduction in tumor numbers in CCL17-deficient mice appeared to be microbiota dependent, as CCL17-deficient mice cohoused with CCL17-competent littermates did not show this phenotype. To determine microbial changes in the single-housed CCL17-deficient mice we analyzed the steady state fecal microbiota of those mice in comparison with that of controls and CCL17-deficient mice cohoused with controls. As the microbiota of CCL17-deficient and competent littermates were very similar, as expected, we merged these two

groups for the statistical analyses. When comparing the microbiota of CCL17-deficient single housed and the cohoused mice, differences both in the alpha- and in the beta diversity of the respective microbiota were detected [Figure 4A, 4B]. The number of observed operational taxonomic units (OTUs) was significantly smaller in feces of single housed CCL17-deficient mice than in the feces of the cohoused groups [Figure 4A]. The Bray-Curtis principal coordinate analysis revealed a significant alteration of the bacterial composition in the feces of single housed CCL17-deficient mice versus cohoused control mice [Figure 4B]. Further analysis using the LEfSE (linear discriminant analysis effect size) method showed a reduced abundance of the genus *Lactobacillus* and the *Proteobacteria* phylum in the feces of cohoused mice, while the genus *Akkermansia*, the *Ruminococcaceae* family and the *Peptococcaceae* family were enriched in the feces of single-housed CCL17-deficient mice [Figure 4C] coinciding with less tumors developing in these mice in the AOM DSS model.

Next, we wanted to investigate the underlying cause of these marked differences in the microbiota of single housed CCL17-deficient mice compared to their cohoused counterparts. Secretory IgA produced constitutively in response to commensals is an important component of the intestinal barrier, regulates microbiota composition and maintains intestinal homeostasis [49, 61]. Bacterial IgA coating has been suggested to influence microbial composition both by promoting bacterial clearance [61] and creating protective niches for the IgA-bound bacteria [62], depending on the environmental setting and the respective bacteria. We found significantly more IgA-coated bacteria in the feces of single-housed CCL17-deficient mice than in control mice [Figure 4D]. IgA levels were significantly elevated in the cecal lumen but not in the serum of single-housed CCL17-deficient mice [Figure 4E], demonstrating that only intestinal and not systemic IgA production is altered in these mice. These results suggest that secretory IgA contributes to the establishment of an altered microbiota in CCL17-deficient mice which is protective against colitis-induced tumor formation.

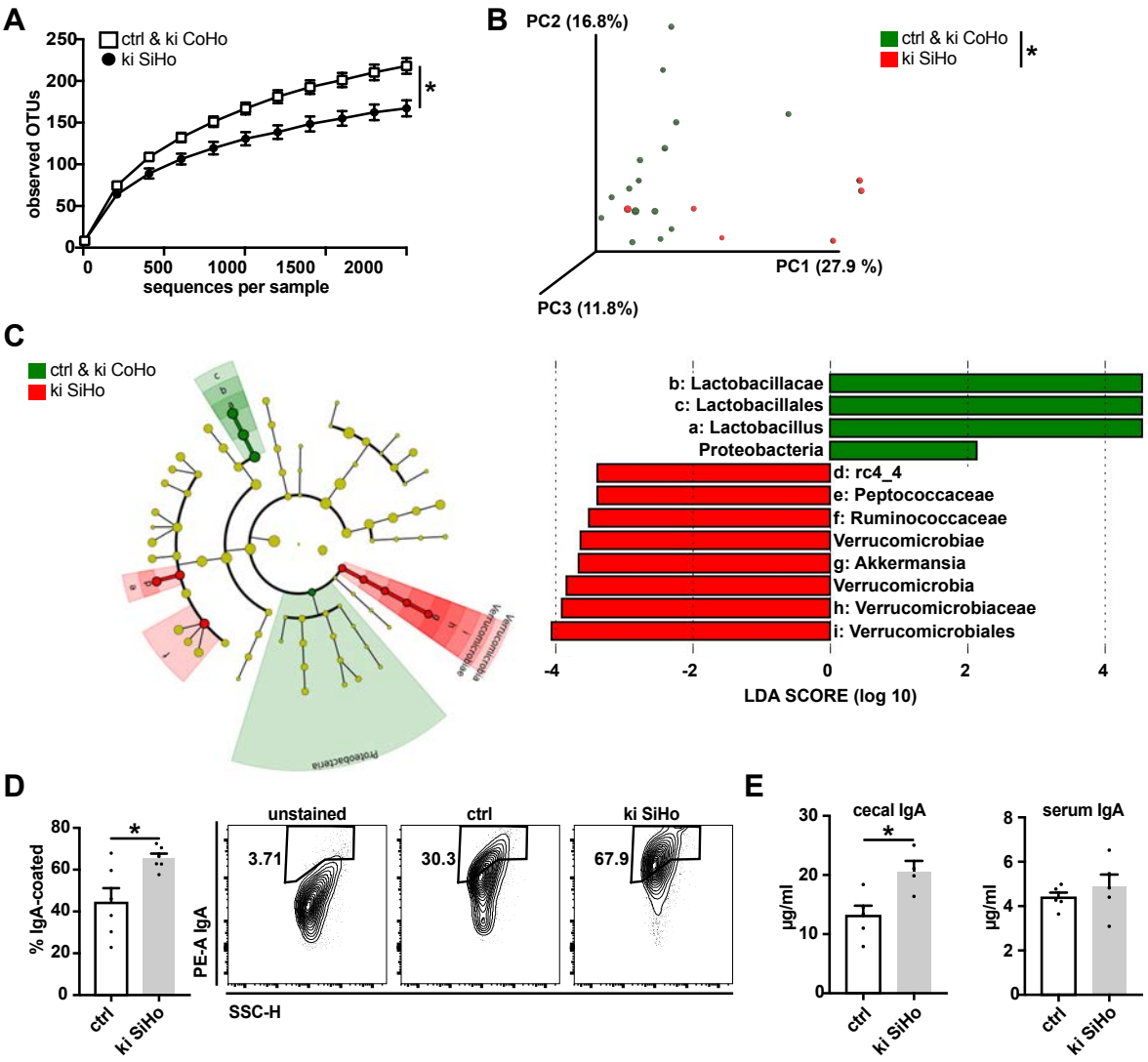

Figure 4 CCL17 deficiency leads to an altered microbiota. A Number of observed OTUs in the feces of steady state ki SiHo vs ctrl& ki CoHo mice. Mean ± SEM (n ≥ 7). *p<0.05 unpaired, two-tailed Student's t-test. **B** Bray-Curtis principal coordinate analysis of the microbiota composition in ki SiHo and ctrl&ki CoHo mice. Each data point represents one mouse. *p<0.05 Adonis (permutational multivariate analysis of variance using the Bray-Curtis distance matrices). **C** Linear discriminant analysis effect size (LEfSE) analysis. Green: taxa enriched in ctrl & ki CoHo, red: taxa enriched in ki SiHo. LDA: Linear discriminant analysis. **D** Left: Percentage of IgA-coated bacteria, determined by flow cytometry. Each data point represents one mouse (n = 5). Mean ± SEM. *p<0.05 unpaired, two-tailed Student's t-test. Right: Representative contour plots of ctrl and ki SiHo fecal samples. **E** Cecal (left) and serum (right) IgA concentration in ctrl and ki SiHo mice. Each data point represents one mouse (n = 5). Mean ± SEM. *p<0.05 unpaired, two-tailed Student's t-test.

Single-housed CCL17-deficient mice show similar weight loss and inflammation after short term AOM DSS treatment

In the AOM DSS model the AOM injection and the first cycle of DSS-induced intestinal inflammation and regeneration are decisive for tumor initiation and early tumor promotion, whereas the following DSS cycles and regeneration phases are important for tumor

maintenance and progression. In order to investigate the events during the initiation phase we injected single-housed CCL17-deficient mice and control mice (wt/ki) with AOM followed by one cycle of DSS and analyzed the mice during the regeneration phase on d4 after stopping exposure to DSS [Figure 5A]. We did not observe significant differences in weight loss during the inflammation phase (day 8 – 12) or in weight gain during the regeneration phase (day 12 – 14) as shown in [Figure 5B]. Histological examination did not reveal major differences in epithelial damage, leucocyte infiltration and regenerative responses of the epithelium [Figure 5C]. Also, the expression of the antimicrobial proteins Muc2 and Reg3g was not altered in single-housed CCL17-deficient mice four days after ending DSS treatment. However, the transcript level ratio of proapoptotic *Bax* and antiapoptotic *Bcl2*, an indicator for apoptotic activity [63] was significantly increased in the colon tissue of these mice, while the relative mRNA expression of the proliferation marker *Pcna* and the tissue repair promoting cytokine *Il22* was not altered. These results indicate increased apoptosis, but comparable proliferative response in the colon of single-housed CCL17-deficient mice during the regeneration phase.

We also analyzed the infiltration by inflammatory cells after short term AOM DSS treatment by flow cytometry and found no difference in the frequency of $CD45^+$ cells (40.0±3.1 % in CCL17-competent vs 39.15±4.85 % in CCL17-deficient single-housed mice) in the colon between the experimental groups. The frequencies of neutrophilic granulocytes, which make up the majority of the myeloid cells, as well as the percentages of monocyte subsets and $MHCII^{hi}$ macrophages within the $CD11b^+$ non-granulocyte fraction were not altered. The composition of the colon DC compartment was also not changed. Only a significantly higher percentage of $MHCII^{lo}$ cells was found in the colon of single-housed CCL17-deficient mice [Figure 5F]. The mRNA expression of the proinflammatory cytokines *Ifng*, *Il17*, *Il12*, *Tnfa*, *Il1b* and *Il6* in whole colon tissue was not altered, indicating a similar inflammatory activity after the short term AOM DSS treatment. It is therefore unlikely that reduced tumor numbers in single housed CCL17-deficient mice are a consequence of reduced inflammation during the early phase of tumor initiation.

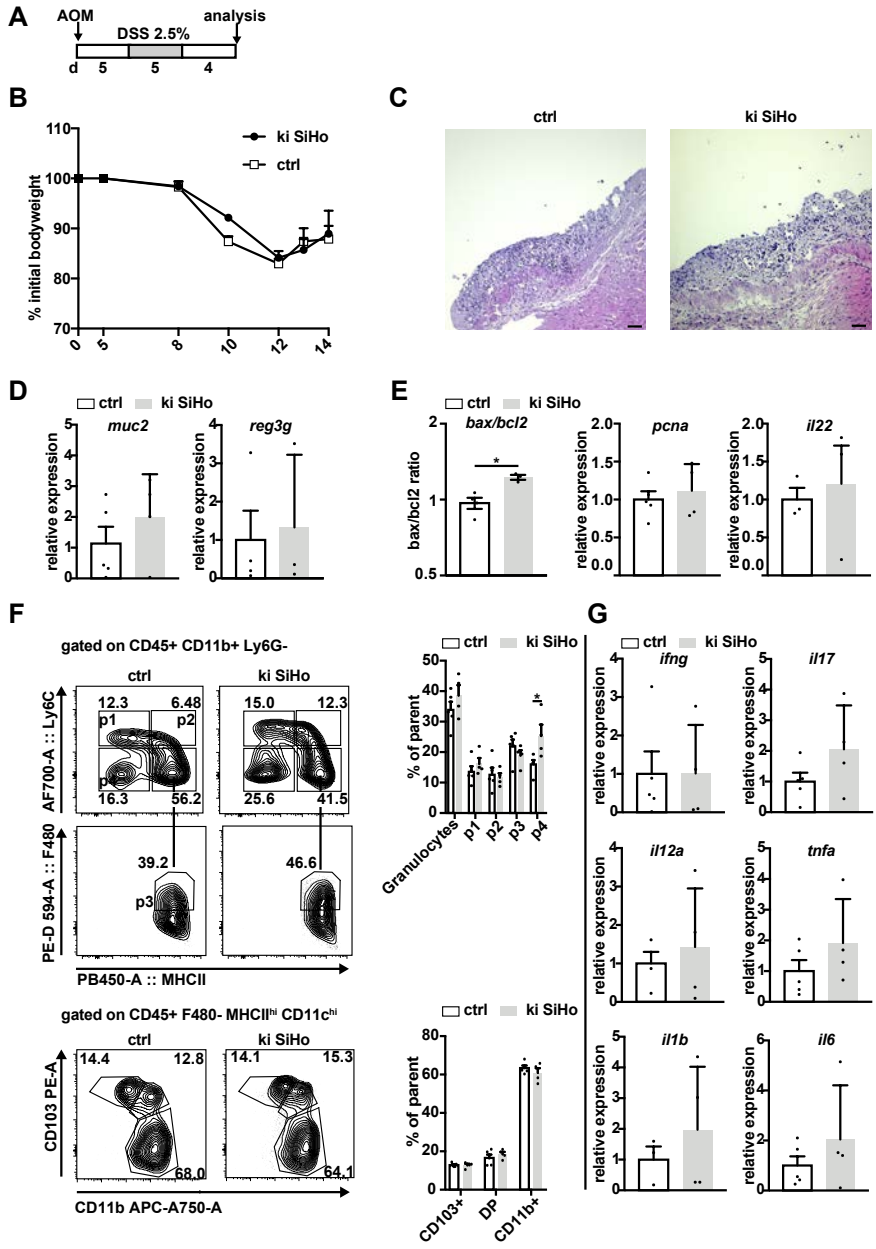

Figure 5 Single housed CCL17-deficient mice show similar weight loss and inflammation after short term AOM DSS treatment. Single-housed CCL17-deficient and control mice were injected AOM followed by one cycle of DSS and were analyzed during the regeneration phase. **A** Experimental scheme of AOM DSS treatment. **B** Relative bodyweight during AOM DSS treatment. Open rectangles: ctrl, filled circles: ki SiHo, Mean ± SEM (n ≥ 4). **C** Representative H&E stained distal colon sections from AOM DSS treated mice. Scale bar: 10 µm. **D** Colonic Relative expression of *Muc2* and *Reg3g* after AOM DSS treatment. Mean ± SEM. Each data point represents one mouse (n = 4). **E** Left: Ratio of *Bax*/*Bcl2* transcript levels. Right: Relative expression of *Pcna* and *Il22*. Mean ± SEM. Each data point represents one mouse (n = 4). *p<0.05 unpaired, two-tailed Mann-Whitney test. **F** Colonic myeloid immune cell infiltration after AOM DSS treatment. Left: gating strategy and representative plots for CD11b+ Ly6G- myeloid cells (upper panel) and dendritic cell subsets (lower panel). Right: Quantification of cell frequencies. Mean ± SEM. Each data point represents one mouse (n = 4). *p<0.05 unpaired, two-tailed Student's t-test. **G** Colonic relative expression of cytokines after AOM DSS treatment. Mean ± SEM. Each data point represents one mouse (n = 4).

Characterization of the tumor immune infiltrate of CCL17-deficient single housed mice reveals altered gene expression signatures in the myeloid cell compartment

Colon tumor development, maintenance and progression is influenced by the tumor microenvironment (TME) which is shaped by innate and adaptive immune cells infiltrating the tumors and by microbiota-dependent signals [64, 65]. In addition, anti-tumor immune responses play a role also in inflammation-driven tumors [10]. As CCL17 is highly expressed in AOM DSS induced tumors by macrophages and DCs, we hypothesized that it might influence the immune cell composition in the tumors. Analysis of the immune cell infiltrate of AOM DSS induced tumors by flow cytometry revealed no differences in the frequencies of $CD45^+$ immune cells, $CD11b^+$ myeloid cells or DCs and no change in the frequencies of monocyte, macrophage and DC subpopulations between single-housed CCL17-deficient mice and the control groups [Figure 6A, 6B]. However, global transcriptome analysis of myeloid cells isolated from AOM DSS induced tumors revealed that monocytes (p1) from tumors of single-housed CCL17-deficient mice were enriched for genes involved in proteasomal degradation (e.g. *Psmc2* and *Psmb1*, which encode for proteasome subunits) and oxidative phosphorylation (e.g. *Uqcr10* encoding for a complex III subunit and multiple genes encoding for the NADH dehydrogenase complex). $Ly6C^{lo}$ $MHCII^{hi}$ (p3) cells from these tumors showed an even stronger enrichment for these gene signatures as well as an enrichment for genes involved in lysosomal activity (e.g. *Psap* and *Hexb*, which are crucial for lipid degradation) indicating increased endocytosis/phagocytosis levels of myeloid cells in colon tumors of single-housed CCL17-deficient mice [Figure 6C]. Moreover, the supernatant of tumor explant cultures of single-housed CCL17-deficient mice contained significantly less IL-1β compared to the controls [Figure 6D]. These results indicate functional differences of the myeloid cell compartment in tumors of CCL17-deficient single housed group, which coincided with reduced tumor numbers.

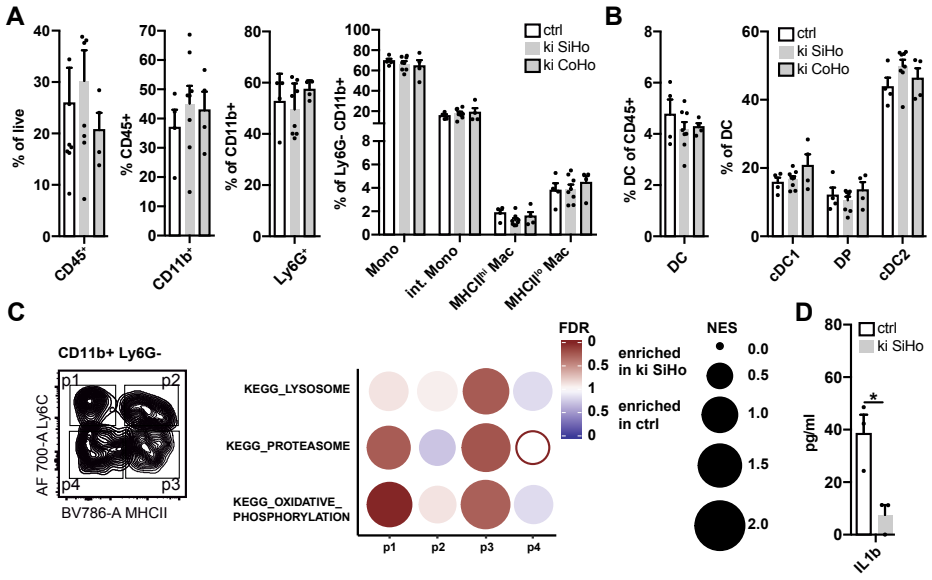

Figure 6 Altered gene expression signatures in tumor associated myeloid cells. Tumor infiltrating immune cells in tumors of ctrl, ki SiHo and ki CoHo were analyzed. **A** Frequency of total immune cells (far left), Percentage of tumor infiltrating CD11b+ myeloid cells (left), granulocytes (right) and monocytes, intermediate monocytes, MHCII^{hi} and MHCII^{lo} macrophages (far right) in tumors of ctrl, ki SiHo and ki CoHo mice. Each data point represents one mouse (n ≥ 4). Mean ± SEM. **B** Percentages of total DCs (left) and DC subsets (right) in tumors of ctrl, ki SiHo and ki CoHo mice. Each data point represents one mouse (n ≥ 4). Mean ± SEM. **C** Gene set enrichment analyses of tumor infiltrating CD11b+ Ly6G- myeloid cell populations p1-p4 from ki SiHo and ctrl mice. The color intensity of the circles denotes the significance level (false discovery rate, FDR); the circle diameter reflects the normalized enrichment score (NES). Blue/red indicates the group in which a signature was positively enriched; n ≥ 4 biological replicates for each group. **D** Concentration of IL-1β in the supernatant of tumor explant cultures from ctrl and ki SiHo mice. Each data point represents one mouse (n = 3). Mean ± SEM. *p<0.05 unpaired, two-tailed Student's t-test.

Innate and adaptive lymphocytes also influence the TME and may have tumor-promoting as well as anti-tumor activity. We found no difference between the experimental groups in the percentages of B cells, but a trend towards lower T cell frequencies in tumors of single housed CCL17-deficient mice [suppl. Figure 3A, B]. The T cell distribution within the tumor tissue was not altered between the groups [suppl. Figure 3C]. The percentages of the CD8-, CD4- and Treg-subsets, as well of NK and NKT cells were similar between the groups [suppl. Figure 3D]. Effector functions of intratumoral lymphocytes, measured by intracellular IFN-ɣ and IL-17, surface CD69 protein levels as well as *Gzmb*, *Il17* and *Ifng* gene expression appeared to be unaltered [suppl. Figure 3E-G]. These results show that the alterations in tumor-associated myeloid cell functionality observed in single housed CCL17-deficient mice are not connected with increased anti-tumor effector T cell responses.

Taken together, we find that the reduced tumor load in CCL17-deficient mice is dependent on the microbiota, but not mediated by reduced inflammation. This phenotype coincides with an

increased ratio of pro- vs anti-apoptotic gene expression in the colon during the early phase of tumor development as well as with functional changes in tumor-infiltrating myeloid cells.

Discussion

We found CCL17 expressed in the steady state colon by the CD11b^{+} dendritic cell subsets, which was observed in other organs as well [27, 32]. While CCL17 is absent in the steady state spleen due to IFN-ɣ signaling in DCs, it can be induced in splenic DCs by systemic application of GalCer, which to IL-4 and GM-CSF secretion by NKT cells [32, 66]. This illustrates that CCL17 expression is highly dependent on external stimuli and is in line with our observation of strong CCL17 induction in DSS induced colon inflammation and AOM/DSS-induced colon tumors. Upregulation of CCL17 expression in intestinal DCs was also observed in another colitis model [26], in skin lesions of an atopic dermatitis model [28] and in the CNS during EAE [27]. CCL17 expression by macrophages was observed in joint inflammation [30] and peritonitis [33], as well as in a subset of TAMs in a melanoma model [67] and in intestinal tumors developing in APC-mutant mice, which is in line with our observations in the CAC model [34]. CCL17 is one of the hallmark genes expressed by M2-polarized macrophages [60]. The present study is the first to provide detailed information about the expression of CCL17 in the colonic monocyte, DC and macrophage subpopulations in inflammation related colon tumorigenesis.

In order to characterize the CCL17 expressing population in AOM DSS induced tumors further, we analyzed the transcriptome of the major non-granulocytic tumor-infiltrating CD11b^{+} myeloid cell populations and found population-specific gene enrichments with functional implications.

In the steady state Ly6C^{hi} MHCII^{lo} monocytes are recruited to the colon where they differentiate via Ly6C^{hi} MHCII^{hi} intermediary cells into Ly6C^{lo} MHCII^{hi} macrophages acquiring a tissue-specific gene signature during the differentiation process [68]. We found an enrichment of hemoglobin-genes in intermediary monocytes, which is in line with findings by Kraft-Terry et. al, who described transcription of hemoglobin genes during early monocyte to macrophage differentiation [69].

Among the genes encoding for known cell surface receptors, we found *Mrc1*, *Cd209a*, and *Cd24a* among the Top 200 highly variable genes. Higher expression of *Cd206* and *Cd209a* in Ly6C^{lo} MHCII^{hi} cells compared to the other analyzed populations could be confirmed on protein level by flow cytometry, while CD24 surface expression was highest in the monocyte subpopulations followed by MHCII^{hi} macrophages and DCs. CD24-deficient mice show reduced susceptibility to DSS-induced colitis and to tumor formation in the AOM/DSS induced model, but the function of CD24 on monocytes and macrophages was not investigated in this study [70]. It was shown that CD24 by interacting with human Siglec 10 or mouse Siglec G dampens the inflammatory response to tissue injury [71]. CD24 expressed on cancer cells by interacting with Siglec G on macrophages inhibits phagocytosis activity against tumor cells [72] and CD24 expressed on tumor-infiltrating myeloid cells could have a similar function. It was shown for example that silencing of CD24 increased phagocytosis of B. burgdorferi and TNF-α induction in RAW macrophages [73]. The C-type lectin CD209a is related to high endocytic activity and the initiation of T cell responses [58]. We found significantly higher *Cd209a* gene expression in Ly6C^{lo}MHCII^{hi} cells which could be confirmed on surface protein level and we observed an enrichment for other genes involved in receptor-mediated endocytosis in this population which at the same time expresses the highest levels of CCL17. Also, the mannose receptor CD206 was found to be significantly higher expressed in Ly6C^{lo}MHCII^{hi} cells with highest expression in MHCII^{hi} macrophages, in line with the report by Schridde et al. who analyzed steady state colonic myeloid cells [68]. CD206 is widely used as a marker for immunosuppressive macrophages in the tumor environment [74-77]. However, we found highest CD206 surface levels on MHCII^{hi} macrophages, while other genes related to immunosuppressive macrophages were not significantly higher expressed in this population and the expression of several pro-inflammatory genes was not significantly lower in MHCII^{hi} macrophages, but in MHCII^{lo} macrophages, compared to the monocyte population which showed the highest expression of pro-inflammatory marker genes. This is consistent with other studies which identified MHCII^{lo} macrophages as the suppressive macrophage population in different tumor models [77, 78]. Thus, our results indicate that the population of MHCII^{hi}

macrophages and cDC2 which contains the CCL17 expressing cells is especially equipped with receptors for antigen uptake and that CD206 might mark macrophages of different functionality in AOM DSS induced colon cancer than in other tumor models, highlighting the importance of the tissue microenvironment for macrophage phenotype and functionality.

Our data shows that CCL17 is expressed by intratumoral myeloid populations, which are relevant for tumor development. Lower tumor number in CCL17-deficient mice indicate a role of CCL17 in AOM DSS induced tumor development itself. However, while inflammation is a major driver in the AOM DSS induced tumor model [50], we did not find overt differences in inflammation between the groups, which is in contrast to our previous results, which we obtained in the acute DSS colitis model with higher doses of DSS [26]. Other studies, finding reduced [79, 80] or increased [81] tumor numbers despite similar inflammation or even a reduced tumor load with increased inflammation [82, 83] illustrate that other factors than inflammation severity can be decisive for tumor induction in this model. Moreover, we found that the difference in tumor multiplicity was abolished when CCL17-deficient mice were obtained from heterozygous breedings and cohoused with CCL17-competent littermates highlighting the importance of the microbiota as has been observed for other knockout mice in the AOM/DSS model [84, 85]. Despite a reduction of the tumor number in CCL17-deficient mice their tumors were not smaller but even slightly larger compared to the other groups. Thus, our results show a reduced tumor number in CCL17-deficient mice without reduction in inflammation severity and tumor size, which is abolished upon cohousing the mice, indicating a role of the microbiota in the protective effect of CCL17 deficiency.

In congruence with the observed effect of separate housing on tumor numbers we found altered alpha- and beta-diversities in single housed CCL17-deficient mice compared to the control groups. The studies of Tschurtschenthaler et al. and Man et al. and the observation that germ-free mice develop higher tumor numbers after AOM DSS treatment [84-87] clearly show that the microbiota composition is a crucial determinant of the tumor number in this model. We found decreased levels of *Proteobacteria* in single-housed CCL17-deficient mice which was associated with lower tumor incidence in other studies [88, 89]. The role of

Akkermansia, which we found increased in single-housed CCL17-deficient mice is not that clear, as both pro- and anti-inflammatory/tumorigenic effects have been reported for increased abundance of this phylum [90-92]. Similarly, Wu et al. have found in the AOM DSS tumor model a positive correlation of tumor multiplicity with the abundance of the *Lactobacillus* phylum, which we found decreased in single housed CCL17-deficient mice, whereas Chen et al. found a decreased abundance upon AOM DSS induced tumor development [93, 94]. One possible underlying mechanism for the altered microbiota composition is a direct, non-redundant effect of CCL17 on the intestinal microbiota. Alterations of the microbiota by chemokine-receptor deficiency have been described before [95]. Chemokines of the C-C family possess a structure similar to defensins and high anti-microbial activity has been shown for the members CCL28 and CCL20 [96-98]. For CCL17 only a low to moderate antimicrobial activity has been shown against *E.coli* and *S.aureus in vitro* at high doses [98], but it cannot be excluded that CCL17 might influence the bacterial composition in the colon directly. Another regulator of the intestinal microbiota is intestinal IgA, produced by plasma cells in the peyers patches (T-cell dependent (TD) IgA production) or in isolated lymphoid follicles (ILF) (T-cell independent (TI) IgA production) [49]. The functional consequences of IgA binding to intestinal bacteria have shown to be diverse and range from protective effects [61, 62, 99-101] to inhibition of bacterial motility [102], enhanced clearance [61] or reduced bacterial fitness [103] e.g. by altering bacterial gene expression [104]. Whether intestinal IgA confers supportive or negative effects on the microbiota was shown to depend on its affinity to its epitope, which can be single- or cross species-specific [61, 105, 106]. Palm et. al found that IgA^+-bacteria from human colitis patients induced colitis when they were transferred to germ-free mice [107], Kau et al. found higher IgA^+ levels in healthy donors compared to their malnutritioned twins [108], whereas D'Auria et al. found specific IgA-coating of rare bacterial taxa such as *Sphingomonadaceae* [109]. We found a significantly higher percentage of IgA-coated fecal bacteria in single-housed CCL17-deficient mice and higher cecal IgA levels with unchanged serum levels. Moreover, we observed a lower number of different fecal OTUs in single-housed CCL17-deficient. Thus, higher IgA-coating may reduce tumorigenic OTUs in the single-housed

CCL17-deficient mice. It has been shown that myeloid cells are able to change the microbiota [92, 110, 111] and that $CD11b^+$ $CD103^+$ dendritic cells, which produce high levels of CCL17 in tumor and normal intestinal tissue are important for TI IgA responses as they are able to support of B cell differentiation [112]. Thus, CCL17 deficiency could lead to an altered microbiota either directly or indirectly by regulating intestinal IgA responses.

As we observed reduced tumor numbers in single-housed CCL17-deficient mice we analyzed the mice after short term AOM DSS treatment to detect changes in early tumor development. No evidence for reduced inflammation or altered proliferative response was found at this early time point. This in contrast to other studies, such as Mc Donough et al., who find increased colitis severity and elevated tumor numbers in Mtg16 deficient mice or Huber et al., who find IL-22 dependent increased proliferation after epithelial damage in IL-22 BP deficient mice and a subsequent increase in tumor number at the end of the AOM DSS treatment [113, 114]. The increased *Bax*/*Bcl2* gene expression ratio in distal colon tissue of single-housed CCL17-deficient mice indicated elevated apoptosis levels after one cycle of DSS treatment. It was shown previously that apoptosis during tumor initiation reduces tumor numbers independent of colitis severity in the AOM DSS model when carcinogen-exposed enterocytes undergo apoptosis instead of forming a tumor [115]. Interestingly, a higher tumor incidence together with decreased tumor sizes and reduced apoptosis levels in the beginning of the treatment have also been observed in mice deficient for Parp–1. In this study Parp–1 was found to increase mutation induced cell death in the early stages and thereby reduced tumor incidence but promoted tumor progression [116]. CCL17 might influence IEC cell death in the early stage and proliferation in the late stage inversely, leading to less but slightly larger tumors after the AOM DSS treatment.

Tumor incidence and progression in the AOM DSS model is not only driven by DSS induced colon inflammation [50], but also influenced by immune cell infiltration and activation in the developing tumors which can have pro- and anti-tumor activity [82]. Therefore, we analyzed the infiltrating immune cells in AOM DSS induced tumors at the end of the treatment.

The observation that effector T cell frequency was not altered in single housed CCL17-deficient mice indicated that the observed reduction in tumor number was not due to an increased T cell response against the tumors. The frequency of Tregs and Th17 cells which have been shown to migrate in response to CCL17 was not altered in the tumors of CCL17-deficient mice indicating that CCL17 is redundant for T cell migration to the tumors in this model. This is in contrast to findings in the syngeneic CT-26 tumor model, in which CCL17 and CCL22 have been shown to play a role for Treg migration [117, 118]. However, these studies focused on downregulation of CCL17 and CCL22 respectively in the CT-26 tumor cell line, while we did not observe CCL17 expression in CD45-negative cells in AOM DSS induced tumors.

We did not find changes in the myeloid cell frequencies. As observed in DSS treated $APC^{Min/+}$ mice (but not in $APC^{1638N/+}$ mice treated with AOM [34]) $MHCII^{lo}$ cells were more abundant than $MHCII^{hi}$ macrophages in AOM/DSS induced tumors [78]. Elevated levels of granulocytes or granulocytic MDSC are associated with increased tumorigenesis [119-122], whereas the role of TAMs appears to be more complex as both protective and protumorigenic effects have been observed [92, 113, 123, 124]. Therefore, we sought to not only determine the abundance but also the functional status of the non-granulocytic myeloid cell populations in the tumor by transcriptomic profiling. Interestingly, we found significantly enriched gene expression for lysosomal and proteasomal processes in monocytes and $Ly6C^{lo}$ $MHCII^{hi}$ cells from tumors of CCL17-deficient single housed mice. Lysosomal and proteasomal activity are crucial for antigen processing, therefore tumor antigen uptake and presentation might be enhanced in monocytes and $Ly6C^{lo}$ $MHCII^{hi}$ cells from tumors of CCL17-deficient single housed mice [125]. Data showing downregulated antigen processing in Irf1-knockout mice, which develop increased numbers of AOM/DSS induced tumors indicate a functional relevance of this effect [121]. Additionally, proteasome inhibition was shown to dampen macrophage pro-inflammatory activity [126]. Functional changes in the myeloid compartment might exert a protective effect in early stages of tumor development. Apart from lysosomal and proteasomal genes, we observed an enrichment in oxidative phosphorylation genes in monocytes and $Ly6C^{lo}$ $MHCII^{hi}$ cells from tumors of CCL17-deficient single housed mice. Studies using *in vitro* differentiated

macrophages have shown a metabolic switch to glycolysis upon LPS/IFN-γ stimulation (M1 polarization) and to oxidative phosphorylation upon M2 polarization with IL-4/IL-13 [127]. Further, the immunosuppressive phenotype of TAMs coincided with increased oxidative phosphorylation (OXPHOS) in several tumor models [128]. However, more recent studies report increased glycolysis instead of increased OXPHOS in suppressive TAMs [129, 130]. Similarly, Soncin et al. show higher glycolytic activity in the $Arg1^{+}$ immunosuppressive macrophage population in colon tumors of DSS treated $APC^{Min/+}$ mice [78]. Thus, transcriptome analysis indicates functional and metabolic alterations in monocytes and $Ly6C^{lo}$ $MHCII^{hi}$ cells from CCL17-deficient single housed mice, which are potentially relevant for tumor incidence and growth. Additionally, functional alterations of the myeloid tumor infiltrating cells in CCL17-deficient single housed mice are also indicated by reduced levels of secreted IL-1β. Elevated levels of IL1-β have been associated with increased AOM/DSS induced tumorigenesis [131, 132]. Further, NLRC4 mediated IL-1β production has been shown to be influenced by the microbiota [133]. Thus, reduced levels of secreted IL1β in the tumor microenvironment might play a protective role in the AOM/DSS induced tumorigenesis in single housed CCL17-deficient mice by e.g. reducing angiogenesis in tumors of CCL17-deficient mice during the tumor initiation phase [134, 135].

Our results show increased CCL17 expression in AOM/DSS induced colonic tumors by myeloid cell populations with relevant functions for tumor induction and progression. Tumor initiation was reduced in single housed CCL17-deficient mice, which showed changes of the microbiota, possibly mediated by increased luminal IgA levels in these mice. Decreased tumor initiation might be caused by elevated apoptosis levels in the early phase of AOM/DSS treatment. Further, changes in myeloid cell functionality in tumors of single housed CCL17-deficient mice coincide with the protective effect in this colon tumor model. Thus, CCL17 influences AOM/DSS induced tumorigenesis on multiple levels, leading to reduced tumor multiplicity.

Acknowledgements

We acknowledge the Core Facility Bioimaging, Biomedical Center, Ludwig-Maximilians-Universität Munich for assistance with confocal microscopy. We would like to thank the BMC Core Facility Flow Cytometry and its manager Dr. Lisa Richter for assistance in flow cytometric analyses and cell sorting.

Funding

RM, MM, SK, and AK were supported by the German Research Foundation (SFB1054/TPA06, KR2199/3-2, KR2199/6- 1, KR2199/9-1) and the Georg and Traud Gravenhorst Stiftung. RM received a Ph.D. scholarship from the Studienstiftung des Deutschen Volkes.

References

1 Bray F, Ferlay J, Soerjomataram I, Siegel RL, Torre LA, Jemal A. Global cancer statistics 2018: GLOBOCAN estimates of incidence and mortality worldwide for 36 cancers in 185 countries. *CA Cancer J Clin* 2018; 68: 394-424.

2 Keum N, Giovannucci E. Global burden of colorectal cancer: emerging trends, risk factors and prevention strategies. *Nat Rev Gastroenterol Hepatol* 2019; 16: 713-732.

3 Rogler G. Chronic ulcerative colitis and colorectal cancer. *Cancer Lett* 2014; 345: 235-241.

4 Grivennikov SI, Cominelli F. Colitis-Associated and Sporadic Colon Cancers: Different Diseases, Different Mutations? *Gastroenterology* 2016; 150: 808-810.

5 Terzic J, Grivennikov S, Karin E, Karin M. Inflammation and colon cancer. *Gastroenterology* 2010; 138: 2101-2114.e2105.

6 Shalapour S, Karin M. Immunity, inflammation, and cancer: an eternal fight between good and evil. *The Journal of clinical investigation* 2015; 125: 3347-3355.

7 Ohtani N. Microbiome and cancer. *Semin Immunopathol* 2015; 37: 65-72.

8 Arthur JC, Perez-Chanona E, Muhlbauer M, Tomkovich S, Uronis JM, Fan TJ, Campbell BJ, Abujamel T, Dogan B, Rogers AB, Rhodes JM, Stintzi A, Simpson KW, Hansen JJ, Keku TO, Fodor AA, Jobin C. Intestinal inflammation targets cancer-inducing activity of the microbiota. *Science* 2012; 338: 120-123.

9 Louis P, Hold GL, Flint HJ. The gut microbiota, bacterial metabolites and colorectal cancer. *Nature reviews Microbiology* 2014; 12: 661-672.

10 Grivennikov SI, Greten FR, Karin M. Immunity, inflammation, and cancer. *Cell* 2010; 140: 883-899.

11 Kong BY, Bolton H, Kim JW, Silveira PA, Fromm PD, Clark GJ. On the Other Side: Manipulating the Immune Checkpoint Landscape of Dendritic Cells to Enhance Cancer Immunotherapy. *Frontiers in Oncology* (Review) 2019; 9.

12 De Oliveira T, Ramakrishnan M, Diamanti MA, Ziegler PK, Brombacher F, Greten FR. Loss of Stat6 affects chromatin condensation in intestinal epithelial cells causing diverse outcome in murine models of inflammation-associated and sporadic colon carcinogenesis. *Oncogene* 2019; 38: 1787-1801.

13 Van der Jeught K, Xu H-C, Li Y-J, Lu X-B, Ji G. Drug resistance and new therapies in colorectal cancer. *World journal of gastroenterology* 2018; 24: 3834-3848.

14 Ganesh K, Stadler ZK, Cercek A, Mendelsohn RB, Shia J, Segal NH, Diaz LA, Jr. Immunotherapy in colorectal cancer: rationale, challenges and potential. *Nat Rev Gastroenterol Hepatol* 2019; 16: 361-375.

15 Marques I, Araújo A, de Mello RA. Anti-angiogenic therapies for metastatic colorectal cancer: current and future perspectives. *World journal of gastroenterology* 2013; 19: 7955-7971.

16 Wunderlich CM, Ackermann PJ, Ostermann AL, Adams-Quack P, Vogt MC, Tran M-L, Nikolajev A, Waisman A, Garbers C, Theurich S, Mauer J, Hövelmeyer N, Wunderlich FT. Obesity exacerbates colitis-associated cancer via IL-6-regulated macrophage polarisation and CCL-20/CCR-6-mediated lymphocyte recruitment. *Nature communications* 2018; 9: 1646.

17 Halama N, Zoernig I, Berthel A, Kahlert C, Klupp F, Suarez-Carmona M, Suetterlin T, Brand K, Krauss J, Lasitschka F, Lerchl T, Luckner-Minden C, Ulrich A, Koch M, Weitz J, Schneider M, Buechler MW, Zitvogel L, Herrmann T, Benner A, Kunz C, Luecke S, Springfeld C, Grabe N, Falk CS, Jaeger D. Tumoral Immune Cell Exploitation in Colorectal Cancer Metastases Can Be Targeted Effectively by Anti-CCR5 Therapy in Cancer Patients. *Cancer Cell* 2016; 29: 587-601.

18 Sierra-Filardi E, Nieto C, Dominguez-Soto A, Barroso R, Sanchez-Mateos P, Puig-Kroger A, Lopez-Bravo M, Joven J, Ardavin C, Rodriguez-Fernandez JL, Sanchez-Torres C, Mellado M, Corbi AL. CCL2 shapes macrophage polarization by GM-CSF and M-CSF: identification of CCL2/CCR2-dependent gene expression profile. *Journal of immunology* 2014; 192: 3858-3867.

19 Wang N, Liu W, Zheng Y, Wang S, Yang B, Li M, Song J, Zhang F, Zhang X, Wang Q, Wang Z. CXCL1 derived from tumor-associated macrophages promotes breast cancer metastasis via activating NF-κB/SOX4 signaling. *Cell Death & Disease* 2018; 9: 880.

20 Forst B, Hansen MT, Klingelhofer J, Moller HD, Nielsen GH, Grum-Schwensen B, Ambartsumian N, Lukanidin E, Grigorian M. Metastasis-inducing S100A4 and RANTES cooperate in promoting tumor progression in mice. *PloS one* 2010; 5: e10374.

21 Inngjerdingen M, Damaj B, Maghazachi AA. Human NK cells express CC chemokine receptors 4 and 8 and respond to thymus and activation-regulated chemokine, macrophage-derived chemokine, and I-309. *Journal of immunology* 2000; 164: 4048-4054.

22 Iellem A, Mariani M, Lang R, Recalde H, Panina-Bordignon P, Sinigaglia F, D'Ambrosio D. Unique chemotactic response profile and specific expression of chemokine receptors CCR4 and CCR8 by CD4(+)CD25(+) regulatory T cells. *The Journal of experimental medicine* 2001; 194: 847-853.

23 Scheu S, Ali S, Ruland C, Arolt V, Alferink J. The C-C Chemokines CCL17 and CCL22 and Their Receptor CCR4 in CNS Autoimmunity. *Int J Mol Sci* 2017; 18: 2306.

24 Imai T, Chantry D, Raport CJ, Wood CL, Nishimura M, Godiska R, Yoshie O, Gray PW. Macrophage-derived chemokine is a functional ligand for the CC chemokine receptor 4. *J Biol Chem* 1998; 273: 1764-1768.

25 Imai T, Baba M, Nishimura M, Kakizaki M, Takagi S, Yoshie O. The T cell-directed CC chemokine TARC is a highly specific biological ligand for CC chemokine receptor 4. *J Biol Chem* 1997; 272: 15036-15042.

26 Heiseke AF, Faul AC, Lehr HA, Forster I, Schmid RM, Krug AB, Reindl W. CCL17 promotes intestinal inflammation in mice and counteracts regulatory T cell-mediated protection from colitis. *Gastroenterology* 2012; 142: 335-345.

27 Ruland C, Renken H, Kuzmanov I, Fattahi Mehr A, Schwarte K, Cerina M, Herrmann A, Otte D-M, Zimmer A, Schwab N, Meuth SG, Arolt V, Klotz L, Förster I, Scheu S, Alferink J. Chemokine CCL17 is expressed by dendritic cells in the CNS during experimental autoimmune encephalomyelitis and promotes pathogenesis of disease. *Brain, Behavior, and Immunity* 2017; 66: 382-393.

28 Stutte S, Quast T, Gerbitzki N, Savinko T, Novak N, Reifenberger J, Homey B, Kolanus W, Alenius H, Forster I. Requirement of CCL17 for CCR7- and CXCR4-dependent migration of cutaneous dendritic cells. *Proceedings of the National Academy of Sciences of the United States of America* 2010; 107: 8736-8741.

29 Weber C, Meiler S, Doring Y, Koch M, Drechsler M, Megens RT, Rowinska Z, Bidzhekov K, Fecher C, Ribechini E, van Zandvoort MA, Binder CJ, Jelinek I, Hristov M, Boon L, Jung S, Korn T, Lutz MB, Forster I, Zenke M, Hieronymus T, Junt T, Zernecke A. CCL17-expressing dendritic cells drive atherosclerosis by restraining regulatory T cell homeostasis in mice. *The Journal of clinical investigation* 2011; 121: 2898-2910.

30 Lee M-C, Saleh R, Achuthan A, Fleetwood AJ, Förster I, Hamilton JA, Cook AD. CCL17 blockade as a therapy for osteoarthritis pain and disease. *Arthritis Research & Therapy* 2018; 20: 62.

31 Alferink J, Lieberam I, Reindl W, Behrens A, Weiß S, Hüser N, Gerauer K, Ross R, Reske-Kunz AB, Ahmad-Nejad P, Wagner H, Förster I. Compartmentalized Production of CCL17 In Vivo : Strong Inducibility in Peripheral Dendritic Cells Contrasts Selective Absence from the Spleen. *The Journal of experimental medicine* 2003; 197: 585-599.

32 Globisch T, Steiner N, Fülle L, Lukacs-Kornek V, Degrandi D, Dresing P, Alferink J, Lang R, Pfeffer K, Beyer M, Weighardt H, Kurts C, Ulas T, Schultze JL, Förster I. Cytokine-dependent regulation of dendritic cell differentiation in the splenic microenvironment. *European journal of immunology* 2014; 44: 500-510.

33 Lee M-C, Lacey DC, Fleetwood AJ, Achuthan A, Hamilton JA, Cook AD. GM-CSF– and IRF4-Dependent Signaling Can Regulate Myeloid Cell Numbers and the Macrophage Phenotype during Inflammation. *The Journal of Immunology* 2019; 202: 3033-3040.

34 Metzger R, Maruskova M, Krebs S, Janssen K-P, Krug AB. Increased Incidence of Colon Tumors in AOM-Treated Apc1638N/+ Mice Reveals Higher Frequency of Tumor

Associated Neutrophils in Colon Than Small Intestine. *Frontiers in Oncology* (Methods) 2019; 9.

35 Mortaz E, Alipoor SD, Adcock IM, Mumby S, Koenderman L. Update on Neutrophil Function in Severe Inflammation. *Frontiers in Immunology* (Review) 2018; 9.

36 Da Silva C, Wagner C, Bonnardel J, Gorvel J-P, Lelouard H. The Peyer's Patch Mononuclear Phagocyte System at Steady State and during Infection. *Frontiers in Immunology* (Review) 2017; 8.

37 Joeris T, Muller-Luda K, Agace WW, Mowat AM. Diversity and functions of intestinal mononuclear phagocytes. *Mucosal immunology* 2017; 10: 845-864.

38 Lande R, Gilliet M. Plasmacytoid dendritic cells: key players in the initiation and regulation of immune responses. *Ann N Y Acad Sci* 2010; 1183: 89-103.

39 Honda K, Yanai H, Negishi H, Asagiri M, Sato M, Mizutani T, Shimada N, Ohba Y, Takaoka A, Yoshida N, Taniguchi T. IRF-7 is the master regulator of type-I interferon-dependent immune responses. *Nature* 2005; 434: 772-777.

40 den Haan JM, Lehar SM, Bevan MJ. CD8(+) but not CD8(-) dendritic cells cross-prime cytotoxic T cells in vivo. *The Journal of experimental medicine* 2000; 192: 1685-1696.

41 Schlitzer A, McGovern N, Teo P, Zelante T, Atarashi K, Low D, Ho AW, See P, Shin A, Wasan PS, Hoeffel G, Malleret B, Heiseke A, Chew S, Jardine L, Purvis HA, Hilkens CM, Tam J, Poidinger M, Stanley ER, Krug AB, Renia L, Sivasankar B, Ng LG, Collin M, Ricciardi-Castagnoli P, Honda K, Haniffa M, Ginhoux F. IRF4 transcription factor-dependent CD11b+ dendritic cells in human and mouse control mucosal IL-17 cytokine responses. *Immunity* 2013; 38: 970-983.

42 Persson EK, Uronen-Hansson H, Semmrich M, Rivollier A, Hagerbrand K, Marsal J, Gudjonsson S, Hakansson U, Reizis B, Kotarsky K, Agace WW. IRF4 transcription-factor-dependent CD103(+)CD11b(+) dendritic cells drive mucosal T helper 17 cell differentiation. *Immunity* 2013; 38: 958-969.

43 Bain CC, Scott CL, Uronen-Hansson H, Gudjonsson S, Jansson O, Grip O, Guilliams M, Malissen B, Agace WW, Mowat AM. Resident and pro-inflammatory macrophages in the colon represent alternative context-dependent fates of the same Ly6Chi monocyte precursors. *Mucosal immunology* 2013; 6: 498-510.

44 Bain CC, Mowat AM. The monocyte-macrophage axis in the intestine. *Cell Immunol* 2014; 291: 41-48.

45 Schreiber HA, Loschko J, Karssemeijer RA, Escolano A, Meredith MM, Mucida D, Guermonprez P, Nussenzweig MC. Intestinal monocytes and macrophages are required for T cell polarization in response to Citrobacter rodentium. *The Journal of experimental medicine* 2013; 210: 2025-2039.

46 Mazzini E, Massimiliano L, Penna G, Rescigno M. Oral tolerance can be established via gap junction transfer of fed antigens from CX3CR1(+) macrophages to CD103(+) dendritic cells. *Immunity* 2014; 40: 248-261.

47 Roberts EW, Broz ML, Binnewies M, Headley MB, Nelson AE, Wolf DM, Kaisho T, Bogunovic D, Bhardwaj N, Krummel MF. Critical Role for CD103+/CD141+ Dendritic Cells Bearing CCR7 for Tumor Antigen Trafficking and Priming of T Cell Immunity in Melanoma. *Cancer Cell* 2016; 30: 324-336.

48 Grivennikov S, Karin E, Terzic J, Mucida D, Yu GY, Vallabhapurapu S, Scheller J, Rose-John S, Cheroutre H, Eckmann L, Karin M. IL-6 and Stat3 are required for survival of intestinal epithelial cells and development of colitis-associated cancer. *Cancer Cell* 2009; 15: 103-113.

49 Pabst O. New concepts in the generation and functions of IgA. *Nat Rev Immunol* 2012; 12: 821-832.

50 Neufert C, Becker C, Neurath MF. An inducible mouse model of colon carcinogenesis for the analysis of sporadic and inflammation-driven tumor progression. *Nat Protoc* 2007; 2: 1998-2004.

51 Biehl LM, Garzetti D, Farowski F, Ring D, Koeppel MB, Rohde H, Schafhausen P, Stecher B, Vehreschild M. Usability of rectal swabs for microbiome sampling in a cohort study of hematological and oncological patients. *PloS one* 2019; 14: e0215428.

52 Caporaso JG, Kuczynski J, Stombaugh J, Bittinger K, Bushman FD, Costello EK, Fierer N, Pena AG, Goodrich JK, Gordon JI, Huttley GA, Kelley ST, Knights D, Koenig JE, Ley RE, Lozupone CA, McDonald D, Muegge BD, Pirrung M, Reeder J, Sevinsky JR, Turnbaugh PJ, Walters WA, Widmann J, Yatsunenko T, Zaneveld J, Knight R. QIIME allows analysis of high-throughput community sequencing data. *Nat Methods* 2010; 7: 335-336.

53 Edgar RC. Search and clustering orders of magnitude faster than BLAST. *Bioinformatics* 2010; 26: 2460-2461.

54 Quast C, Pruesse E, Yilmaz P, Gerken J, Schweer T, Yarza P, Peplies J, Glockner FO. The SILVA ribosomal RNA gene database project: improved data processing and web-based tools. *Nucleic Acids Res* 2013; 41: D590-596.

55 Segata N, Izard J, Waldron L, Gevers D, Miropolsky L, Garrett WS, Huttenhower C. Metagenomic biomarker discovery and explanation. *Genome Biology* 2011; 12: R60.

56 Pfaffl MW. A new mathematical model for relative quantification in real-time RT-PCR. *Nucleic acids research* 2001; 29: e45-e45.

57 Weber J, de la Rosa J, Grove CS, Schick M, Rad L, Baranov O, Strong A, Pfaus A, Friedrich MJ, Engleitner T, Lersch R, Öllinger R, Grau M, Menendez IG, Martella M, Kohlhofer U, Banerjee R, Turchaninova MA, Scherger A, Hoffman GJ, Hess J, Kuhn LB, Ammon T, Kim J, Schneider G, Unger K, Zimber-Strobl U, Heikenwälder M, Schmidt-Supprian M, Yang F, Saur D, Liu P, Steiger K, Chudakov DM, Lenz G, Quintanilla-Martinez L, Keller U, Vassiliou GS, Cadiñanos J, Bradley A, Rad R. PiggyBac transposon tools for recessive screening identify B-cell lymphoma drivers in mice. *Nature communications* 2019; 10: 1415.

58 Schetters STT, Kruijssen LJW, Crommentuijn MHW, Kalay H, Ochando J, den Haan JMM, Garcia-Vallejo JJ, van Kooyk Y. Mouse DC-SIGN/CD209a as Target for Antigen Delivery and Adaptive Immunity. *Frontiers in Immunology* (Original Research) 2018; 9.

59 Scodeller P, Simón-Gracia L, Kopanchuk S, Tobi A, Kilk K, Säälik P, Kurm K, Squadrito ML, Kotamraju VR, Rinken A, De Palma M, Ruoslahti E, Teesalu T. Precision Targeting of Tumor Macrophages with a CD206 Binding Peptide. *Scientific Reports* 2017; 7: 14655.

60 Murray PJ. Macrophage Polarization. *Annu Rev Physiol* 2017; 79: 541-566.

61 Moor K, Diard M, Sellin ME, Felmy B, Wotzka SY, Toska A, Bakkeren E, Arnoldini M, Bansept F, Co AD, Völler T, Minola A, Fernandez-Rodriguez B, Agatic G, Barbieri S, Piccoli L, Casiraghi C, Corti D, Lanzavecchia A, Regoes RR, Loverdo C, Stocker R, Brumley DR, Hardt W-D, Slack E. High-avidity IgA protects the intestine by enchaining growing bacteria. *Nature* 2017; 544: 498-502.

62 Chagwedera DN, Ang QY, Bisanz JE, Leong YA, Ganeshan K, Cai J, Patterson AD, Turnbaugh PJ, Chawla A. Nutrient Sensing in CD11c Cells Alters the Gut Microbiota to Regulate Food Intake and Body Mass. *Cell Metabolism* 2019; 30: 364-373.e367.

63 Perlman H, Zhang X, Chen MW, Walsh K, Buttyan R. An elevated bax/bcl-2 ratio corresponds with the onset of prostate epithelial cell apoptosis. *Cell Death Differ* 1999; 6: 48-54.

64 Binnewies M, Roberts EW, Kersten K, Chan V, Fearon DF, Merad M, Coussens LM, Gabrilovich DI, Ostrand-Rosenberg S, Hedrick CC, Vonderheide RH, Pittet MJ, Jain RK, Zou W, Howcroft TK, Woodhouse EC, Weinberg RA, Krummel MF. Understanding the tumor immune microenvironment (TIME) for effective therapy. *Nature medicine* 2018; 24: 541-550.

65 Noguti J, Chan AA, Bandera B, Brislawn CJ, Protic M, Sim MS, Jansson JK, Bilchik AJ, Lee DJ. Both the intratumoral immune and microbial microenvironment are linked to recurrence in human colon cancer: results from a prospective, multicenter nodal ultrastaging trial. *Oncotarget* 2018; 9: 23564-23576.

66 Valente M, Dolen Y, van Dinther E, Vimeux L, Fallet M, Feuillet V, Figdor CG. Cross-talk between iNKT cells and CD8 T cells in the spleen requires the IL-4/CCL17 axis for the generation of short-lived effector cells. *Proceedings of the National Academy of Sciences of the United States of America* 2019; 116: 25816-25827.

67 Perry CJ, Muñoz-Rojas AR, Meeth KM, Kellman LN, Amezquita RA, Thakral D, Du VY, Wang JX, Damsky W, Kuhlmann AL, Sher JW, Bosenberg M, Miller-Jensen K, Kaech SM. Myeloid-targeted immunotherapies act in synergy to induce inflammation and antitumor immunity. *The Journal of experimental medicine* 2018; 215: 877-893.

68 Schridde A, Bain CC, Mayer JU, Montgomery J, Pollet E, Denecke B, Milling SWF, Jenkins SJ, Dalod M, Henri S, Malissen B, Pabst O, McL Mowat A. Tissue-specific differentiation of colonic macrophages requires TGFbeta receptor-mediated signaling. *Mucosal immunology* 2017; 10: 1387-1399.

69 Kraft-Terry SD, Gendelman HE. Proteomic biosignatures for monocyte–macrophage differentiation. *Cellular Immunology* 2011; 271: 239-255.

70 Naumov I, Zilberberg A, Shapira S, Avivi D, Kazanov D, Rosin-Arbesfeld R, Arber N, Kraus S. CD24 knockout prevents colorectal cancer in chemically induced colon carcinogenesis and in APC(Min)/CD24 double knockout transgenic mice. *Int J Cancer* 2014; 135: 1048-1059.

71 Chen GY, Tang J, Zheng P, Liu Y. CD24 and Siglec-10 selectively repress tissue damage-induced immune responses. *Science* 2009; 323: 1722-1725.

72 Barkal AA, Brewer RE, Markovic M, Kowarsky M, Barkal SA, Zaro BW, Krishnan V, Hatakeyama J, Dorigo O, Barkal LJ, Weissman IL. CD24 signalling through macrophage Siglec-10 is a target for cancer immunotherapy. *Nature* 2019; 572: 392-396.

73 Carreras-Gonzalez A, Barriales D, Palacios A, Montesinos-Robledo M, Navasa N, Azkargorta M, Pena-Cearra A, Tomas-Cortazar J, Escobes I, Pascual-Itoiz MA, Hradiska J, Kopecky J, Gil-Carton D, Prados-Rosales R, Abecia L, Atondo E, Martin I, Pellon A, Elortza F, Rodriguez H, Anguita J. Regulation of macrophage activity by surface receptors contained within Borrelia burgdorferi-enriched phagosomal fractions. *PLoS Pathog* 2019; 15: e1008163.

74 Mantovani A, Allavena P, Sica A. Tumour-associated macrophages as a prototypic type II polarised phagocyte population: role in tumour progression. *European Journal of Cancer* 2004; 40: 1660-1667.

75 Luo Y, Zhou H, Krueger J, Kaplan C, Lee S-H, Dolman C, Markowitz D, Wu W, Liu C, Reisfeld RA, Xiang R. Targeting tumor-associated macrophages as a novel strategy against breast cancer. *The Journal of clinical investigation* 2006; 116: 2132-2141.

76 Movahedi K, Schoonooghe S, Laoui D, Houbracken I, Waelput W, Breckpot K, Bouwens L, Lahoutte T, De Baetselier P, Raes G, Devoogdt N, Van Ginderachter JA. Nanobody-based targeting of the macrophage mannose receptor for effective in vivo imaging of tumor-associated macrophages. *Cancer Res* 2012; 72: 4165-4177.

77 Georgoudaki AM, Prokopec KE, Boura VF, Hellqvist E, Sohn S, Ostling J, Dahan R, Harris RA, Rantalainen M, Klevebring D, Sund M, Brage SE, Fuxe J, Rolny C, Li F, Ravetch JV, Karlsson MC. Reprogramming Tumor-Associated Macrophages by Antibody Targeting Inhibits Cancer Progression and Metastasis. *Cell reports* 2016; 15: 2000-2011.

78 Soncin I, Sheng J, Chen Q, Foo S, Duan K, Lum J, Poidinger M, Zolezzi F, Karjalainen K, Ruedl C. The tumour microenvironment creates a niche for the self-renewal of tumour-promoting macrophages in colon adenoma. *Nature communications* 2018; 9: 582.

79 Singh K, Coburn LA, Asim M, Barry DP, Allaman MM, Shi C, Washington MK, Luis PB, Schneider C, Delgado AG, Piazuelo MB, Cleveland JL, Gobert AP, Wilson KT. Ornithine Decarboxylase in Macrophages Exacerbates Colitis and Promotes Colitis-Associated Colon Carcinogenesis by Impairing M1 Immune Responses. *Cancer Research* 2018; 78: 4303-4315.

80 Viennois E, Merlin D, Gewirtz AT, Chassaing B. Dietary Emulsifier-Induced Low-Grade Inflammation Promotes Colon Carcinogenesis. *Cancer Res* 2017; 77: 27-40.

81 Hu B, Elinav E, Huber S, Booth CJ, Strowig T, Jin C, Eisenbarth SC, Flavell RA. Inflammation-induced tumorigenesis in the colon is regulated by caspase-1 and NLRC4. *Proceedings of the National Academy of Sciences* 2010; 107: 21635-21640.

82 Kesselring R, Glaesner J, Hiergeist A, Naschberger E, Neumann H, Brunner Stefan M, Wege Anja K, Seebauer C, Köhl G, Merkl S, Croner Roland S, Hackl C, Stürzl M, Neurath Markus F, Gessner A, Schlitt H-J, Geissler Edward K, Fichtner-Feigl S. IRAK-M Expression in Tumor Cells Supports Colorectal Cancer Progression through Reduction of Antimicrobial Defense and Stabilization of STAT3. *Cancer Cell* 2016; 29: 684-696.

83 Barrett CW, Fingleton B, Williams A, Ning W, Fischer MA, Washington MK, Chaturvedi R, Wilson KT, Hiebert SW, Williams CS. MTGR1 Is Required for Tumorigenesis in the Murine AOM/DSS Colitis-Associated Carcinoma Model. *Cancer Research* 2011; 71: 1302-1312.

84 Tschurtschenthaler M, Wang J, Fricke C, Fritz TMJ, Niederreiter L, Adolph TE, Sarcevic E, Künzel S, Offner FA, Kalinke U, Baines JF, Tilg H, Kaser A. Type I interferon signalling in the intestinal epithelium affects Paneth cells, microbial ecology and epithelial regeneration. *Gut* 2014; 63: 1921-1931.

85 Man SM, Zhu Q, Zhu L, Liu Z, Karki R, Malik A, Sharma D, Li L, Malireddi RK, Gurung P, Neale G, Olsen SR, Carter RA, McGoldrick DJ, Wu G, Finkelstein D, Vogel P, Gilbertson RJ, Kanneganti TD. Critical Role for the DNA Sensor AIM2 in Stem Cell Proliferation and Cancer. *Cell* 2015; 162: 45-58.

86 Zhan Y, Chen P-J, Sadler WD, Wang F, Poe S, Nunez G, Eaton KA, Chen GY. Gut microbiota protects against gastrointestinal tumorigenesis caused by epithelial injury. *Cancer Research* 2013: canres.0827.2013.

87 Lee YP, Chiu CC, Lin TJ, Hung SW, Huang WC, Chiu CF, Huang YT, Chen YH, Chen TH, Chuang HL. The germ-free mice monocolonization with Bacteroides fragilis improves azoxymethane/dextran sulfate sodium induced colitis-associated colorectal cancer. *Immunopharmacol Immunotoxicol* 2019; 41: 207-213.

88 Klimesova K, Kverka M, Zakostelska Z, Hudcovic T, Hrncir T, Stepankova R, Rossmann P, Ridl J, Kostovcik M, Mrazek J, Kopecny J, Kobayashi KS, Tlaskalova-Hogenova H. Altered gut microbiota promotes colitis-associated cancer in IL-1 receptor-associated kinase M-deficient mice. *Inflammatory bowel diseases* 2013; 19: 1266-1277.

89 Cevallos SA, Lee J-Y, Tiffany CR, Byndloss AJ, Johnston L, Byndloss MX, Bäumler AJ. Increased Epithelial Oxygenation Links Colitis to an Expansion of Tumorigenic Bacteria. *MBio* 2019; 10: e02244-02219.

90 Malik A, Sharma D, Zhu Q, Karki R, Guy CS, Vogel P, Kanneganti T-D. IL-33 regulates the IgA-microbiota axis to restrain IL-1α–dependent colitis and tumorigenesis. *The Journal of clinical investigation* 2016; 126: 4469-4481.

91 Li S, Fu C, Zhao Y, He J. Intervention with α-Ketoglutarate Ameliorates Colitis-Related Colorectal Carcinoma via Modulation of the Gut Microbiome. *BioMed research international* 2019; 2019: 8020785-8020785.

92 Marelli G, Erreni M, Anselmo A, Taverniti V, Guglielmetti S, Mantovani A, Allavena P. Heme-oxygenase-1 Production by Intestinal CX3CR1(+) Macrophages Helps to Resolve Inflammation and Prevents Carcinogenesis. *Cancer Res* 2017; 77: 4472-4485.

93 Wu M, Li J, An Y, Li P, Xiong W, Li J, Yan D, Wang M, Zhong G. Chitooligosaccharides Prevents the Development of Colitis-Associated Colorectal Cancer by Modulating the Intestinal Microbiota and Mycobiota. *Frontiers in Microbiology* (Original Research) 2019; 10.

94 Chen L, Jiang B, Zhong C, Guo J, Zhang L, Mu T, Zhang Q, Bi X. Chemoprevention of colorectal cancer by black raspberry anthocyanins involved the modulation of gut microbiota and SFRP2 demethylation. *Carcinogenesis* 2018; 39: 471-481.

95 Cao S, Su X, Zeng B, Yan H, Huang Y, Wang E, Yun H, Zhang Y, Liu F, Li W, Wei H, Che Y, Yang R. The Gut Epithelial Receptor LRRC19 Promotes the Recruitment of Immune Cells and Gut Inflammation. *Cell reports* 2016; 14: 695-707.

96 Wolf M, Moser B. Antimicrobial activities of chemokines: not just a side-effect? *Front Immunol* 2012; 3: 213.

97 Hieshima K, Ohtani H, Shibano M, Izawa D, Nakayama T, Kawasaki Y, Shiba F, Shiota M, Katou F, Saito T, Yoshie O. CCL28 has dual roles in mucosal immunity as a chemokine with broad-spectrum antimicrobial activity. *Journal of immunology* 2003; 170: 1452-1461.

98 Yang D, Chen Q, Hoover DM, Staley P, Tucker KD, Lubkowski J, Oppenheim JJ. Many chemokines including CCL20/MIP-3alpha display antimicrobial activity. *J Leukoc Biol* 2003; 74: 448-455.

99 Grootjans J, Krupka N, Hosomi S, Matute JD, Hanley T, Saveljeva S, Gensollen T, Heijmans J, Li H, Limenitakis JP, Ganal-Vonarburg SC, Suo S, Luoma AM, Shimodaira Y, Duan J, Shih DQ, Conner ME, Glickman JN, Fuhler GM, Palm NW, de Zoete MR, van der Woude CJ, Yuan G-C, Wucherpfennig KW, Targan SR, Rosenstiel P, Flavell RA, McCoy KD, Macpherson AJ, Kaser A, Blumberg RS. Epithelial endoplasmic reticulum stress orchestrates a protective IgA response. *Science* 2019; 363: 993-998.

100 Donaldson GP, Ladinsky MS, Yu KB, Sanders JG, Yoo BB, Chou WC, Conner ME, Earl AM, Knight R, Bjorkman PJ, Mazmanian SK. Gut microbiota utilize immunoglobulin A for mucosal colonization. *Science* 2018; 360: 795-800.

101 Fadlallah J, El Kafsi H, Sterlin D, Juste C, Parizot C, Dorgham K, Autaa G, Gouas D, Almeida M, Lepage P, Pons N, Le Chatelier E, Levenez F, Kennedy S, Galleron N, de Barros J-PP, Malphettes M, Galicier L, Boutboul D, Mathian A, Miyara M, Oksenhendler E, Amoura Z, Doré J, Fieschi C, Ehrlich SD, Larsen M, Gorochov G. Microbial ecology perturbation in human IgA deficiency. *Science Translational Medicine* 2018; 10: eaan1217.

102 Cullender Tyler C, Chassaing B, Janzon A, Kumar K, Muller Catherine E, Werner Jeffrey J, Angenent Largus T, Bell ME, Hay Anthony G, Peterson Daniel A, Walter J, Vijay-Kumar M, Gewirtz Andrew T, Ley Ruth E. Innate and Adaptive Immunity Interact to Quench Microbiome Flagellar Motility in the Gut. *Cell Host & Microbe* 2013; 14: 571-581.

103 Peterson DA, McNulty NP, Guruge JL, Gordon JI. IgA Response to Symbiotic Bacteria as a Mediator of Gut Homeostasis. *Cell Host & Microbe* 2007; 2: 328-339.

104 Nakajima A, Vogelzang A, Maruya M, Miyajima M, Murata M, Son A, Kuwahara T, Tsuruyama T, Yamada S, Matsuura M, Nakase H, Peterson DA, Fagarasan S, Suzuki K. IgA regulates the composition and metabolic function of gut microbiota by promoting symbiosis between bacteria. *The Journal of experimental medicine* 2018; 215: 2019-2034.

105 Pabst O, Slack E. IgA and the intestinal microbiota: the importance of being specific. *Mucosal immunology* 2020; 13: 12-21.

106 Sterlin D, Fadlallah J, Slack E, Gorochov G. The antibody/microbiota interface in health and disease. *Mucosal immunology* 2020; 13: 3-11.

107 Palm NW, de Zoete MR, Cullen TW, Barry NA, Stefanowski J, Hao L, Degnan PH, Hu J, Peter I, Zhang W, Ruggiero E, Cho JH, Goodman AL, Flavell RA. Immunoglobulin A coating identifies colitogenic bacteria in inflammatory bowel disease. *Cell* 2014; 158: 1000-1010.

108 Kau AL, Planer JD, Liu J, Rao S, Yatsunenko T, Trehan I, Manary MJ, Liu TC, Stappenbeck TS, Maleta KM, Ashorn P, Dewey KG, Houpt ER, Hsieh CS, Gordon JI. Functional characterization of IgA-targeted bacterial taxa from undernourished Malawian children that produce diet-dependent enteropathy. *Sci Transl Med* 2015; 7: 276ra224.

109 D'Auria G, Peris-Bondia F, Džunková M, Mira A, Collado MC, Latorre A, Moya A. Active and secreted IgA-coated bacterial fractions from the human gut reveal an under-represented microbiota core. *Scientific Reports* 2013; 3: 3515.

110 Malik A, Sharma D, Malireddi RKS, Guy CS, Chang T-C, Olsen SR, Neale G, Vogel P, Kanneganti T-D. SYK-CARD9 Signaling Axis Promotes Gut Fungi-Mediated Inflammasome Activation to Restrict Colitis and Colon Cancer. *Immunity* 2018; 49: 515-530.e515.

111 Kim Y-I, Song J-H, Ko H-J, Kweon M-N, Kang C-Y, Reinecker H-C, Chang S-Y. CX3CR1+ Macrophages and CD8+ T Cells Control Intestinal IgA Production. *The Journal of Immunology* 2018; 201: 1287-1294.

112 Flores-Langarica A, Müller Luda K, Persson EK, Cook CN, Bobat S, Marshall JL, Dahlgren MW, Hägerbrand K, Toellner KM, Goodall MD, Withers DR, Henderson IR, Johansson Lindbom B, Cunningham AF, Agace WW. CD103+CD11b+ mucosal classical dendritic cells initiate long-term switched antibody responses to flagellin. *Mucosal immunology* 2018; 11: 681-692.

113 McDonough EM, Barrett CW, Parang B, Mittal MK, Smith JJ, Bradley AM, Choksi YA, Coburn LA, Short SP, Thompson JJ, Zhang B, Poindexter SV, Fischer MA, Chen X, Li J, Revetta FL, Naik R, Washington MK, Rosen MJ, Hiebert SW, Wilson KT, Williams CS. MTG16 is a tumor suppressor in colitis-associated carcinoma. *JCI Insight* 2017; 2: e78210.

114 Huber S, Gagliani N, Zenewicz LA, Huber FJ, Bosurgi L, Hu B, Hedl M, Zhang W, O'Connor W, Jr., Murphy AJ, Valenzuela DM, Yancopoulos GD, Booth CJ, Cho JH, Ouyang W, Abraham C, Flavell RA. IL-22BP is regulated by the inflammasome and modulates tumorigenesis in the intestine. *Nature* 2012; 491: 259-263.

115 Greten FR, Eckmann L, Greten TF, Park JM, Li Z-W, Egan LJ, Kagnoff MF, Karin M. IKKβ Links Inflammation and Tumorigenesis in a Mouse Model of Colitis-Associated Cancer. *Cell* 2004; 118: 285-296.

116 Dorsam B, Seiwert N, Foersch S, Stroh S, Nagel G, Begaliew D, Diehl E, Kraus A, McKeague M, Minneker V, Roukos V, Reissig S, Waisman A, Moehler M, Stier A, Mangerich A, Dantzer F, Kaina B, Fahrer J. PARP-1 protects against colorectal tumor induction, but promotes inflammation-driven colorectal tumor progression. *Proceedings of the National Academy of Sciences of the United States of America* 2018; 115: E4061-e4070.

117 Hirata A, Hashimoto H, Shibasaki C, Narumi K, Aoki K. Intratumoral IFN-α gene delivery reduces tumor-infiltrating regulatory T cells through the downregulation of tumor CCL17 expression. *Cancer Gene Therapy* 2019; 26: 334-343.

118 Anz D, Rapp M, Eiber S, Koelzer VH, Thaler R, Haubner S, Knott M, Nagel S, Golic M, Wiedemann GM, Bauernfeind F, Wurzenberger C, Hornung P, Veit, Scholz C, Mayr D, Rothenfusser S, Endres S, Bourquin C. Suppression of intratumoral CCL22 by type I interferon inhibits migration of regulatory T cells and blocks cancer progression. *Cancer Research* 2015: canres.3499.2014.

119 Katoh H, Wang D, Daikoku T, Sun H, Dey SK, Dubois RN. CXCR2-expressing myeloid-derived suppressor cells are essential to promote colitis-associated tumorigenesis. *Cancer Cell* 2013; 24: 631-644.

120 Wang T, Fan C, Yao A, Xu X, Zheng G, You Y, Jiang C, Zhao X, Hou Y, Hung MC, Lin X. The Adaptor Protein CARD9 Protects against Colon Cancer by Restricting Mycobiota-Mediated Expansion of Myeloid-Derived Suppressor Cells. *Immunity* 2018; 49: 504-514.e504.

121 Jeyakumar T, Fodil N, Van Der Kraak L, Meunier C, Cayrol R, McGregor K, Langlais D, Greenwood CMT, Beauchemin N, Gros P. Inactivation of Interferon Regulatory Factor 1 Causes Susceptibility to Colitis-Associated Colorectal Cancer. *Sci Rep* 2019; 9: 18897.

122 Chen X, Takemoto Y, Deng H, Middelhoff M, Friedman RA, Chu TH, Churchill MJ, Ma Y, Nagar KK, Tailor YH, Mukherjee S, Wang TC. Histidine decarboxylase (HDC)-expressing granulocytic myeloid cells induce and recruit Foxp3+ regulatory T cells in murine colon cancer. *OncoImmunology* 2017; 6: e1290034.

123 Ke Z, Wang C, Wu T, Wang W, Yang Y, Dai Y. PAR2 deficiency enhances myeloid cell-mediated immunosuppression and promotes colitis-associated tumorigenesis. *Cancer Lett* 2020; 469: 437-446.

124 Hull MA, Cuthbert RJ, Ko CWS, Scott DJ, Cartwright EJ, Hawcroft G, Perry SL, Ingram N, Carr IM, Markham AF, Bonifer C, Coletta PL. Paracrine cyclooxygenase-2 activity by macrophages drives colorectal adenoma progression in the Apc (Min/+) mouse model of intestinal tumorigenesis. *Sci Rep* 2017; 7: 6074.

125 Roche PA, Cresswell P. Antigen Processing and Presentation Mechanisms in Myeloid Cells. *Microbiol Spectr* 2016; 4.

126 Qureshi AA, Guan XQ, Reis JC, Papasian CJ, Jabre S, Morrison DC, Qureshi N. Inhibition of nitric oxide and inflammatory cytokines in LPS-stimulated murine macrophages by resveratrol, a potent proteasome inhibitor. *Lipids Health Dis* 2012; 11: 76-76.

127 Freemerman AJ, Johnson AR, Sacks GN, Milner JJ, Kirk EL, Troester MA, Macintyre AN, Goraksha-Hicks P, Rathmell JC, Makowski L. Metabolic reprogramming of macrophages: glucose transporter 1 (GLUT1)-mediated glucose metabolism drives a proinflammatory phenotype. *J Biol Chem* 2014; 289: 7884-7896.

128 Wang S, Liu R, Yu Q, Dong L, Bi Y, Liu G. Metabolic reprogramming of macrophages during infections and cancer. *Cancer Letters* 2019; 452: 14-22.

129 Netea-Maier RT, Smit JWA, Netea MG. Metabolic changes in tumor cells and tumor-associated macrophages: A mutual relationship. *Cancer Letters* 2018; 413: 102-109.

130 Arts RJ, Plantinga TS, Tuit S, Ulas T, Heinhuis B, Tesselaar M, Sloot Y, Adema GJ, Joosten LA, Smit JW, Netea MG, Schultze JL, Netea-Maier RT. Transcriptional and metabolic reprogramming induce an inflammatory phenotype in non-medullary thyroid carcinoma-induced macrophages. *Oncoimmunology* 2016; 5: e1229725.

131 Song J, Chen Z, Geng T, Wang M, Yi S, Liu K, Zhou W, Gao J, Song W, Tang H. Deleting MyD88 signaling in myeloid cells promotes development of adenocarcinomas of the colon. *Cancer Letters* 2018; 433: 65-75.

132 Wang Y, Wang K, Han GC, Wang RX, Xiao H, Hou CM, Guo RF, Dou Y, Shen BF, Li Y, Chen GJ. Neutrophil infiltration favors colitis-associated tumorigenesis by activating the interleukin-1 (IL-1)/IL-6 axis. *Mucosal immunology* 2014; 7: 1106-1115.

133 Franchi L, Kamada N, Nakamura Y, Burberry A, Kuffa P, Suzuki S, Shaw MH, Kim Y-G, Núñez G. NLRC4-driven production of IL-1β discriminates between pathogenic and commensal bacteria and promotes host intestinal defense. *Nature immunology* 2012; 13: 449-456.

134 Voronov E, Shouval DS, Krelin Y, Cagnano E, Benharroch D, Iwakura Y, Dinarello CA, Apte RN. IL-1 is required for tumor invasiveness and angiogenesis. *Proceedings of the National Academy of Sciences* 2003; 100: 2645-2650.

135 Dai L, Cui X, Zhang X, Cheng L, Liu Y, Yang Y, Fan P, Wang Q, Lin Y, Zhang J, Li C, Mao Y, Wang Q, Su X, Zhang S, Peng Y, Yang H, Hu X, Yang J, Huang M, Xiang R, Yu D, Zhou Z, Wei Y, Deng H. SARI inhibits angiogenesis and tumour growth of human colon cancer through directly targeting ceruloplasmin. *Nature communications* 2016; 7: 11996-11996.

Supplementary material

Supplementary Figures and extended materials

Supplementary Figure 1

Supplementary Figure 2

Supplementary Figure 3

Supplementary table 1 antibodies used for flow cytometry

Supplementary table 2 primer probe sets

Supplementary file Top_200_HVG.pdf

Supplementary file GO term analysis.xlsx

Supplementary file RNASeq_Readcounts.xlsx

Supplementary Figure 1

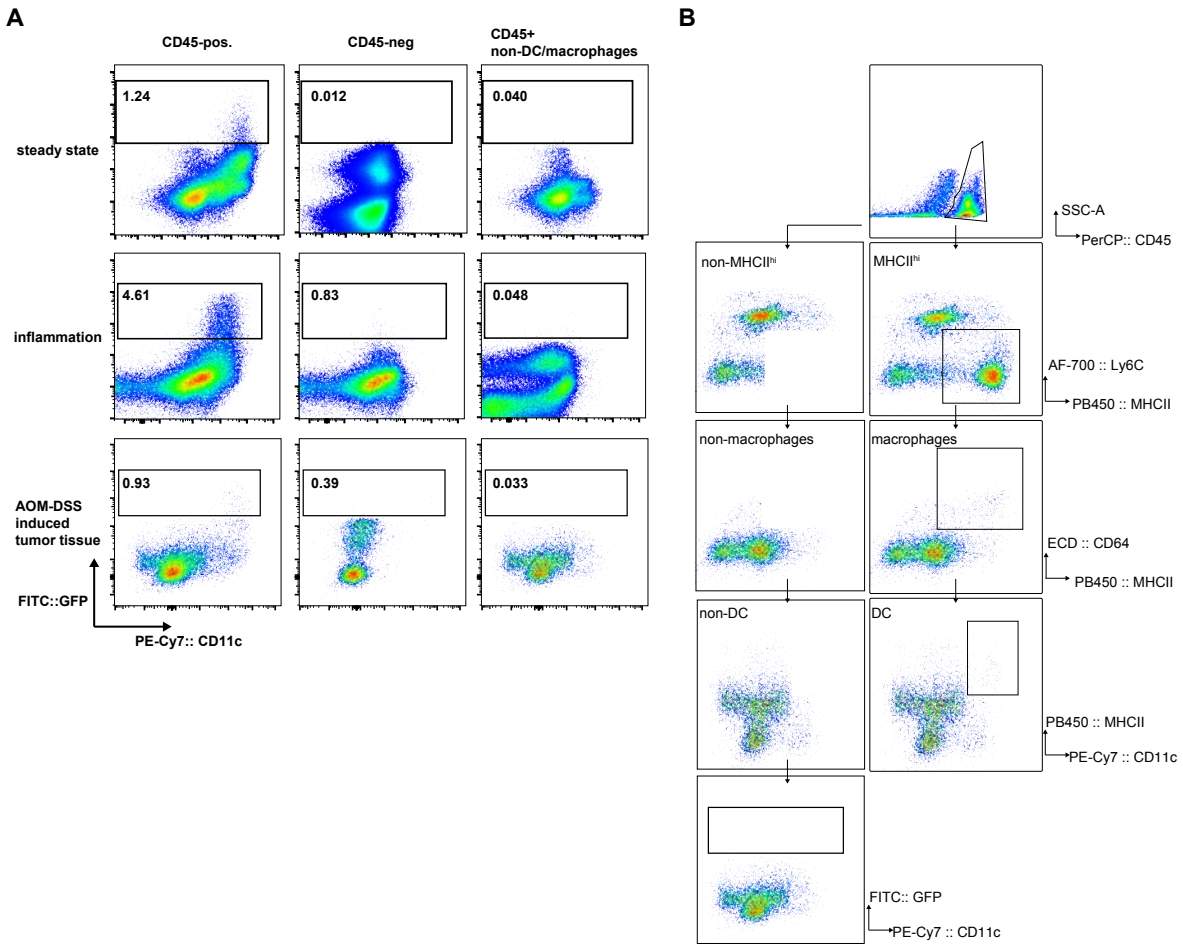

Supplementary Figure 1 (related to Figure 1): A Representative dot plots, showing GFP+ cell frequencies within CD45+ cells (left), CD45- cells (middle) and CD45+ non-DCs/macrophages in steady state (top), inflammatory (middle) colon tissue and AOM-DSS induced colon tumors (bottom). **B** Gating strategy for CD45+ non-DCs/macrophages.

Supplementary Figure 2

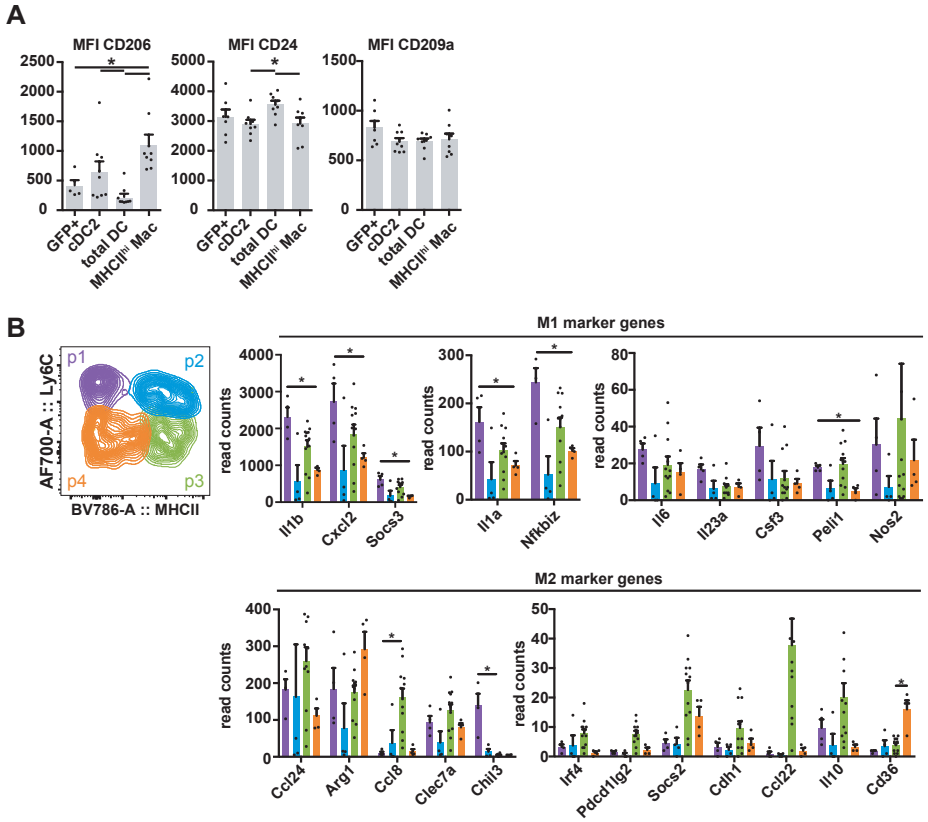

Supplementary Figure 2 (related to Figure 2). **A** MFI of CD206, CD24 and CD209a on tumor infiltrating GFP+ cells, cDC2, total DCs and MHCII^{hi} macrophages. Mean ± SEM. Each data point represents pooled tumors (similar size) of one mouse (n ≥ 4). **B** Left. Gating strategy used for population sorting for subsequent gene expression analysis. Right: M1 (top) and M2 (bottom) marker gene expression in the sorted populations (from left to right: p1-p4). Mean ± SEM. Each data point represents pooled tumors (similar size) of one mouse (n ≥ 4).

Supplementary Figure 3

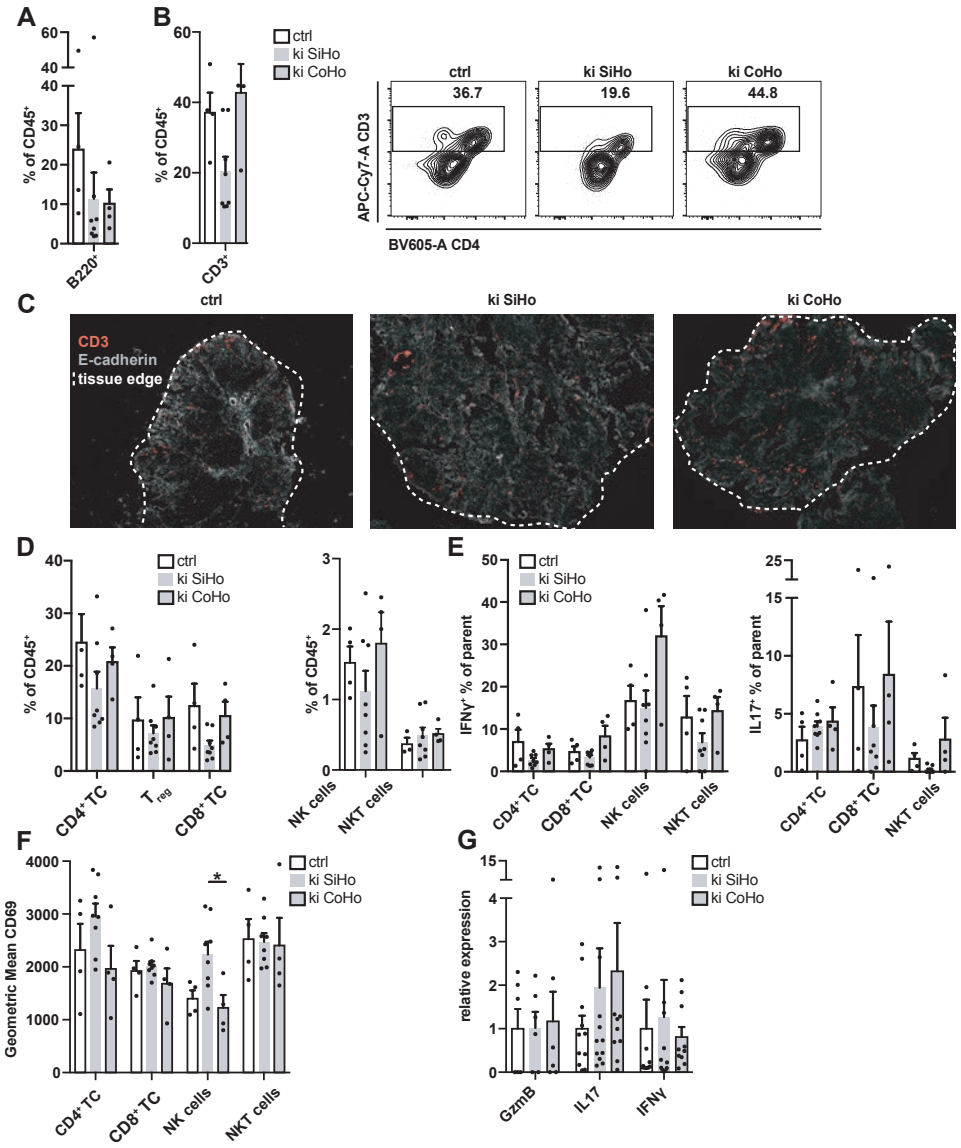

Supplementary Figure 3 (related to Figure 6): A Frequency of B220+ cells. Each data point represents one mouse (n ≥ 4). Mean ± SEM. **B** T cell frequencies in ctrl, ki SiHo and ki CoHo tumors (left). Representative contour plots (right). Each data point represents one mouse (n ≥ 4). Mean ± SEM. **C** Representative tumor cryosections from ctrl, ki SiHo and ki CoHo mice, stained for CD3 (red) and E-Cadherin (grey). Dashed lines highlight tissue edges. Scale bar: 10 µm. **D** Percentages of CD4+, Treg and CD8+ T cell subsets (left) and NK and NKT cells (right) in tumors of ctrl, ki SiHo and ki CoHo mice. Each data point represents one mouse (n ≥ 4). Mean ± SEM. **E** Percentages of IFN-γ-expressing cells (left) and IL-17-expressing cells (right) in tumors of ctrl, ki SiHo and ki CoHo mice. Each data point represents one mouse (n ≥ 4). Mean ± SEM. **F** Geometric mean of CD69 on CD4+, CD8+ T cells, NK cells and NKT cells in tumors of ctrl, ki SiHo and ki CoHo mice. Each data point represents one mouse (n ≥ 4). Mean ± SEM. **G** Relative gene expression of *gzmb*, *il17* and *ifng* in tumors of ctrl, ki SiHo and ki CoHo mice. Each data point represents one mouse (n ≥ 6). Mean ± SEM.

Supplementary table 1 antibodies used for flow cytometry

Reagent/Resource	Source	Cat.no.	Clone	Dilution
anti-mouse Ly6C-AF700	Biolegend	128024	HK1.4	1:200
anti-mouse MHCII-BV421	Biolegend	107631	M5/114.15.2	1:300
anti-mouse CD64-PE-Dazzle-594	Biolegend	139319	X54-5/7.1	1:150
anti-mouse F4/80-PE-Dazzle-594	Biolegend	123145	BM8	1:200
anti-mouse CD103-PE	BD Bioscience	557495	2E7	1:150
anti-mouse CD11b-APC-Cy7	Biolegend	101226	M1/70	1:300
anti-mouse CD24 BV605	Biolegend	101827	M1/69	1:200
anti-mouse CD209a APC	Thermo	17-2092-80	LWC06	1:200
anti-mouse CD13 BV421	BD Bioscience	564354	R3-242	1:200
anti-mouse CD206 AF647	Biolegend	141712	C068C2	1:150
anti-mouse CD45 PerCP	Biolegend	109828	104	1:300
anti-mouse Ly6G BV650	Biolegend	109828	1A8	1:200
anti-mouse CD11c PE-Cy7	Biolegend	117318	N418	1:400
anti-mouse B220 BV605	Biolegend	103244	RA3-6B2	1:200
anti-mouse CD3 APC-Cy7	Thermo	47-0031-82	145-2C11	1:200
anti-mouse CD4 BV605	Biolegend	100548	RM4-5	1:200
anti-mouse Foxp3 PE-Cy7	Thermo	25-5773-80	FJK-16a	1:200
anti-mouse CD8 AF700	Biolegend	100729	53-6.7	1:200
anti-mouse NK1.1 BV650	Biolegend	108735	PK136	1:200
anti-mouse IL-17A APC	Thermo	17-7177-81	eBio17B7	1:200
anti-mouse IFNɣ PE	BD Bioscience	108736	XMG1.2	1:200

anti-mouse CD69 V450	BD Bioscience	560690	H1.2F3	1:200
anti-mouse IgA PE	Thermo	12-4204-81	mA-6E1	1:125

Supplementary table 2 primer probe sets

Target	Source	Identifier
Bax	Thermo	Mm00432051_m1
Bcl2	Thermo	Mm00477631_m1
Ccl17	Thermo	Mm01244826_g1
Ccl2	Thermo	Mm00441242_m1
Csf2	Thermo	Mm01290062_m1
Cxcl10	Thermo	Mm00445235_m1
Cxcl13	IDT	Mm.PT.58.31389616
Cxcl2	Thermo	Mm00437121_m1
Gzmb	Thermo	Mm00442837_m1
Hprt	IDT	Mm.PT.39a.22214828
Ifng	Thermo	Mm99999071_m1
Il12a	Thermo	Mm00434169_m1
Il17a	Thermo	Mm00439619_m1
Il1b	Thermo	Mm00434228_m1
Il22	Thermo	Mm00444241_m1
Il23a	IDT	Mm00518984_m1
IL6	Thermo	Mm00446190_m1
Muc2	Thermo	Mm01276696_m1
Pcna	IDT	Mm.PT.58.3320736
Reg3g	Thermo	Mm00441127_m1
Tnf	Thermo	Mm00443258_m1

frontiers in Oncology

METHODS
published: 02 October 2019
doi: 10.3389/fonc.2019.01001

Increased Incidence of Colon Tumors in AOM-Treated *Apc*$^{1638N/+}$ Mice Reveals Higher Frequency of Tumor Associated Neutrophils in Colon Than Small Intestine

Rebecca Metzger[1], *Mahulena Maruskova*[1], *Sabrina Krebs*[1], *Klaus-Peter Janssen*[2] *and Anne B. Krug*[1]*

[1] *Biomedical Center, Institute for Immunology, Ludwig-Maximilians-University Munich, Munich, Germany,* [2] *Department of Surgery, Klinikum rechts der Isar, Technische Universität München, Munich, Germany*

OPEN ACCESS

Edited by:
Michael J. Wargovich,
The University of Texas Health Science Center at San Antonio, United States

Reviewed by:
Feng Wei,
Tianjin Medical University Cancer Institute and Hospital, China
Toru Furukawa,
Tohoku University School of Medicine, Japan

**Correspondence:*
Anne B. Krug
anne.krug@med.uni-muenchen.de

Specialty section:
This article was submitted to Gastrointestinal Cancers, a section of the journal Frontiers in Oncology

Received: 02 August 2019
Accepted: 17 September 2019
Published: 02 October 2019

Citation:
Metzger R, Maruskova M, Krebs S, Janssen K-P and Krug AB (2019) Increased Incidence of Colon Tumors in AOM-Treated Apc$^{1638N/+}$ Mice Reveals Higher Frequency of Tumor Associated Neutrophils in Colon Than Small Intestine. Front. Oncol. 9:1001. doi: 10.3389/fonc.2019.01001

Colorectal cancer (CRC) is one of the most common cancers and a major cause of mortality. Mice with truncating *Apc* germline mutations have been used as a standard model of CRC, but most of the *Apc*-mutated lines develop multiple tumors in the proximal small intestine and rarely in the colon precluding detailed analysis of colon tumor microenvironment. Our aim was to develop a model with higher resemblance to human CRC and to characterize tumor infiltrating immune cells in spontaneously developing colon tumors compared to small intestinal tumors. Therefore, the *Apc*$^{1638N/+}$ line was treated repeatedly with azoxymethane (AOM) and 90% colon tumor incidence and 4 to 5 colon tumors per mouse were achieved. Of note, AOM treatment specifically increased the tumor burden in the colon, but not in the small intestine. Histological grading and WNT-signaling activity did not differ significantly between small intestinal and colon tumors with some lesions progressing to invasive adenocarcinoma in both locations. However, characterization of the intratumoral myeloid cell compartment revealed a massive infiltration of colon tumors with neutrophils – 6-fold higher than in small intestinal tumors. Moreover, CCL17-expressing macrophages and dendritic cells accumulated in the tumors indicating the establishment of a tumor-promoting immunosuppressive environment. Thus, *Apc*$^{1638N/+}$ mice treated with AOM are a suitable and straightforward model to study the influence of immune cells and chemokines on colon carcinogenesis.

Keywords: colorectal cancer, mouse model, adenomatous polyposis coli, azoxymethane, tumor immunology and microenvironment, tumor-associated neutrophils, tumor-associated macrophages, dendritic cells

INTRODUCTION

Colorectal cancer (CRC) is one of the most prevalent cancers worldwide, and one of the leading causes of cancer-related morbidity and mortality, especially in countries with "Western" life style. Aberrant WNT signaling plays an important role in initiation of human colorectal carcinogenesis. Loss of the adenomatous polyposis coli (*APC*) tumor suppressor is not only the

cause of familial adenomatous polyposis, but also 80–90% of sporadic CRC harbor loss of function mutations—mostly truncating nonsense mutations—in the *APC* gene (1). The second *APC* allele is inactivated by promoter methylation, chromosomal loss, or additional mutations leading to biallelic loss (loss of heterozygosity, LOH) or inactivation of *APC* (2, 3). As a result, **β**-catenin is not degraded, accumulates and translocates to the nucleus where it acts as a transcriptional coactivator inducing the expression of WNT target genes including c-Myc, Cyclin D1, and osteopontin which promote proliferation and ultimately tumor formation (2, 4). Additional mutations, e.g., in *KRAS*, *PTEN*, *PIK3CA*, *TGFBR1*, *TGFBR2*, *SMAD2*, *SMAD4,* and *TP53* are found in *APC*-mutated sporadic CRC, which promote tumor progression. In contrast, CRC lacking *APC* mutations are frequently associated with mutations in mismatch repair genes (2).

Mice heterozygous for truncating germline mutations of *Apc*, such as the *Apc*$^{Min/+}$ line on C57BL/6 background (5) have been used for decades as a preclinical model. A major disadvantage of the frequently used *Apc*$^{Min/+}$ model is however that the mice quickly develop multiple adenomas in the small intestine (SI), and only few polyps in the colon, which leads to a life span of <6 months on the C57BL/6 background (2). Further, progression of these lesions to invasive adenocarcinoma is very rare (2).

Apc$^{1638N/+}$ mice were generated by inserting a neomycin cassette in antisense orientation into exon 15, resulting in chain termination at codon 1638 and production of an unstable protein. These mice develop intestinal adenomas and adenocarcinomas, which was attributed to somatic loss of the wildtype *Apc* allele (6) or rather *Apc* mutations as described in a more recent publication (7). In comparison to *Apc*$^{Min/+}$ mice the *Apc*$^{1638N/+}$ mice develop less tumors with longer latency and show progression to invasive adenocarcinomas, as well as splenomegaly and desmoid formation, thus more closely resembling human CRC. Although colon tumors develop in *Apc*$^{1638N/+}$ mice, their incidence and number is low and their formation takes 10–12 months (2, 6, 8). Treating *Apc*$^{1638N/+}$ mice with "Western style" diet (9) or crossing them with other genetically engineered mutant or knockout mice (6, 10–17) promotes multiplicity and sometimes progression of tumors in SI and/or colon. Similarly, conditional knockout of *Apc* in colonic epithelial cells leads to selective colon tumor formation (18, 19).

However, mice carrying several mutant or transgenic alleles are cumbersome to work with for mechanistic studies, which require crossing these models with additional knockout or transgenic mice. Moreover, when using a Cre-mediated knockout of *Apc* in colonic epithelial cells for tumor formation, alternative recombinase systems need to be used for conditional gene knockouts in other cell types.

Induction of colitis by administration of dextran sodium sulfate (DSS) greatly accelerates adenoma and adenocarcinoma formation in the colon of *Apc*$^{Min/+}$ mice (20, 21), but this model is not suitable to study tumorigenesis in the absence of overt inflammation, which would better mimick human CRC pathogenesis. Administration of azoxymethan (AOM), an alkylating agent that produces free radicals, to C57BL/6 mice leads to low incidence tumor formation in the colon by causing mutations in **β**-catenin (22). AOM treatment increased incidence and numbers of colon adenomas and adenocarcinomas in adult *Apc*$^{Min/+}$ mice (23) and in young or neonatal *Apc*$^{Min/+}$ mice, but these mice still had a predominance of small intestinal tumors and a short life span (24–26). The histological features of tumors from these mice have been described but a detailed characterization e.g., regarding immune cell infiltration is lacking.

Studies performed in the *Apc*$^{Min/+}$ model indicate that tumors are controlled by the adaptive immune system (27, 28). However, regulatory T cells and myeloid cells, such as tumor associated neutrophilic granulocytes (TAN) and monocytic cells (functionally described as myeloid derived suppressor cells, MDSC) as well as tumor associated macrophages (TAM) together shape the tumor microenvironment to promote tumor growth and to limit the anti-tumor immune response (29–33). A subpopulation of TAMs isolated from subcutaneous tumor models was shown to secrete CCL17 as a hallmark of M2-like macrophage polarization (34). Unfortunately, the low incidence and number of spontaneous colon tumors in *Apc*$^{Min/+}$ and *Apc*$^{1638N/+}$ mice precludes a detailed characterization of immune cell infiltrates including TAMs and TANs in spontaneously developing colon tumors. We therefore established an accelerated *Apc*$^{1638N/+}$ model which is suitable for further investigations of the tumor microenvironment and anti-tumor immune responses in spontaneously forming colon tumors. In this study we show that repeated administration of AOM to *Apc*$^{1638N/+}$ mice leads to a higher incidence and an increased number of tumors in the colon and shortens experimental time to 6–7 months.

RESULTS

Repeated Injection of AOM Leads to Higher Incidence and Multiplicity of Colon Tumors and Decreased Survival in *Apc*$^{1638N/+}$ Mice

To generate more colon tumors in a shorter experimental time, adult C57BL/6 mice carrying one CCL17-eGFP knock- in allele as a reporter for CCL17 expression received weekly AOM injections for 6 weeks, and were followed by clinical assessment until anemia was clinically apparent or other criteria for euthanasia were reached (**Figure 1A**). While the number of colon tumors per mouse (**Figure 1B**) was significantly higher in AOM treated vs. untreated *Apc*$^{1638N/+}$ mice (median 3 vs. 0; mean ±SEM 4.3 ±0.8 vs. 0.3 ±0.2), the number of macroscopically visible tumors in the SI was slightly reduced in AOM treated vs. untreated *Apc*$^{1638N/+}$ mice (median 3 vs. 5; mean ±SEM 4.0 ±0.6 vs. 5.8 ± 0.7). Survival time was significantly reduced in AOM treated *Apc*$^{1638N/+}$ mice with a median survival time of 193 days compared to 312 days in untreated mice (**Figure 1C**). The cumulative incidence of colon tumor development increased 6-fold from 15 to 90% after the administration of AOM, with a 5.7-fold higher relative risk for colon tumor development with AOM treatment ($p < 0.0001$,

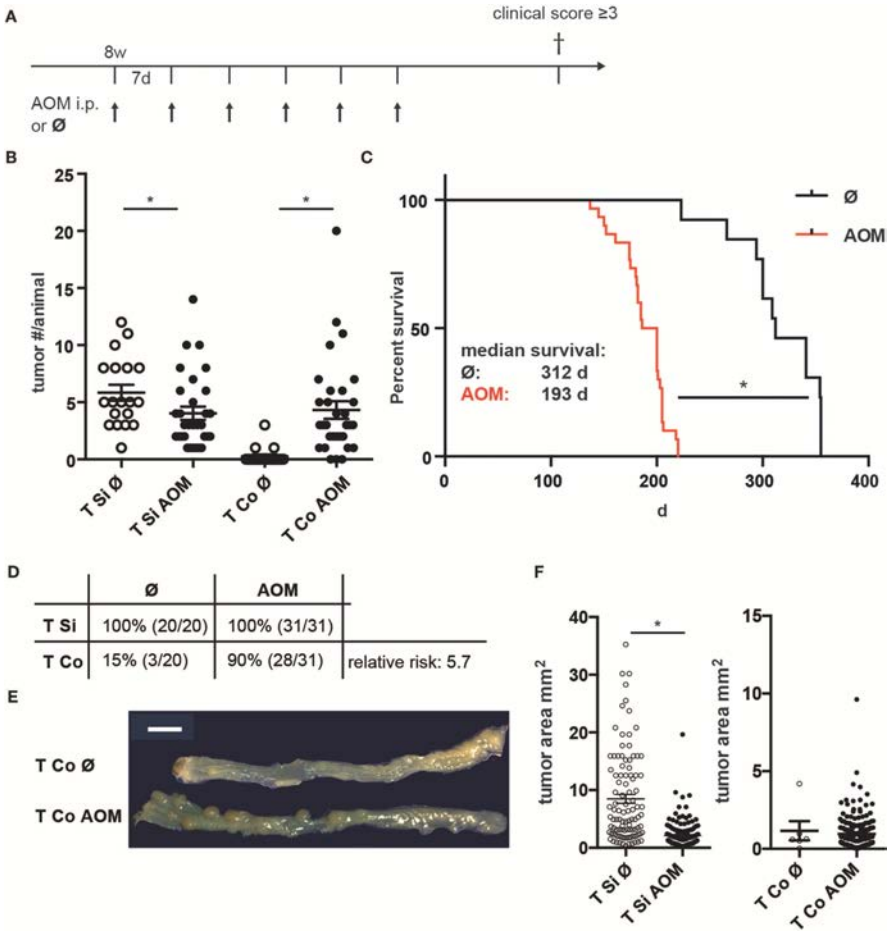

FIGURE 1 | Increased incidence and number of colon tumors in AOM-treated APC$^{1638N/+}$ mice. (A) Experimental scheme. *Apc*$^{1638N/+}$ mice received weekly i.p. injections of AOM from age 8 to 14 weeks and were sacrificed when reaching criteria for euthanasia. (B) Number of tumors in small intestine (Si) and colon (Co) in untreated (n = 19) and AOM-treated (n = 31) mice (Mann–Whitney test). (C) Kaplan-Meier survival analysis (log-rank test). (D) Tumor incidence in Si and Co (Chi-square analysis). (E) Representative macroscopic image of colon tumors in untreated and AOM-treated *Apc*$^{1638N/+}$ mice. Scale bar: 1 cm. (F) Tumor sizes of Si and Co tumors (Si untreated: n = 103, Si AOM: n = 150, Co untreated: n = 5, Co AOM: n = 189, *$p < 0.0001$, Mann–Whitney test). *$p < 0.05$.

Chi-square test, **Figure 1D**). Colon tumors were macroscopically similar and were localized in the distal half of the colon in AOM treated and untreated *Apc*$^{1638N/+}$ mice (**Figure 1E**). Interestingly, tumors in the SI were found to be significantly smaller in the AOM-treated mice (median 1.3 vs. 5.3 mm^2; **Figure 1F**).

Thus, administration of AOM to adult C57BL/6 *Apc*$^{1638N/+}$ mice specifically accelerates tumor development in the colon, but not in the small intestine leading to a higher incidence and multiplicity of colon tumors.

AOM-Treated *Apc*$^{1638N/+}$ Mice Develop Highly Proliferative Colon Tumors With Active Wnt Signaling and Aberrant Accumulation of β-Catenin

Histopathological examination of tissue sections from colon and SI tumors at the time points of sacrifice revealed low grade and high grade intraepithelial neoplasia (IEN) with distorted crypt architecture, high nuclear to cytoplasmic ratio, and elongated stratified hyperchromatic nuclei, which

in high grade IEN reached the luminal side. In some tumors invasion of the muscularis mucosae with stromal and inflammatory reactions was observed indicating progression to adenocarcinoma (**Figure 2A**). Low grade IEN, high grade IEN and occasionally adenocarcinomas were detected in intestinal tumors of both AOM-treated and untreated mice. High grade IEN was observed in colon tumors from AOM treated mice (6/9), but not in SI tumors of AOM treated mice (0/4) (**Figure 2A**).

Expression of canonical Wnt target genes, such as the stemness marker *Leucine-rich repeat-containing G-protein coupled receptor 5* (*Lgr5*) (35) and *osteopontin* (*Opn, Spp1*) (4) on mRNA level was significantly higher in SI and colon tumors in comparison to normal intestinal tissue. A trend towards higher expression of *Lgr5* and *Opn* in colon tumors of AOM treated *Apc*$^{1638N/+}$ mice was observed (**Figure 2B**, upper panels). Strong **β**-catenin staining with cytoplasmic and nuclear localization [in contrast to membranous staining found in normal epithelium (4, 36)] was detected in all tumors with a trend toward a higher proportion of nuclear **β**-catenin staining in AOM-treated mice (**Figure 2B**, lower panels). Ki67 staining in tumor tissue sections confirmed the high percentage of proliferating cells in the tumors (representative result shown in **Figure 2C**, lower panel). Accordingly, expression of *Proliferating cell nuclear antigen* (*Pcna*) mRNA was significantly higher in colon tumors compared to normal colon tissue and slightly higher in colon tumors of AOM treated than untreated mice (**Figure 2B**). Thus, tumors developing in AOM-treated *Apc*$^{1638N/+}$ mice are highly proliferative and show aberrant distribution of **β**-catenin and active WNT signaling.

Comparison of Immune Cell Infiltrates in Small Intestinal and Colon Tumors Reveals Preferential Accumulation of Neutrophilic Granulocytes in Colon Tumors

Immune cell infiltrates in human colorectal cancer are an important prognostic factor. Tumors in SI and colon of both AOM treated and untreated mice were strongly infiltrated with CD45$^+$ cells (**Supplementary Figures 1, 2**). These were localized below the neoplastic epithelium either distributed throughout the tumor or forming clusters (**Supplementary Figure 2**). In all tumors CD45$^+$ cells contained a substantial proportion of T lymphocytes, including CD4$^+$ and CD8$^+$ T cells as well as CD4$^+$ Foxp3$^+$ regulatory T cells and a smaller more variable proportion of CD19$^+$ B lymphocytes (**Supplementary Figure 1**). CD11b$^+$ myeloid cells — encompassing granulocytic and monocytic cells as well as TAM and CD11b$^+$ DCs — were less frequent in SI tumors from AOM-treated than untreated mice (24.1 ±6.1 vs. 53.2 ±7.0, mean ±SEM, $p = 0.024$; **Figure 3A**). In contrast, AOM treatment did not seem to alter the frequency of CD11b$^+$ cells in colon tumors (**Figure 3A**). Ly6G^{hi} CD11b$^+$ neutrophilic granulocytes were 6-fold more abundant in colon tumors than in SI tumors (AOM treated mice: 59.4 ±23.2% vs. 19.5 ±13.9% of CD11b+ cells, $p < 0.005$) (**Figure 3B**). The percentage of Ly6G^{hi} CD11b$^+$ cells was greatly increased in tumors compared to lamina propria of the same AOM-treated *Apc*$^{1638N/+}$ mice in both SI and colon indicating active recruitment of neutrophilic granulocytes to tumors in both locations, but preferential accumulation in colon tumors (**Supplementary Figure 2B**). Within the CD11b$^+$ Ly6G$^-$ compartment the proportions of Ly6C^{hi} MHCII$^-$ monocytic cells, Ly6C^{hi} MHCII$^+$ intermediate cells, Ly6C$^-$ MHCII^{hi} CD64$^+$ macrophages and Ly6C$^-$ MHCII^{lo} CD64$^+$ macrophages were similar in colon and SI tumors and not altered by AOM treatment (**Figure 3C**). The frequency of DCs within CD45$^+$ tumor infiltrating cells was not significantly different between the experimental groups and the tumor locations (**Figure 3D**). CCL2 and CXCL10, showed higher relative mRNA expression levels in tumors than in normal lamina propria of tumor bearing *Apc*$^{1638N/+}$ mice (**Figure 3E**) correlating with the recruitment of myeloid cells and T lymphocytes into the tumors.

Distinct Subpopulations of Tumor Infiltrating Myeloid Cells Shape the Intestinal Tumor Microenvironment

Programmed cell death ligand 1 (PD-L1) interacts with Programmed cell death 1 (PD1) on effector T cells, NK cells and TAMs inhibiting their anti-tumor activity. PD-L1 staining was not detectable on CD45- tumor cells by flow cytometry (**Figure 4B**) but was found to be expressed on the surface of all myeloid cell subsets within colon and SI tumors irrespective of AOM treatment. Expression levels were highest in Ly6C^{hi} MHCII$^-$ followed by Ly6C^{hi} MHCII$^+$ monocytic cells and then MHCII^{hi} and MHCII^{lo} TAM subsets (**Figure 4A**) We detected lower PD-L1 expression on monocytes from the tumors than from lamina propria (**Figure 4B**) indicating that the tumor microenvironment is less inductive for PD-L1 expression than the lamina propria.

CCL17 expression in the intestine is restricted to DCs in the steady state (37, 38), but is also expressed by immunosuppressive M2 polarized macrophages within tumors (34). Using *Apc*$^{1638N/+}$ CCL17$^{eGFP/+}$ reporter knockin mice (37) CCL17 expression could be detected in TAMs and DCs in tumors of AOM (**Figure 4C**) at significantly higher levels than in normal lamina propria of tumor bearing mice. Immunofluorescence staining of tumor tissue sections showed infiltrates of CCL17^{eGFP} expressing cells, part of which stained positively for the DC marker CD11c confirming our results from flow cytometric analysis (**Figure 4D**). Thus, the tumor microenvironment which is established in colon and SI tumors of *Apc*$^{1638N/+}$ mice favors CCL17 expression in TAMs and DCs.

DISCUSSION

In this study we show that repeated AOM injections increase the incidence and multiplicity of colon tumors in mice with the *Apc*$^{1638N/+}$ germline mutation and shorten experiment time while reducing the small intestinal tumor burden. Tumors developing in AOM treated *Apc*$^{1638N/+}$ mice express WNT target genes and show aberrant accumulation of **β**- catenin, as expected for WNT driven carcinogenesis. Strikingly, comparison of immune cell infiltrates between colonic and SI tumors revealed a significantly higher frequency of neutrophilic

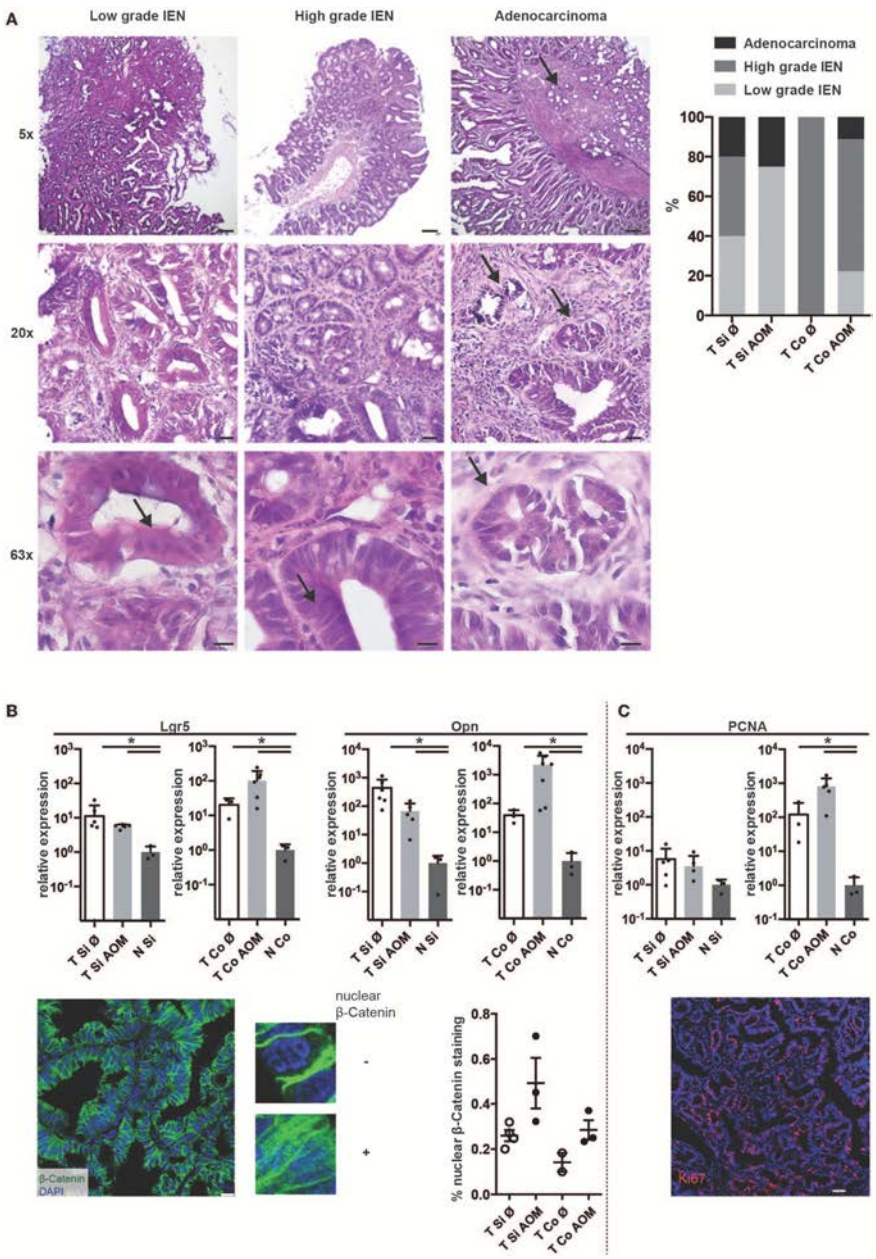

FIGURE 2 | AOM-treatment leads to the development of high-grade colonic lesions with active Wnt-signaling and proliferation. (A) Exemplary images of H&E stained cryosections of tumors isolated from AOM-treated and non-treated *Apc*$^{1638N/+}$ mice (taken with 5×, 20×, and 63×objectives). Scale bars: 100 μm (5×), 25 μm

(Continued)

FIGURE 2 | (20×), 10 μm (63×). Arrows indicate features of cell dedifferentiation and dysplasia such as pseudo-stratification, increased nucleus/cytoplasm ratios and abnormal nuclei positioning as well as invasion of the muscularis mucosae in adenocarcinomas. Proportions of low grade IEN, high grade IEN and adenocarcinoma are shown in the graph (Si untreated, $n = 5$; Si AOM $n = 4$; Co untreated, $n = 1$; Co AOM, $n = 9$). (B) Upper panel: relative mRNA expression of WNT target genes *Lgr5* and *Opn* in tumors and normal intestinal tissue from tumor-bearing mice was measured by qRT-PCR (fold-change compared to normal tissue average, log(10) scale, mean + SEM, $n = 3$–6). Lower panel, left: representative image of immuno-fluorescence staining for β-Catenin in cryosections of a colon tumor. Scale bar: 50 μm. Zoomed images show nuclear and extranuclear localization of β-Catenin. Green: β-Catenin, blue: DAPI, 63× magnification. Right: quantification of nuclear β-Catenin staining of total β-Catenin staining in one field of view per mouse. Symbols indicate tumors from individual mice; mean + SEM ($n = 2$–3). (C) Upper panel: relative mRNA expression of *Pcna* in tumors and normal intestinal tissue from tumor-bearing mice was measured by qRT-PCR (fold-change compared to normal tissue average, log(10) scale, mean + SEM, $n = 3$–6, unpaired, two-tailed *t*-test). Lower panel: representative Ki67 staining of intestinal tumor tissue of an *Apc*$^{1638N/+}$ mouse (20×, red: Ki67, blue: DAPI, Scale bar: 50 μm). *$p < 0.05$.

granulocytes in colon tumors. Further, increased expression of CCL17 in DCs and M2-like TAMs within tumors compared to intestinal lamina propria indicates the establishment of a tumor-promoting immunosuppressive environment. Thus, AOM treated *Apc*$^{1638N/+}$ mice can be used as a model of early colon carcinogenesis to further investigate the interplay of immune cells, stromal cells, and cancer cells in the tumor microenvironment.

Repeated AOM administration has been used previously as a model for sporadic CRC. A sufficient incidence of colon tumors can be achieved by AOM administration in the susceptible A/J strain but not in the C57BL/6 strain (39), which is the background of the majority of genetically engineered mouse lines, e.g., for functional studies of relevant immune cell types. Therefore, we sought to combine *Apc*$^{1638N/+}$ mutant mice with AOM treatment and observed greatly increased incidence and multiplicity of colon tumors, demonstrating a synergistic effect of the truncating *Apc*$^{1638N/+}$ mutation and AOM-induced mutations, which led to increased cytoplasmic and nuclear accumulation of β-catenin and upregulation of canonical WNT target genes.

Besides the slightly reduced number of small intestinal tumors, their size was reduced and the majority showed low grade IEN in AOM treated *Apc*$^{1638N/+}$ mice. This is probably due to the earlier termination of the experiment and demonstrates that AOM is specifically affecting the colon. Histologically, high grade IENs and invasive adenocarcinomas were found with comparable frequency in 5–7 months old AOM treated *Apc*$^{1638N/+}$ mice as in 10–12 months old untreated *Apc*$^{1638N/+}$ mice. Thus, AOM treatment accelerated tumor progression, but did not lead to deeper tissue invasion beyond the bowel wall or to metastasis. An increased incidence and number of colon tumors was also reported in *Apc*$^{min/+}$ mice after repeated AOM treatment (23, 24, 26, 40). However, *Apc*$^{min/+}$ mice have a much higher spontaneous tumor burden in the small intestine, and therefore a shorter life time that precludes further progression of lesions along the adenoma-carcinoma sequence. The AOM treated *Apc*$^{1638N/+}$ mice in the present study provide the opportunity to assess the influence of additional risk factors and immune responses on both, lesion incidence and progression to invasive carcinoma. It was shown in a recent study that administration of AOM alone or combined with *Citrobacter rodentium* infection increased proliferation and Dclk1-positive cancer stem cell frequency in intestinal tumors of *Apc*$^{1638N/+}$ mice indicating enhanced tumorigenesis in line with our results (41). However, the impact of AOM administration on tumor multiplicity and progression was not reported in this publication. Comparison of small intestinal and colon tumors revealed that neutrophilic granulocytes marked by CD11b and Ly6G expression are massively recruited and dominate the myeloid cell infiltrate in colon tumors but not small intestinal tumors. This shows that location has a great impact on the composition of immune cell infiltrates in intestinal tumors, but the regulation of this preferential accumulation of neutrophilic cells in colon tumors is not known. Intratumoral CD11b$^+$ Ly6-G^{high} cells consist of classical neutrophils (TANs) and/or pathologically activated immunosuppressive PMN-MDSC, which accumulate in the tumors, but are also found in blood, spleen and bone marrow of tumor bearing mice. TANs are heterogeneous and can have anti-tumor or protumor activity. Their prognostic role in CRC is controversial (42, 43). Although it was shown recently that neutrophils can limit tumor progression in the very early phase of murine CRC models by restricting tumor-associated bacteria and inflammatory responses (44), the majority of reports provide evidence for a tumor supporting role of TANs. PMN-MDSC, which develop at later stages, are by definition immunosuppressive and promote tumor initiation, progression and dissemination (43).

Accumulation of neutrophils/PMN-MDSCs in small intestinal and colon tumors of *Apc*$^{1638N/+}$ mice correlated with increased expression of CCL2 compared to normal intestinal tissue with slightly higher expression in colon tumors. Chun et al. also reported increased CCL2 expression in colitis associated colon cancer, sporadic CRC as well as precancerous colorectal lesions in humans and in mouse models (45). In these models CCL2 was shown to be required for PMN-MDSC and M- MDSC accumulation in the tumors and enhanced the T cell suppressive function of PMN-MDSC (45). In addition to CCL2, CXCR2 ligands including CXCL1, CXCL2, CXCL3, and CXCL8 produced by CRC cells and neutrophils themselves were found to be responsible for recruitment of CXCR2$^+$ neutrophils/PMN-MDSCs to colon tumors (46–48). We have shown earlier that specific colon microbiota in human patients are correlated with chemokine production and infiltration of immune cell subsets (49). Preferential recruitment of neutrophilic cells to colon tumors vs. small intestinal tumors could therefore involve site-specific microbiota signals and inflammatory responses (50), but also genetic mechanisms of tumor initiation, which differ between tumor locations in the intestine (7).

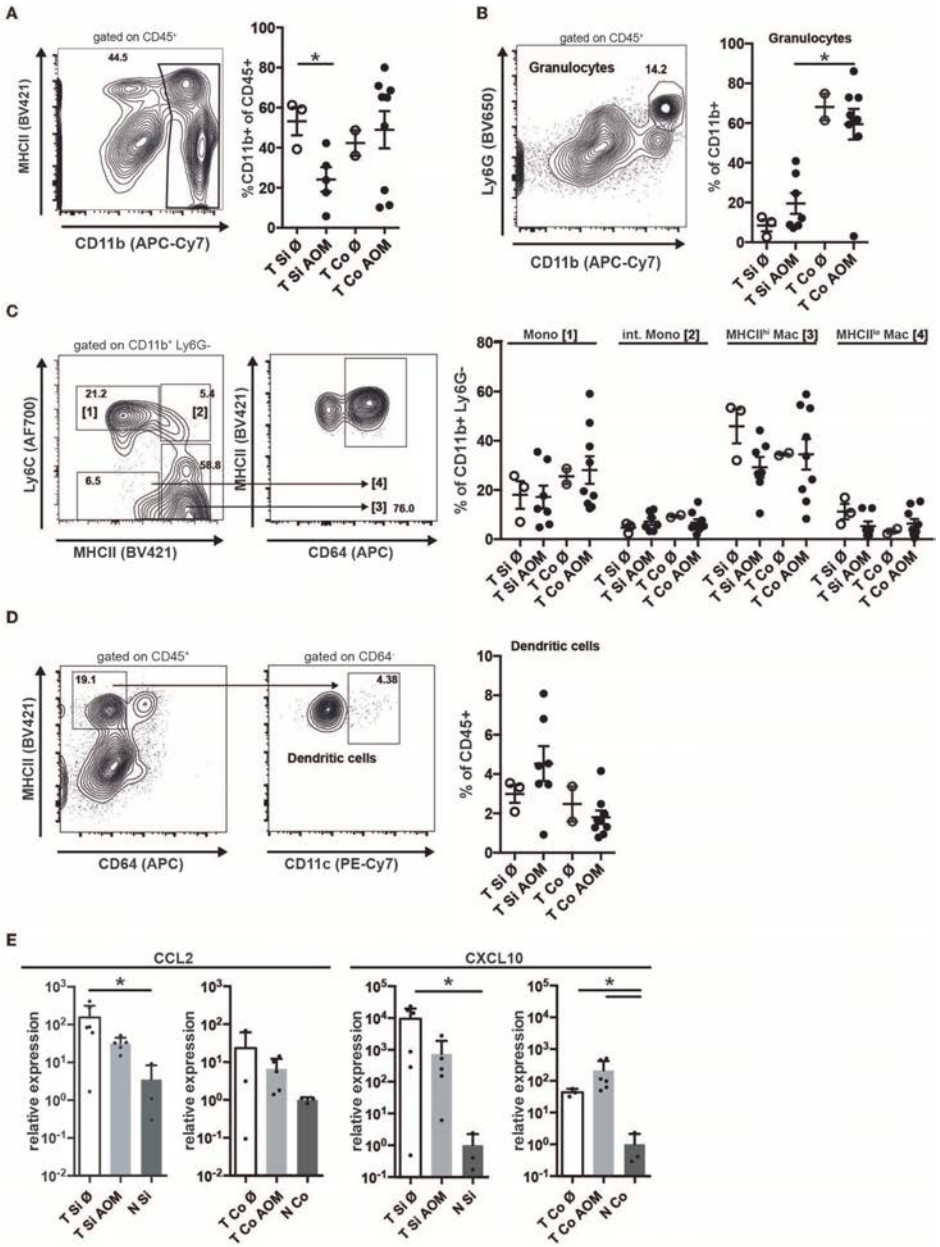

FIGURE 3 | Accumulation of granulocytes in intestinal tumors correlates with chemokine expression and is enhanced in colon tumors. (A) Representative contour plot of intratumoral (AOM treated colon tumor) immune cells stained for MHCII and CD11b, showing the gating for CD11b$^+$ cells. The percentages of CD11b$^+$ cells of all

(Continued)

FIGURE 3 | CD45$^+$ cells in Si and Co tumors of untreated and AOM treated *Apc*$^{1638N/+}$ mice are shown in the graph. (B) Representative dot plot of intratumoral CD45$^+$ immune cells stained for Ly6G and CD11b, showing the gating for CD11b$^+$ Ly6G$^+$ granulocytic cells. The percentages of CD11b$^+$ Ly6G$^+$ cells of all CD11b$^+$ cells are shown in the graph. (C) Gating strategy for monocytes (Mono), intermediate monocytes (int. Mono), and MHCII$^{lo/hi}$ macrophages within the intratumoral CD11b$^+$ Ly6G$^-$ population. The percentages of the indicated populations within the CD11b$^+$ Ly6G$^-$ cells are shown in the graph. (D) Gating strategy for intratumoral DCs and frequency of DCs within CD45$^+$ cells. (A–D) Each symbol represents an individual mouse. Horizontal bars indicate mean, error bars indicate SEM, n = 2–9. (E) Relative mRNA expression of the chemokines CCL2 and CXCL10 in tumors and normal intestinal tissue from AOM-treated and untreated *Apc*$^{1638N/+}$ mice measured by qRT-PCR [fold-change compared to normal tissue, log(10) scale]. Symbols indicate individual mice, horizontal bars: mean, error bars: SEM, n = 3–6, unpaired, two-tailed t-test. *$p < 0.05$.

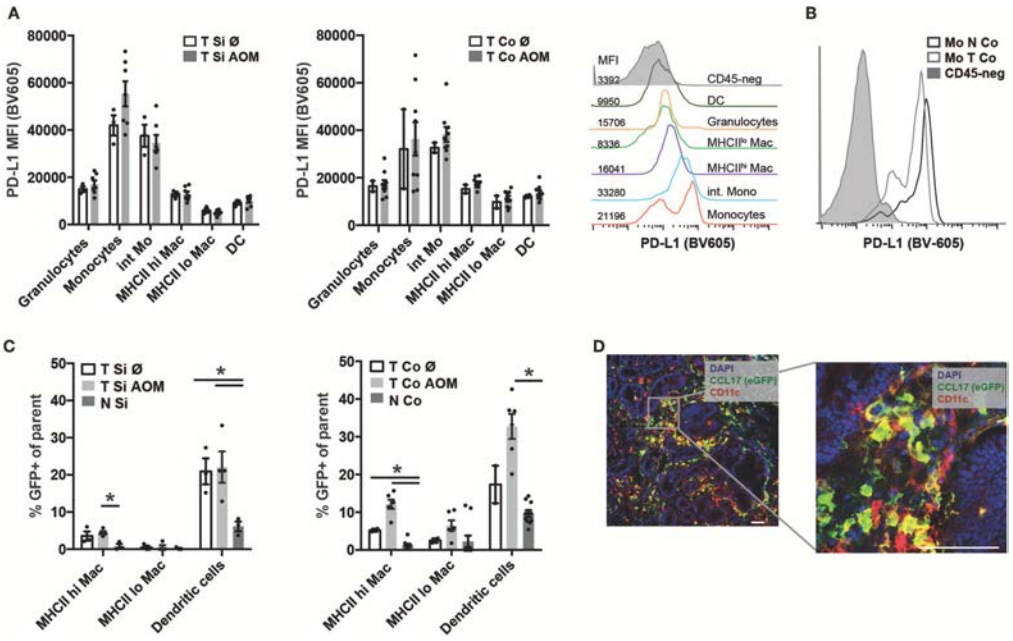

FIGURE 4 | PD-L1 and CCL17 (eGFP) expression in intestinal tumors indicates establishment of a tumor promoting microenvironment. (A) PD-L1 mean fluorescence intensity (MFI) of the indicated myeloid cell populations in Si and Co tumors of untreated and AOM treated *Apc*$^{1638N/+}$ mice. Representative histogram overlay of the PD-L1 fluorescence signal in the indicated myeloid cell populations (colored histograms) and CD45-negative tumor cells (gray histogram) from colonic intratumoral cells of an AOM-treated mouse. (B) Representative histogram overlay of the PD-L1 fluorescence signal in monocytes from tumor (light gray, open histogram) and normal (dark gray, open histogram) tissue, compared to CD45-negative cells (gray, filled histogram) from colonic intratumoral cells of an AOM-treated mouse. (C) CCL17-eGFP expression was detected by flow cytometry in macrophages and DCs in tumors and normal lamina propria of *Apc*$^{1638N/+}$;CCL17-eGFP-reporter mice. The percentages of GFP$^+$ cells within the indicated populations are shown. (A,C) Each symbol represents an individual mouse. Horizontal bars: mean, error bars: SEM, n = 2–9, unpaired two-tailed t-test. (D) Immunofluorescence staining (left: 20×magnification, scale bar 50 μm) of Si tumor tissue of an AOM-treated mouse. Blue: nuclear staining (DAPI), red: CD11c, green: CCL17-reporter (eGFP). *$p < 0.05$.

Further investigation of tumor infiltrating myeloid cells in intestinal tumors of AOM-treated and untreated *Apc*$^{1638N/+}$ mice confirmed the presence of all subpopulations of monocytes, macrophages and DCs with comparable frequencies in small intestinal and colon tumors. PD-L1 was expressed on tumor-infiltrating monocytic cells, albeit at lower levels than in colon lamina propria. But macrophages, granulocytes and DCs showed only low level expression mimicking the situation in human CRC, where low PD-L1 expression correlates with poor response to PD-1 blockade (51). Successful therapy with pembrolizumab (anti-PD-1) is restricted to the subgroup of mismatch repair deficient CRC which show higher PD-L1 expression (mainly in tumor-associated immune cells) (52). Thus, our model is suitable for investigating regulation of PD-L1 expression in colon tumors and testing therapeutic approaches, which aim to increase responsiveness to checkpoint inhibition.

Using *Apc*$^{1638N/+}$ CCL17-eGFP reporter mice, we found that TAMs and DCs upregulate expression of CCL17 in the microenvironment of small intestinal and colon tumors developing in *Apc*$^{1638N/+}$ mice. CCL17 expression has been used

as a marker for M2-like immunosuppressive TAMs and was shown to correlate with Treg frequencies in tumors in line with its ability to attract Tregs expressing CCR4 (34, 53). Therapeutic strategies targeting TAMs (such as CSF-1R inhibitors) were shown to be effective in syngeneic subcutaneous tumor models, but only in combination with immune stimulation or checkpoint blockade (34, 54). Further studies are required to identify novel target molecules, which prevent or revert the immunosuppressive and tumor promoting functions of TAMs and other tumor-infiltrating myeloid cell subpopulations in spontaneously developing cancers, such as the CRC model described here.

The model described here also allows assessing the phenotype of diverse complete and conditional knockout mouse strains with a simple breeding strategy since only one mutated *Apc* allele is necessary, whereas Cre recombinase or complex husbandry regimes are not required for colon tumor formation. This is advantageous compared to models of conditional *Apc* deletion, such as in *Cdx2p-Cre*; *Apc*$^{+/Loxp}$ mice (18, 19) or *Fabpl- Cre*; *Apc*$^{15lox/+}$ mice (55) or *Villin-Cre; Tp53* $^{Loxp/Loxp}$ mice treated with AOM which require backcrossing to the FVB background (56).

We conclude that *Apc*$^{1638N/+}$ mice treated with AOM are a suitable and robust model of colon carcinogenesis and will be useful to develop new strategies for prevention and immunotherapy of CRC.

MATERIALS AND METHODS

Mice

Mice were bred and held in the animal facility of the Institute for Immunology, LMU Munich, Germany under SPF conditions. Health monitoring was performed according to the recommendations of the Federation of European Laboratory Animal Science Association (FELASA). Sentinels occasionally tested positive for *Helicobacter* spp. All experimental procedures involving mice were performed in accordance with the regulations of and were approved by the local government (Regierung von Oberbayern, license no: 55.2-1-54-2532-36-2013). *Apc*$^{1638N/+}$ mice (8) were crossed with CCL17-eGFP reporter mice (37) (all kept on C57BL6/N-background for >10 generations). Starting at the age of 8 weeks mice were injected with 10 mg/kg Azoxymethane (AOM) i.p. weekly for 6 weeks [as described (56)] or were left untreated. Mice were sacrificed by cervical dislocation when reaching criteria for euthanasia, which included clinical signs of anemia.

Tissue Processing and Single Cell Preparation

The intestines were cut longitudinally, washed with ice-cold PBS and the number, location and size of tumors was recorded. Visible tumors were excised and randomly selected tumors were fixed in 4% PFA for 1 h at 4°C and subsequently incubated in 20% sucrose o/n at 4°C. Tumors were then embedded in OCT (Leica, Wetzlar, Germany) and stored in −80°C. For the generation of single cell suspensions remaining tumor and normal intestinal tissue was cut into 5 mm long pieces and incubated with 2 mM DTT, 10 mM HEPES, 10 mM EDTA for 10 min in a shaking incubator (125 rpm) to dissociate the epithelial layer and then digested with DNAse (0.5 µg/ml), Collagenase D (2.5 µg/ml), Collagenase V (5 µg/ml), and Collagenase IV (157 Wuensch Units/ml) in RPMI-1640 for 30 min at 37°C with gentle shaking before passing through 100 and 70 µm cell strainers.

Histology

Cryosections (5–8 µm) were incubated in Hematoxylin solution (Merck, Darmstadt, Germany), washed in H2O and subsequently stained in Eosin solution (J.T. Baker, Philipsburg, USA), washed in H2O, dehydrated and mounted with Roti®-Histokitt (Carl Roth, Karlsruhe, Germany). Histological assessment and grading was performed using a Leica DM2500 after consultation with a pathologist.

Immunofluorescence Staining

Cyrosections (5–8 µm) were incubated with phosphate buffered saline (PBS) containing 5% goat serum (Vector Labs, Burlingame, USA) and 0.5% Triton-X-100 and then stained with primary antibodies: anti-Ki67 (cat. #12202, Cell signaling technology, Danvers, USA), anti-CD45-FITC (#11-0454-82, Thermo Fisher, Waltham, USA), anti-GFP (#ab6556, Abcam, Cambridge, UK), anti-CD11c (#550283, BD-Bioscience, Franklin Lakes, USA), anti-β-Catenin (#ab22656, Abcam). In case of unlabeled primary antibodies fluorochrome-labeled secondary antibodies were used (#A11008, #A11001, #A21236 Molecular Probes, Eugene, USA). For staining nuclei DAPI (Sigma-Aldrich, St. Louis, USA) was used. Imaging was conducted with a Leica SP8X WLL upright confocal microscope (Leica, Germany).

Flow Cytometry

Single cell suspensions from normal or tumor tissues, processed as described above, were incubated for 10 min with Fc-blocking reagent (anti-CD16/32 producing hybridoma supernatant) before staining with fluorescently labeled surface antibodies, purchased from Biolegend (CD4, #100547, CD8, #100730, CD19, #115522, MHCII, #107632, CD11b, #101226, Ly6G, #127641, CD64, #139305, CD11c, #117318) and Thermo Fisher (CD3, #47-0031-82, Foxp3, #25-5773-80). For Foxp3-staining the Foxp3-Fix/Perm buffer kit was used according to the manufacturers protocol. The Cytoflex S flow cytometer (Beckman Coulter, Brea, USA) was used and the data were analyzed using FlowJo v. 10 (Tree Star Inc., Ashland, USA).

RNA Isolation and qRT-PCR

RNA was isolated from OCT-embedded tissue sections using the RNeasy-FFPE Kit (Qiagen, Hilden, Germany) according to the manufacturers protocol. RNA was reverse-transcribed using SuperScript III (Thermo Fisher). For qRT-PCR UPL primer/probe sets for Lgr5, Opn, Ccl2, Cxcl10 (probes: Roche Diagnostics, Rotkreuz, Switzerland; primers: Metabion, Planegg, Germany) or Taqman assays for Hprt1 (Thermo Fisher) were used and qPCR was performed on a LightCycler 480 Real-Time PCR system (Roche). The 2^-ddCT method was used to quantify relative mRNA expression.

Statistical Analysis

Statistical analysis was performed with GraphPad Prism version 6.0 (GraphPad Software Inc., La Jolla, CA, USA). Normally distributed data was analyzed by unpaired or paired two-tailed *t*-test. Not normally distributed data was analyzed using the Mann-Whitney test. For multiple testing the Holm-Sidak correction method (alpha = 0.05) was used. Survival was analyzed by Kaplan-Meier analysis and log-rank test. The Chi-square test was used to assess relative risk.

DATA AVAILABILITY STATEMENT

All datasets generated for this study are included in the manuscript/**Supplementary Files**.

ETHICS STATEMENT

The animal study was reviewed and approved by Regierung von Oberbayern.

AUTHOR CONTRIBUTIONS

RM designed and performed experiments and analyzed and interpreted data. SK and MM performed experiments. K-PJ analyzed and interpreted data. AK conceived the project, designed experiments, analyzed and interpreted data, and wrote the manuscript.

FUNDING

RM, MM, SK, and AK were supported by the German Research Foundation (SFB1054/TPA06, KR2199/3-2, KR2199/6- 1, KR2199/9-1) and the Georg and Traud Gravenhorst Stiftung. RM received a Ph.D. scholarship from the Studienstiftung des Deutschen Volkes. K-PJ was funded by the German Research Foundation (SFB1371/P10).

ACKNOWLEDGMENTS

This work was part of the thesis of RM. We acknowledge the Core Facility Bioimaging, Biomedical Center, Ludwig-Maximilians-Universität Munich for assistance with confocal microscopy. We would like to thank J. Slotta-Huspenina, Institute of Pathology, Technical University Munich, for consultation regarding histological assessment.

SUPPLEMENTARY MATERIAL

The Supplementary Material for this article can be found online at: https://www.frontiersin.org/articles/10.3389/fonc.2019.01001/full#supplementary-material

REFERENCES

1. Powell SM, Zilz N, Beazer-Barclay Y, Bryan TM, Hamilton SR, Thibodeau SN, et al. APC mutations occur early during colorectal tumorigenesis. *Nature.* (1992) 359:235–7. doi: 10.1038/359235a0
2. Jackstadt R, Sansom OJ. Mouse models of intestinal cancer. *J Pathol.* (2016) 238:141–51. doi: 10.1002/path.4645
3. Aghabozorgi AS, Bahreyni A, Soleimani A, Bahrami A, Khazaei M, Ferns GA, et al. Role of adenomatous polyposis coli (APC) gene mutations in the pathogenesis of colorectal cancer; current status and perspectives. *Biochimie.* (2019) 157:64–71. doi: 10.1016/j.biochi.2018.11.003
4. Rohde F, Rimkus C, Friederichs J, Rosenberg R, Marthen C, Doll D, et al. Expression of osteopontin, a target gene of de-regulated Wnt signaling, predicts survival in colon cancer. *Int J Cancer.* (2007) 121:1717–23. doi: 10.1002/ijc.22868
5. Su LK, Kinzler KW, Vogelstein B, Preisinger AC, Moser AR, Luongo C, et al. Multiple intestinal neoplasia caused by a mutation in the murine homolog of the APC gene. *Science.* (1992) 256:668–70. doi: 10.1126/science.1350108
6. Smits R, Ruiz P, Diaz–Cano S, Luz A, Jagmohan–Changur S, Breukel C, et al. E-cadherin and adenomatous polyposis coli mutations are synergistic in intestinal tumor initiation in mice. *Gastroenterology.* (2000) 119:1045–53. doi: 10.1053/gast.2000.18162
7. Haigis KM, Hoff PD, White A, Shoemaker AR, Halberg RB, Dove WF. Tumor regionality in the mouse intestine reflects the mechanism of loss of Apc function. *Proc Natl Acad Sci USA.* (2004) 101:9769–73. doi: 10.1073/pnas.0403338101
8. Fodde R, Edelmann W, Yang K, van Leeuwen C, Carlson C, Renault B, et al. A targeted chain-termination mutation in the mouse Apc gene results in multiple intestinal tumors. *Proc Natl Acad Sci USA.* (1994) 91:8969–73. doi: 10.1073/pnas.91.19.8969
9. Lipkin M, Yang K, Edelmann W, Newmark H, Fan KH, Risio M, et al. Inherited and acquired risk factors in colonic neoplasia and modulation by chemopreventive interventions. *J Cell Biochem Suppl.* (1996) 25:136–41. doi: 10.1002/(SICI)1097-4644(1996)25+<136::AID-JCB19>3.0.CO;2-M
10. Alberici P, Jagmohan-Changur S, De Pater E, Van Der Valk M, Smits R, Hohenstein P, et al. Smad4 haploinsufficiency in mouse models for intestinal cancer. *Oncogene.* (2006) 25:1841–51. doi: 10.1038/sj.onc.1209226
11. Janssen KP, Alberici P, Fsihi H, Gaspar C, Breukel C, Franken P, et al. APC and oncogenic KRAS are synergistic in enhancing Wnt signaling in intestinal tumor formation and progression. *Gastroenterology.* (2006) 131:1096–109. doi: 10.1053/j.gastro.2006.08.011
12. Gravaghi C, Bo J, Laperle KM, Quimby F, Kucherlapati R, Edelmann W, et al. Obesity enhances gastrointestinal tumorigenesis in Apc-mutant mice. *Int J Obes.* (2008) 32:1716–9. doi: 10.1038/ijo.2008.149
13. Kucherlapati MH, Yang K, Fan K, Kuraguchi M, Sonkin D, Rosulek A, et al. Loss of Rb1 in the gastrointestinal tract of Apc1638N mice promotes tumors of the cecum and proximal colon. *Proc Natl Acad Sci USA.* (2008) 105:15493–8. doi: 10.1073/pnas.0802933105
14. Yang K, Popova NV, Yang WC, Lozonschi I, Tadesse S, Kent S, et al. Interaction of Muc2 and Apc on Wnt signaling and in intestinal tumorigenesis: potential role of chronic inflammation. *Cancer Res.* (2008) 68:7313–22. doi: 10.1158/0008-5472.CAN-08-0598
15. Fre S, Pallavi SK, Huyghe M, Lae M, Janssen KP, Robine S, et al. Notch and Wnt signals cooperatively control cell proliferation and tumorigenesis in the intestine. *Proc Natl Acad Sci USA.* (2009) 106:6309–14. doi: 10.1073/pnas.0900427106
16. Kress E, Skah S, Sirakov M, Nadjar J, Gadot N, Scoazec JY, et al. Cooperation between the thyroid hormone receptor TRalpha1 and the WNT pathway in the induction of intestinal tumorigenesis. *Gastroenterology.* (2010) 138:1863–74. doi: 10.1053/j.gastro.2010.01.041
17. Bong YS, Assefnia S, Tuohy T, Neklason DW, Burt RW, Ahn J, et al. A role for the vitamin D pathway in non-intestinal lesions in genetic and carcinogen models of colorectal cancer and in familial adenomatous polyposis. *Oncotarget.* (2016) 7:80508–20. doi: 10.18632/oncotarget.12768
18. Hinoi T, Akyol A, Theisen BK, Ferguson DO, Greenson JK, Williams BO, et al. Mouse model of colonic adenoma-carcinoma progression based on somatic Apc inactivation. *Cancer Res.* (2007) 67:9721–30. doi: 10.1158/0008-5472.CAN-07-2735

19. Feng Y, Sentani K, Wiese A, Sands E, Green M, Bommer GT, et al. Sox9 induction, ectopic Paneth cells, and mitotic spindle axis defects in mouse colon adenomatous epithelium arising from conditional biallelic Apc inactivation. *Am J Pathol.* (2013) 183:493–503. doi: 10.1016/j.ajpath.2013.04.013
20. Cooper HS, Everley L, Chang WC, Pfeiffer G, Lee B, Murthy S, et al. The role of mutant Apc in the development of dysplasia and cancer in the mouse model of dextran sulfate sodium–induced colitis. *Gastroenterology.* (2001) 121:1407–16. doi: 10.1053/gast.2001.29609
21. Soncin I, Sheng J, Chen Q, Foo S, Duan K, Lum J, et al. The tumour microenvironment creates a niche for the self-renewal of tumour-promoting macrophages in colon adenoma. *Nat Commun.* (2018) 9:582. doi: 10.1038/s41467-018-02834-8
22. Yang D, Zhang M, Gold B. Origin of somatic mutations in beta-catenin versus adenomatous polyposis coli in colon cancer: random mutagenesis in animal models versus nonrandom mutagenesis in humans. *Chem Res Toxicol.* (2017) 30:1369–75. doi: 10.1021/acs.chemrestox.7b00092
23. Issa AY, Volate SR, Muga SJ, Nitcheva D, Smith T, Wargovich MJ. Green tea selectively targets initial stages of intestinal carcinogenesis in the AOM-ApcMin mouse model. *Carcinogenesis.* (2007) 28:1978–84. doi: 10.1093/carcin/bgm161
24. Suzui M, Okuno M, Tanaka T, Nakagama H, Moriwaki H. Enhanced colon carcinogenesis induced by azoxymethane in min mice occurs via a mechanism independent of beta-catenin mutation. *Cancer Lett.* (2002) 183:31–41. doi: 10.1016/S0304-3835(02)00114-3
25. Paulsen JE, Steffensen IL, Namork E, Eide TJ, Alexander J. Age-dependent susceptibility to azoxymethane-induced and spontaneous tumorigenesis in the Min/+ mouse. *Anticancer Res.* (2003) 23:259–65.
26. Mollersen L, Paulsen JE, Alexander J. Loss of heterozygosity and nonsense mutation in Apc in azoxymethane-induced colonic tumours in min mice. *Anticancer Res.* (2004) 24:2595–9. Available online at: http://ar.iiarjournals.org/content/24/5A/2595.abstract
27. Rao VP, Poutahidis T, Ge Z, Nambiar PR, Boussahmain C, Wang YY, et al. Innate immune inflammatory response against enteric bacteria *Helicobacter hepaticus* induces mammary adenocarcinoma in mice. *Cancer Res.* (2006) 66:7395–400. doi: 10.1158/0008-5472.CAN-06-0558
28. Zhang C, Hou D, Wei H, Zhao M, Yang L, Liu Q, et al. Lack of interferon-gamma receptor results in a microenvironment favorable for intestinal tumorigenesis. *Oncotarget.* (2016) 7:42099–109. doi: 10.18632/oncotarget.9867
29. Nakanishi Y, Nakatsuji M, Seno H, Ishizu S, Akitake-Kawano R, Kanda K, et al. COX-2 inhibition alters the phenotype of tumor-associated macrophages from M2 to M1 in ApcMin/+ mouse polyps. *Carcinogenesis.* (2011) 32:1333–9. doi: 10.1093/carcin/bgr128
30. Akeus P, Langenes V, Kristensen J, von Mentzer A, Sparwasser T, Raghavan S, et al. Treg-cell depletion promotes chemokine production and accumulation of CXCR3(+) conventional T cells in intestinal tumors. *Eur J Immunol.* (2015) 45:1654–66. doi: 10.1002/eji.201445058
31. Elliott LA, Doherty GA, Sheahan K, Ryan EJ. Human tumor-infiltrating myeloid cells: phenotypic and functional diversity. *Front Immunol.* (2017) 8:86. doi: 10.3389/fimmu.2017.00086
32. Akeus P, Szeponik L, Ahlmanner F, Sundstrom P, Alsen S, Gustavsson B, et al. Regulatory T cells control endothelial chemokine production and migration of T cells into intestinal tumors of APC(min/+) mice. *Cancer Immunol Immunother.* (2018) 67:1067–77. doi: 10.1007/s00262-018-2161-9
33. Zhong X, Chen B, Yang Z. The role of tumor-associated macrophages in colorectal carcinoma progression. *Cell Physiol Biochem.* (2018) 45:356–65. doi: 10.1159/000486816
34. Perry CJ, Munoz-Rojas AR, Meeth KM, Kellman LN, Amezquita RA, Thakral D, et al. Myeloid-targeted immunotherapies act in synergy to induce inflammation and antitumor immunity. *J Exp Med.* (2018) 215:877–93. doi: 10.1084/jem.20171435
35. Barker N, van Es JH, Kuipers J, Kujala P, van den Born M, Cozijnsen M, et al. Identification of stem cells in small intestine and colon by marker gene Lgr5. *Nature.* (2007) 449:1003–7. doi: 10.1038/nature06196
36. Henderson BR. Nuclear-cytoplasmic shuttling of APC regulates beta-catenin subcellular localization and turnover. *Nat Cell Biol.* (2000) 2:653–60. doi: 10.1038/35023605
37. Alferink J, Lieberam I, Reindl W, Behrens A, Weiss S, Huser N, et al. Compartmentalized production of CCL17 *in vivo*: strong inducibility in peripheral dendritic cells contrasts selective absence from the spleen. *J Exp Med.* (2003) 197:585–99. doi: 10.1084/jem.20021859
38. Heiseke AF, Faul AC, Lehr HA, Forster I, Schmid RM, Krug AB, et al. CCL17 promotes intestinal inflammation in mice and counteracts regulatory T cell-mediated protection from colitis. *Gastroenterology.* (2012) 142:335–45. doi: 10.1053/j.gastro.2011.10.027
39. Chen J, Huang XF. The signal pathways in azoxymethane-induced colon cancer and preventive implications. *Cancer Biol Ther.* (2009) 8:1313–7. doi: 10.4161/cbt.8.14.8983
40. Souris JS, Zhang HJ, Dougherty U, Chen NT, Waller JV, Lo LW, et al. A novel mouse model of sporadic colon cancer induced by combination of conditional Apc genes and chemical carcinogen in the absence of Cre recombinase. *Carcinogenesis.* (2019) bgz050. doi: 10.1093/carcin/bgz050
41. Roy BC, Ahmed I, Ramalingam S, Jala V, Haribabu B, Ramamoorthy P, et al. Co-localization of autophagy-related protein p62 with cancer stem cell marker dclk1 may hamper dclk1's elimination during colon cancer development and progression. *Oncotarget.* (2019) 10:2340–54. doi: 10.18632/oncotarget.26684
42. Wikberg ML, Ling A, Li X, Oberg A, Edin S, Palmqvist R. Neutrophil infiltration is a favorable prognostic factor in early stages of colon cancer. *Hum Pathol.* (2017) 68:193–202. doi: 10.1016/j.humpath.2017.08.028
43. Zhou J, Nefedova Y, Lei A, Gabrilovich D. Neutrophils and PMN-MDSC: their biological role and interaction with stromal cells. *Semin Immunol.* (2018) 35:19–28. doi: 10.1016/j.smim.2017.12.004
44. Triner D, Devenport SN, Ramakrishnan SK, Ma X, Frieler RA, Greenson JK, et al. Neutrophils restrict tumor-associated microbiota to reduce growth and invasion of colon tumors in mice. *Gastroenterology.* (2019) 156:1467–82. doi: 10.1053/j.gastro.2018.12.003
45. Chun E, Lavoie S, Michaud M, Gallini CA, Kim J, Soucy G, et al. CCL2 Promotes colorectal carcinogenesis by enhancing polymorphonuclear myeloid-derived suppressor cell population and function. *Cell Rep.* (2015) 12:244–57. doi: 10.1016/j.celrep.2015.06.024
46. Katoh H, Wang D, Daikoku T, Sun H, Dey SK, Dubois RN. CXCR2-expressing myeloid-derived suppressor cells are essential to promote colitis-associated tumorigenesis. *Cancer Cell.* (2013) 24:631–44. doi: 10.1016/j.ccr.2013.10.009
47. Ogawa R, Yamamoto T, Hirai H, Hanada K, Kiyasu Y, Nishikawa G, et al. Loss of SMAD4 promotes colorectal cancer progression by recruiting tumor-associated neutrophils via the CXCL1/8-CXCR2 axis. *Clin Cancer Res.* (2019) 25:2887–99. doi: 10.1158/1078-0432.CCR-18-3684
48. Doll D, Keller L, Maak M, Boulesteix AL, Siewert JR, Holzmann B, et al. Differential expression of the chemokines GRO-2, GRO-3, and interleukin-8 in colon cancer and their impact on metastatic disease and survival. *Int J Colorectal Dis.* (2010) 25:573–81. doi: 10.1007/s00384-010-0901-1
49. Cremonesi E, Governa V, Garzon JFG, Mele V, Amicarella F, Muraro MG, et al. Gut microbiota modulate T cell trafficking into human colorectal cancer. *Gut.* (2018) 67:1984–94. doi: 10.1136/gutjnl-2016-313498
50. Tomkovich S, Yang Y, Winglee K, Gauthier J, Muhlbauer M, Sun X, et al. Locoregional effects of microbiota in a preclinical model of colon carcinogenesis. *Cancer Res.* (2017) 77:2620–32. doi: 10.1158/0008-5472.CAN-16-3472
51. Topalian SL, Hodi FS, Brahmer JR, Gettinger SN, Smith DC, McDermott DF, et al. Safety, activity, and immune correlates of anti-PD-1 antibody in cancer. *N Engl J Med.* (2012) 366:2443–54. doi: 10.1056/NEJMoa1200690
52. Le DT, Durham JN, Smith KN, Wang H, Bartlett BR, Aulakh LK, et al. Mismatch repair deficiency predicts response of solid tumors to PD-1 blockade. *Science.* (2017) 357:409–13. doi: 10.1126/science.aan6733
53. Akeus P, Langenes V, von Mentzer A, Yrlid U, Sjoling A, Saksena P, et al. Altered chemokine production and accumulation of regulatory T cells in intestinal adenomas of APC(Min/+) mice. *Cancer Immunol Immunother.* (2014) 63:807–19. doi: 10.1007/s00262-014-1555-6
54. Hoves S, Ooi CH, Wolter C, Sade H, Bissinger S, Schmittnaegel M, et al. Rapid activation of tumor-associated macrophages boosts preexisting

tumor immunity. *J Exp Med.* (2018) 215:859–76. doi: 10.1084/jem.20171440

55. Robanus-Maandag EC, Koelink PJ, Breukel C, Salvatori DC, Jagmohan-Changur SC, Bosch CA, et al. A new conditional Apc-mutant mouse model for colorectal cancer. *Carcinogenesis.* (2010) 31:946–52. doi: 10.1093/carcin/bgq046
56. Schwitalla S, Ziegler PK, Horst D, Becker V, Kerle I, Begus-Nahrmann Y, et al. Loss of p53 in enterocytes generates an inflammatory microenvironment enabling invasion and lymph node metastasis of carcinogen-induced colorectal tumors. *Cancer Cell.* (2013) 23:93–106. doi: 10.1016/j.ccr.2012.11.014

Conflict of Interest: The authors declare that the research was conducted in the absence of any commercial or financial relationships that could be construed as a potential conflict of interest.

Supplemental information

Increased incidence of colon tumors in AOM-treated *Apc*$^{1638N/+}$ mice reveals higher frequency of tumor associated neutrophils in colon than small intestine

Rebecca Metzger, Mahulena Maruskova, Sabrina Krebs, Klaus-Peter Janssen, Anne B Krug

Inventory of supplemental information:

Supplementary figure 1:

(A) Percentages of CD45+ immune cells in tumors of untreated and AOM-treated *Apc*$^{1638N/+}$ mice. (B) Percentages of CD3^{+} T cells, CD4^{+} T-helper cells, CD4^{+} Foxp3^{+} Treg cells and CD19^{+} B cells of all CD45^{+} cells in tumors of untreated and AOM-treated *Apc*$^{1638N/+}$ mice. Each symbol represents an individual mouse. Horizontal bars: mean, error bars: SEM, n=2-9, unpaired two-tailed t-test (not significant).

Supplementary figure 2:

(A) Representative images of CD45 (red) immunofluorescence staining (20x magnification) of small intestinal tumor tissue from untreated (left) and AOM-treated (right) *Apc*$^{1638N/+}$ mice. (B) Percentages of indicated immune cell populations of all CD45^{+} cells in Si and Co tumor lesions (grey, filled bars) and normal intestinal tissue (open bars) of the same individual AOM-treated *Apc*$^{1638N/+}$ mice. Each symbol represents an individual mouse. Lines connect paired values (n=3-6, paired, two-tailed t-test). *$p<0.05$

Supplementary figure 1

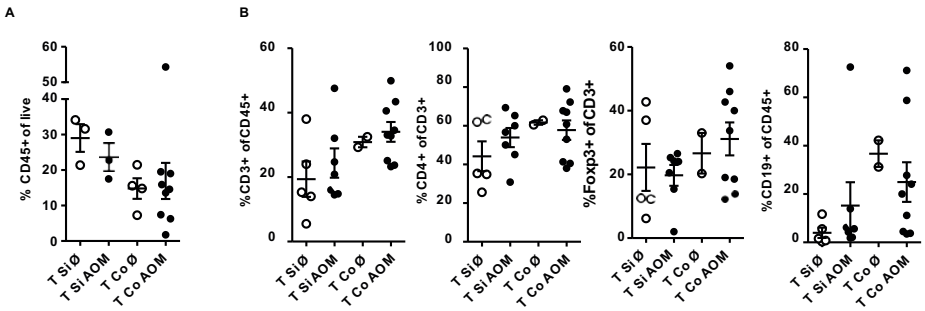

Supplementary figure 2

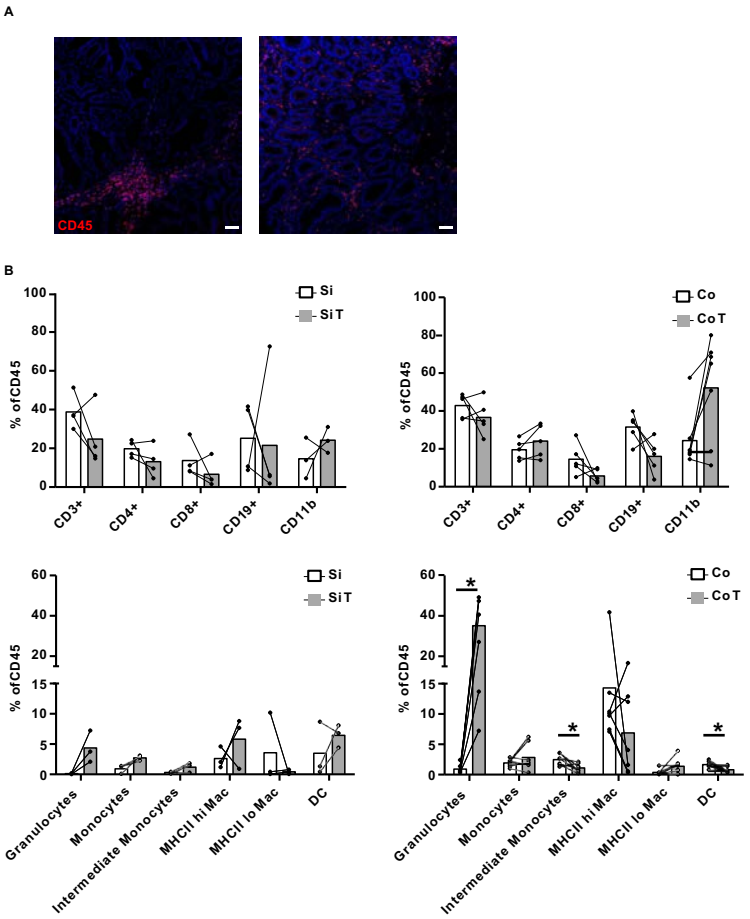

7. References

1 Breedveld A, Groot Kormelink T, van Egmond M, de Jong EC. Granulocytes as modulators of dendritic cell function. *Journal of leukocyte biology* 2017; 102: 1003-1016.

2 Fournier BM, Parkos C. The role of neutrophils during intestinal inflammation. *Mucosal immunology* 2012; 5: 354-366.

3 Wéra O, Lancellotti P, Oury C. The Dual Role of Neutrophils in Inflammatory Bowel Diseases. *J Clin Med* 2016; 5: 118.

4 Zindl CL, Lai J-F, Lee YK, Maynard CL, Harbour SN, Ouyang W *et al*. IL-22-producing neutrophils contribute to antimicrobial defense and restitution of colonic epithelial integrity during colitis. *Proceedings of the National Academy of Sciences of the United States of America* 2013; 110: 12768-12773.

5 Wikberg ML, Ling A, Li X, Öberg Å, Edin S, Palmqvist R. Neutrophil infiltration is a favorable prognostic factor in early stages of colon cancer. *Human Pathology* 2017; 68: 193-202.

6 Zhou J, Nefedova Y, Lei A, Gabrilovich D. Neutrophils and PMN-MDSC: Their biological role and interaction with stromal cells. *Seminars in Immunology* 2018; 35: 19-28.

7 Muzaki ARBM, Tetlak P, Sheng J, Loh SC, Setiagani YA, Poidinger M *et al*. Intestinal CD103+CD11b− dendritic cells restrain colitis via IFN-γ-induced anti-inflammatory response in epithelial cells. *Mucosal immunology* 2016; 9: 336-351.

8 Stagg AJ. Intestinal Dendritic Cells in Health and Gut Inflammation. *Frontiers in Immunology* (Mini Review) 2018; 9.

9 Roberts EW, Broz ML, Binnewies M, Headley MB, Nelson AE, Wolf DM *et al*. Critical Role for CD103+/CD141+ Dendritic Cells Bearing CCR7 for Tumor Antigen Trafficking and Priming of T Cell Immunity in Melanoma. *Cancer Cell* 2016; 30: 324-336.

10 Binnewies M, Mujal AM, Pollack JL, Combes AJ, Hardison EA, Barry KC *et al*. Unleashing Type-2 Dendritic Cells to Drive Protective Antitumor CD4(+) T Cell Immunity. *Cell* 2019; 177: 556-571.e516.

11 Bain CC, Bravo-Blas A, Scott CL, Gomez Perdiguero E, Geissmann F, Henri S *et al*. Constant replenishment from circulating monocytes maintains the macrophage pool in the intestine of adult mice. *Nature immunology* 2014; 15: 929-937.

12 Yona S, Kim KW, Wolf Y, Mildner A, Varol D, Breker M *et al*. Fate mapping reveals origins and dynamics of monocytes and tissue macrophages under homeostasis. *Immunity* 2013; 38: 79-91.

13 Bain CC, Schridde A. Origin, Differentiation, and Function of Intestinal Macrophages. *Frontiers in Immunology* (Review) 2018; 9.

14 Soncin I, Sheng J, Chen Q, Foo S, Duan K, Lum J *et al*. The tumour microenvironment creates a niche for the self-renewal of tumour-promoting macrophages in colon adenoma. *Nature communications* 2018; 9: 582.

15 Georgoudaki AM, Prokopec KE, Boura VF, Hellqvist E, Sohn S, Ostling J *et al*. Reprogramming Tumor-Associated Macrophages by Antibody Targeting Inhibits Cancer Progression and Metastasis. *Cell reports* 2016; 15: 2000-2011.

16 Olingy CE, Dinh HQ, Hedrick CC. Monocyte heterogeneity and functions in cancer. *Journal of Leukocyte Biology* 2019; 106: 309-322.

17 Inngjerdingen M, Damaj B, Maghazachi AA. Human NK cells express CC chemokine receptors 4 and 8 and respond to thymus and activation-regulated chemokine, macrophage-derived chemokine, and I-309. *Journal of immunology* 2000; 164: 4048-4054.

18 Iellem A, Mariani M, Lang R, Recalde H, Panina-Bordignon P, Sinigaglia F *et al*. Unique chemotactic response profile and specific expression of chemokine receptors CCR4 and CCR8 by CD4(+)CD25(+) regulatory T cells. *The Journal of experimental medicine* 2001; 194: 847-853.

19 Perry CJ, Muñoz-Rojas AR, Meeth KM, Kellman LN, Amezquita RA, Thakral D *et al*. Myeloid-targeted immunotherapies act in synergy to induce inflammation and antitumor immunity. *The Journal of experimental medicine* 2018; 215: 877-893.

20 Françozo MCS, Costa FRC, Guerra-Gomes IC, Silva JS, Sesti-Costa R. Dendritic cells and regulatory T cells expressing CCR4 provide resistance to coxsackievirus B5-induced pancreatitis. *Scientific Reports* 2019; 9: 14766.

21 Yogo Y, Fujishima S, Inoue T, Saito F, Shiomi T, Yamaguchi K *et al*. Macrophage derived chemokine (CCL22), thymus and activation-regulated chemokine (CCL17), and CCR4 in idiopathic pulmonary fibrosis. *Respiratory Research* 2009; 10: 80.

22 Stutte S, Quast T, Gerbitzki N, Savinko T, Novak N, Reifenberger J *et al*. Requirement of CCL17 for CCR7- and CXCR4-dependent migration of cutaneous dendritic cells. *Proceedings of the National Academy of Sciences of the United States of America* 2010; 107: 8736-8741.

23 Weber C, Meiler S, Doring Y, Koch M, Drechsler M, Megens RT *et al*. CCL17-expressing dendritic cells drive atherosclerosis by restraining regulatory T cell homeostasis in mice. *The Journal of clinical investigation* 2011; 121: 2898-2910.

24 Heiseke AF, Faul AC, Lehr HA, Forster I, Schmid RM, Krug AB *et al*. CCL17 promotes intestinal inflammation in mice and counteracts regulatory T cell-mediated protection from colitis. *Gastroenterology* 2012; 142: 335-345.

25 Corrêa-Oliveira R, Fachi JL, Vieira A, Sato FT, Vinolo MAR. Regulation of immune cell function by short-chain fatty acids. *Clin Transl Immunology* 2016; 5: e73-e73.

26 Kaur R, Thakur S, Rastogi P, Kaushal N. Resolution of Cox mediated inflammation by Se supplementation in mouse experimental model of colitis. *PloS one* 2018; 13: e0201356.

27 Sindrilaru A, Peters T, Wieschalka S, Baican C, Baican A, Peter H *et al*. An unrestrained proinflammatory M1 macrophage population induced by iron impairs wound healing in humans and mice. *The Journal of clinical investigation* 2011; 121: 985-997.

28 Werner T, Wagner SJ, Martínez I, Walter J, Chang J-S, Clavel T *et al*. Depletion of luminal iron alters the gut microbiota and prevents Crohn's disease-like ileitis. *Gut* 2011; 60: 325-333.

29 Markota A, Metzger R, Heiseke AF, Jandl L, Dursun E, Eisenächer K *et al*. Comparison of iron-reduced and iron-supplemented semisynthetic diets in T cell transfer colitis. *PloS one* 2019; 14: e0218332.

30 Grivennikov SI, Cominelli F. Colitis-Associated and Sporadic Colon Cancers: Different Diseases, Different Mutations? *Gastroenterology* 2016; 150: 808-810.

31 Griffith JW, Sokol CL, Luster AD. Chemokines and Chemokine Receptors: Positioning Cells for Host Defense and Immunity. *Annual Review of Immunology* 2014; 32: 659-702.

32 Mollica Poeta V, Massara M, Capucetti A, Bonecchi R. Chemokines and Chemokine Receptors: New Targets for Cancer Immunotherapy. *Frontiers in Immunology* (Mini Review) 2019; 10.

33 Poh AR, Love CG, Masson F, Preaudet A, Tsui C, Whitehead L *et al*. Inhibition of Hematopoietic Cell Kinase Activity Suppresses Myeloid Cell-Mediated Colon Cancer Progression. *Cancer cell* 2017; 31: 563-575.e565.

34 Metzger R, Maruskova M, Krebs S, Janssen K-P, Krug AB. Increased Incidence of Colon Tumors in AOM-Treated Apc1638N/+ Mice Reveals Higher Frequency of Tumor Associated Neutrophils in Colon Than Small Intestine. *Frontiers in Oncology* (Methods) 2019; 9.

8. Acknowledgements

I want to thank everyone without whom this thesis would not have been possible.

First of all I want to thank Prof. Dr. Anne Krug for giving me the possibility to conduct this thesis in her laboratory and for her trustful support and guidance. I also want to warmly thank my co-supervisors Prof. Dr. Thomas Brocker and PD Dr. Hubertus Hochrein for their input and support. Further, I want to thank our collaborators Prof. Dr. K.P. Janssen, Prof. Bärbel Stecher and Prof. Roland Rad.

I am deeply thankful to all AG Krug members for the good times and the discussions about science and beyond.

Moreover, I want to acknowledge PD Dr. Steffen Dietzel and Dr. Andreas Thomae for being always helpful and supportive regarding microscopy and Dr. Lisa Richter for her input and advice in flow cytometry.

I also want to thank all members of the institute for immunology for the collaborative and helpful atmosphere.

9. Curriculum Vitae

REBECCA METZGER

LMU LUDWIG-MAXIMILIANS-UNIVERSITÄT MÜNCHEN

Dean's Office
Medical Faculty

MMRS

Confirmation of congruency between printed and electronic version of the doctoral thesis

Metzger, Rebecca

Surname, first name

Street

Zip code, town

Country

I hereby declare that the electronic version of the submitted thesis, entitled

Effector functions and dependencies of myeloid cell subsets in colitis, colitis associated cancer and sporadic intestinal cancer

is congruent with the printed version both in content and format.

München, 28.11.2020

Place, date

Rebecca Metzger

Signature doctoral candidate